Infrared Airglow and Contamination Modeling

S.M. Adler-Golden
A. Berk
P.K. Acharya
L.S. Bernstein

Spectral Sciences, Inc.
99 South Bedford Street #7
Burlington, MA 01803-5169
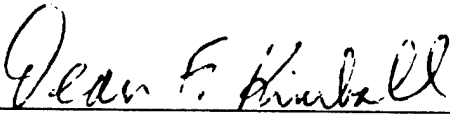

October 1999

Final Report

May 1993-March 1999

AIR FORCE RESEARCH LABORATORY
Space Vehicles Directorate
29 Randolph Rd
AIR FORCE MATERIEL COMMAND
Hanscom AFB, MA 01731-3010

20020815 057

This technical report has been reviewed and is approved for publication.

DEAN F. KIMBALL
DEAN F. KIMBALL
Contract Manager
AFRL/VSSS

GERALD J. ZDYB
Acting Deputy Chief
AFRL/VSSS

REPORT DOCUMENT PAGE

Public reporting burden for this collection of information is estimated to average 1 hour per response, including the time for reviewing instructions, searching existing date sources, gathering and maintaining the data needed, and completing and reviewing the collection of information Send comments regarding this burden estimate or any other aspect of this collection of information, including suggestions for reducing this burden, to Washington Headquarters Services, Directorate for Information Operations Reports, 1215 Jefferson Davis Highway, Suite 1204, Arlington, VA 22202-4302, and to the office of Management and Budget, Paperwork Reduction Project (0704-0188), Washington, DC 20503.

1. AGENCY USE ONLY (Leave Blank)	2. REPORT DATE October 1999	3. REPORT TYPE AND DATES COVERED Final Scientific and Technical Report

4. TITLE AND SUBTITLE Infrared Airglow and Contamination Modeling	5. FUNDING NUMBERS C F19628-93-C-0049
6. AUTHOR(S) S.M. Aldler-Golden, A. Berk, P.K. Acharya, L.S. Bernstein	PE 63215C PR S321 TA GD WU BS

7. PERFORMING ORGANIZATION NAME(S) AND ADDRESS(ES) Spectral Sciences, Inc. 99 South Bedford Street Burlington, MA 01803	8. PERFORMING ORGANIZATION REPORT NUMBER SSI-TR-333

9. SPONSORING/MONITORING AGENCY NAME(S) AND ADDRESS(ES) AFRL/VSBM 29 Randolph Road Hanscom AFB, MA 01731-3010	10. SPONSORING/MONITORING AGENCY REPORT NUMBER AFRL-VS-TR-1999-1544

11. SUPPLEMENTARY NOTES

12a. DISTRIBUTION/AVAILABILITY STATEMENT Approved for public release; distribution unlimited	12b DISTRIBUTION CODE

13. ABSTRACT *(Maximum 200 words)*

This report describes work performed to evaluate our understanding of infrared (IR) atmospheric phenomenology through comprehensive analysis of spectral and in-band radiance field data. Computer models of atmospheric IR radiation used for these analyses include the standard AFRL codes MODTRAN, SHARC, and SAMM. MODTRAN is a rapid, local thermodynamic equilibrium (LTE) code for low- to moderate-resolution spectra. SHARC calculates emission and transmission spectra in the 2-40 μm region for arbitrary line-of-sight (LOS) paths between 50 and 300 km for both quiescent and auroral conditions. SAMM is the result of integrating MODTRAN and SHARC into a single, seamless code with a unified and correlated radiative transport algorithm applicable at altitudes from ground to 300 km. Detailed comparisons of the models with spectral and in-band radiance data from the CIRRIS-1A Shuttle experiment demonstrate the predictive capabilities of the background models, as well as the variability of IR atmospheric radiance over time and geographic location. In addition, MODTRAN upgrades which address the data/model comparisons and the investigation into the accuracy of MODTRAN in selected radiation transfer applications are discussed.

14. SUBJECT TERMS Infrared Radiation MWIR LWIR Atmospheric Radiance CIRRIS-1A LTE non-LTE Radiative Transfer	15 NUMBER OF PAGES 122
	16. PRICE CODE

17. SECURITY CLASSIFICATION OR REPORT Unclassified	18. SECURITY CLASSIFICATION OF THE PAGE Unclassified	19. SECURITY CLASSIFICATION OF ABSTRACT Unclassified	20. LIMITATION OF ABSTRACT Same as Report

TABLE OF CONTENTS

TABLE OF CONTENTS (Continued)

Section

Page

LIST OF FIGURES

LIST OF FIGURES (Continued)

LIST OF TABLES

GLOSSARY

A^+	Aerosol Plus
AFRL/VSBM	Air Force Research Lab/Background Clutter Mitigation Branch
ATLAS	Atmospheric Laboratory for Applications and Science
BM	Band Model
BMDO	Ballistic Missile Defense Organization
CG	Curtis-Godson
CIRRIS	Cryogenic Infrared Radiance Instrumentation for Shuttle
CK	Correlated-k
CO_2	Carbon Dioxide
FOV	Field of View
FP	Focal Plane
FWHM	Full Width at Half Maximum
H_2O	Water
HITRAN	High-resolution transmission molecular absorption
HNO_3	Nitric Acid
ICRCCM	Intercomparison of Radiation Codes used in Climate Models
IR	Infrared Radiation
LBL	Line-by-line
LOS	Line of Sight
LTE	Local Thermodynamic Equilibrium
LWIR	Long Wave Infrared
MODTRAN	Moderate Spectral Resolution Atmospheric Transmission Model
NBM	Narrow Band Model
NAM	Navy Aerosol Model
NRL	Naval Research Lab
NO	Nitric Oxide
NOVAM	Naval Oceanic Vertical Aerosol Model
O_3	Ozone
OH	Hydroxyl
RH	Relative Humidity
RMS	Root Mean Square

GLOSSARY (Continued)

SAMM	Sharc And Modtran Merged
SHARC	Strategic High-altitude Atmospheric Radiation Code
SWIR	Short Wave Infrared
SPIRE	Spectral Infrared Rocket Experiment
SSGM	Strategic Scene Generation Model
SUSIM	Solar Ultraviolet Spectral Irradiance Monitor
SSI	Spectral Sciences, Inc.
SSBUV	Shuttle Solar Backscatter Ultraviolet
SZA	Solar Zenith Angle
UARS	Upper Atmosphere Research Satellite
USS	User Supplied Spectra
UV	Ultraviolet
VNBM	Very Narrow Band Model
WBM	Wide Band Model
1-D	One Dimensional

1.0 INTRODUCTION

The calculation of infrared (IR) radiance and transmittance spectra is of fundamental importance in many areas of atmospheric science. These include modeling the atmospheric energy budget for global climate change predictions, analyzing data from remote sounding experiments, and understanding the impact of the atmosphere on target detection. The usefulness of the models and codes used in simulations lies in the fundamental understanding of the underlying physics and chemistry that give rise to these atmospheric effects. The overall objective of this effort is to evaluate our understanding of IR atmospheric phenomenology through comprehensive analysis of spectral and in-band radiance field data, and to transition these results into practical models for inclusion into existing atmospheric simulation codes.

Available computer codes for atmospheric IR radiation that have gained wide use include several developed and maintained by AFRL/VS. MODTRAN [Berk *et al.*, 1998] is a rapid, local thermodynamic equilibrium (LTE) code for low- to moderate-resolution spectra. FASCODE [Clough *et al.*, 1988] is a high-resolution, line-by-line code that can be used in both LTE and non-LTE applications; however, the non-LTE molecular state populations must be externally generated. SHARC, the Strategic High-altitude Atmospheric Radiation Code [Sundberg *et al.*, 1995] calculates emission and transmittance spectra in the 2-40 μm region for arbitrary line-of-sight (LOS) paths between 30 and 300 km with sufficient accuracy, speed, and resolution (1.0 cm^{-1}) to be useful for a wide range of applications. It incorporates the IR bands of NO, CO_2, O_3, H_2O, OH, CO, and CH_4 found in the quiescent atmosphere, including minor isotopic bands of CO_2 and H_2O. It also accounts for auroral production and excitation of CO_2, NO, and NO+ caused by the flux of energetic solar electrons. SAMM [Sharma *et al.*, 1996], SHARC and MODTRAN Merged, was developed by integrating MODTRAN and SHARC into a single, seamless code with a unified and correlated radiative transport algorithm applicable at altitudes from ground to 300 km.

This Final Report summarizes the work performed by Spectral Sciences, Inc. (SSI) under the Infrared Airglow and Contamination Modeling and Interpretation program. The overall objectives of the program are to interpret and model recent infrared airglow observations using first-principles radiation codes. The main tasks of this effort include: (1) analyzing data from the CIRRIS-1A Shuttle experiment through comparisons with calculations using the SHARC, SAMM and/or

MODTRAN codes, (2) providing MODTRAN upgrades which address the data/model comparisons, and (3) investigating the accuracy of MODTRAN in selected radiation transfer applications.

The report is organized as follows: Section 2 presents a summary of a detailed spectral and radiometric analysis of the CIRRIS-1A data using SAMM; section 3 describes the addition of a correlated-k capability to MODTRAN; a summary of Band Model Calculations of Atmospheric Fluxes and Cooling Rates is given in Section 4; the creation of a MODTRAN input file from radiosonde measurements is described in Section 5; Section 6 discusses improvements to MODTRAN accuracy for remote sensing; the new solar irradiance data sets incorporated in MODTRAN is presented in Section 7; next, the incorporation of NOVAM aerosol model into MODTRAN 3.7/4.0 is described in Section 8; finally, upgrades to the MODTRAN 3.7/4.0 aerosol and cloud models are discussed in Section 9.

2.0 SPECTRAL AND RADIOMETRIC COMPARISONS OF CIRRIS-1A DATA AND SAMM

Atmospheric infrared (IR) radiation constitutes the background against which targets are viewed by many space-based optical sensors. The operability of these system elements is limited by the ability to discriminate target signatures from the atmospheric optical background. The cost-effective acquisition of IR sensors for tactical, theater, and strategic weapon systems requires accurate, validated atmospheric IR radiance models for generating environment simulations over a wide range of wavelengths, lines of sight, and atmospheric conditions.

The highly successful April 1991 CIRRIS-1A mission [Ahmadjian *et al.*, 1990] on the space shuttle STS-39 and the development of the SAMM atmospheric optical background code [Sharma *et al.*, 1996] provide a unique opportunity for a comprehensive comparison of high-quality spectral and radiometric data with code calculations. This section describes a systematic comparison of CIRRIS atmospheric IR radiance measurements with SAMM code calculations, and the generation of a database of matched overlay plots. The CIRRIS spectral data were taken with a Michelson interferometer and a Si:As detector array (focal plane 3), and include limb views for tangent heights ranging from near the ground to over 200 km during different times of the day and night and over a wide latitude range in both hemispheres. Medium-wavelength-IR spectra were also taken in near-nadir, mostly sunlit viewing geometries. In addition, in-band radiance profiles were measured using filtered radiometers (in focal planes 1 and 2) for eight wavelength bandpasses.

The CIRRIS-1A-SAMM database contains approximately 70 1-cm^{-1}-resolution spectra and 70 radiometer profiles measured by the CIRRIS experiment for non-auroral atmospheric conditions. The SAMM calculations used to compare with these data are based on 24 model atmospheres, corresponding to eight geographic locations along the shuttle orbit and three levels of geomagnetic activity. The calculations properly account for the CIRRIS-1A instrument wavelength response, resolution, and field of view. The CIRRIS-1A data were evaluated for near-field contamination and other experimental artifacts. The agreement between the calculated and observed data is found to be generally good, typically within a factor of two for in-band radiances. The discrepancies are due mainly to the assumed profiles of temperature and certain minor species and to the current lack of mechanisms in SAMM for the quiescent daytime chemiluminescence from NO high-v,J states and from NO$^+$, which are important, new emission process discovered in the CIRRIS-1A data.

3

This section discusses the overall methodology and key results of the study. A more detailed presentation of the results, including basic technical documentation on the database files and software, and complete sets of radiometric and spectral comparison plots are contained in a technical report by [Adler-Golden et al. 1994]. The CIRRIS-1A-SAMM database is available from the Air Force Research Laboratory (AFRL/VS). It is planned that the database will be incorporated into the BMDO Strategic Scene Generation Model (SSGM) as well as the AFRL/VS integrated optical background code PLEXUS.

2.1 SAMM Calculations

2.1.1 Code Overview

SSI and AFRL developed the SAMM code [Sharma et al., 1996] for self-consistently calculating atmospheric radiance and transmittance from 0 to 300 km for the 2 to 40 μm spectral range. The code smoothly integrates the high-altitude, non-LTE SHARC [Sundberg et al., 1995] algorithms with the MODTRAN [Berk et al., 1998] model for lower altitudes. SAMM includes a first-principles vibrational non-LTE calculation above 30 km, auroral and terminator phenomenologies with multiple atmospheric regions, aerosol, cloud, and rain models, single and multiple scattering, and 1 cm^{-1} spectral binning for an effective resolution of about 2 cm^{-1}. The input model atmosphere profile is selected by the user. The spectra and radiance profiles in the CIRRIS-SAMM data base were calculated using a pre-released Version of SAMM.

2.1.2 Inputs

For the CIRRIS-SAMM database, SAMM calculations were performed using model atmosphere profiles generated using the December 1993 version of the SHARC/SAMM Atmosphere Generator (SAG) [Adler-Golden, 1993]. SAG incorporates the NASA MSISE-90 empirical model [Hedin, 1991] for temperature and major species, AFGL [Anderson et al., 1986] and NRL [Summers, 1993] climatology databases for minor species, and additional photochemical and empirical models for CO_2, H_2O, odd oxygen, and NO. The atmosphere profiles are a function of the local time, latitude, Julian day, solar flux indices F10.7 and F10.7A, and the geomagnetic activity index Ap. The solar zenith angle is a function of the local time and latitude and is input separately to SAMM.

4

To span the range of conditions covered during the CIRRIS flight, SAG and SAMM were run for eight geographic conditions and three Ap values, for a total of 24 model atmospheres. The geographic conditions were selected to evenly sample the latitudes and solar zenith angles along the vehicle orbit (see Figure 1). For each atmosphere, the line of sight (LOS) spectral radiances from 200 cm^{-1} to 5000 cm^{-1} (2 to 50 μm) were calculated for 38 tangent views between -10 km and 240 km and two downward views (0° and 30° to the nadir) using the same observer location and LOS azimuth angle. Table 1 lists the SAMM input variables pertaining to the geographic conditions and the LOS geometries at a tangent height of 100 km. These are based on actual CIRRIS viewing conditions during Blocks 12A and 16. Table 2 lists additional input parameters required for SAG and SAMM. Initial SAMM calculations showed that using the Mie phase function for aerosol scattering gives an artificial discontinuity in the radiance profile at 30 km, due to the transition in MODTRAN between the stratospheric and thermospheric aerosol models. For subsequent calculations the Henyey-Greenstein phase function with the default asymmetry parameter value of 0.9 was used, and these results are presented in the database.
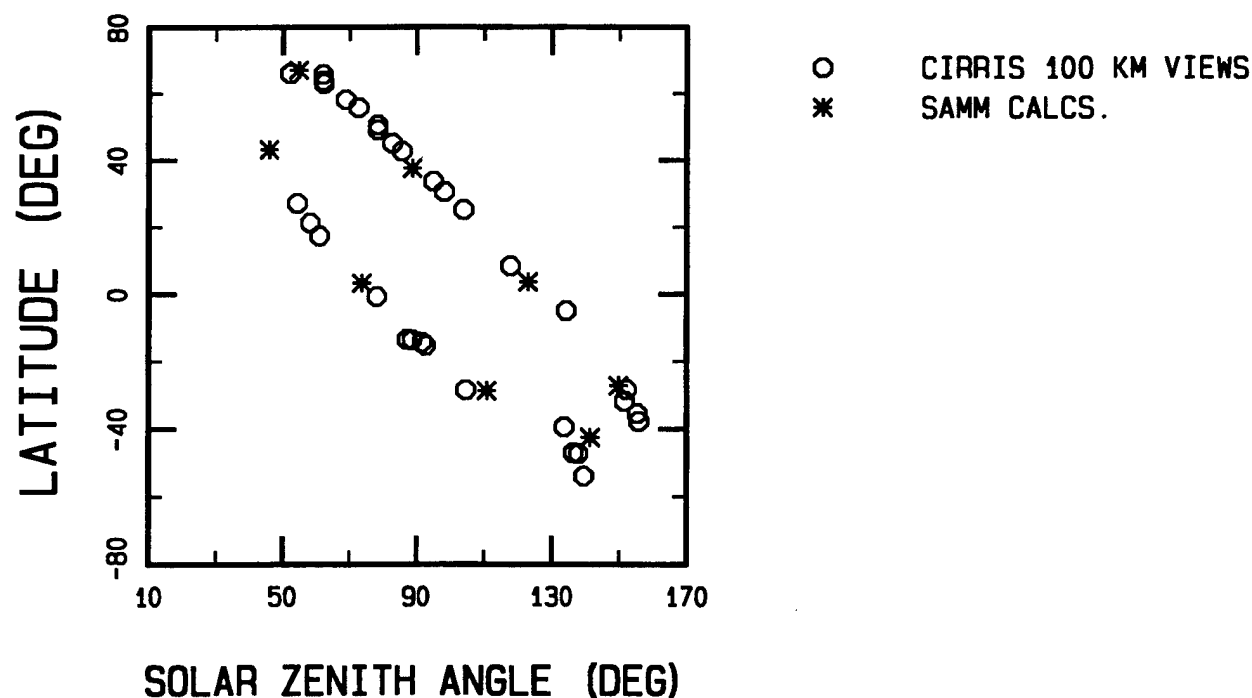
Figure 1. CIRRIS Viewing Geometries at 100 km Tangent Height During Non-Auroral Data Blocks

5

Table 1. Geographic and LOS Geometry Inputs for SAMM Calculations (Tangent Height = 100 km)

Atmosphere Description	Local Time (hr)	Tangent Pt SZA (deg)	Observer[a]			Tangent PT		Sun
			Lat (deg)	Long (deg)	LOS Az (deg)	Lat (deg)	Long (deg)	GMT (hr)
MidLat Night	1.92	149.9	-32.3	30.7	-66.6	-26.6	17.7	0.66
LowLat Night	3.59	122.9	5.0	55.1	-94.9	3.8	42.5	0.85
MidLat Day	5.31	88.7	40.2	82.1	-94.7	38.0	66.1	1.03
HighLat Day	10.37	54.7	56.2	151.6	-25.9	66.9	137.5	1.23
MidLat Day	14.78	45.9	32.4	40.0	14.7	44.5	44.4	11.86
LowLat Day	16.88	73.6	-5.2	246.6	30.7	5.7	253.0	0.11
MidLat Night	19.03	110.8	-40.6	274.0	28.2	-29.2	280.8	0.29
HighLat Night	21.90	141.6	-57.1	326.9	-15.0	-44.9	322.4	0.45
[a] at 260 km altitude								

Table 2. Additional Inputs for SAMM and SAG

Parameter	Value
Ap	18 (Low), 42 (Mean), 80 (High)
Julian day	119
F10.7	158
F10.7A	221
Aerosol model	Maritime
Scattering phase function	Henyey-Greenstein, g=0.9

2.1.3 Outputs

Each SAMM run for a given atmosphere generates a file containing the spectral radiance versus wavenumber for each LOS specified in the input list. For comparison with the CIRRIS data, the SAMM output spectra were interpolated between tangent heights, integrated over the detector vertical footprint, and degraded in spectral resolution, as described in Subsection 2.5. The calculation of the in-band radiance profiles is also discussed below.

2.1.4 In-Band Radiance Computations

To compare with the CIRRIS radiometer data, in-band radiance profiles were computed by convolving each SAMM spectrum with the effective radiometer response functions, which were measured by Utah State University in collaboration with AFRL [Bingham, 1991]. The approximate wavelengths for 25% of peak response are listed in Table 3.

Table 3. CIRRIS-1A Radiometer Filter Bandpasses

Filter	Bandpass (μm)[a]	Major Radiators
0	8.5 - 18	$CO_2(v_2)$, $O_3(v_3)$
1	4.1 - 4.5	$CO_2(v_3)$, $CO(\Delta v=1)$, $NO^+(\Delta v=1)$
2	4.9 - 7.0	$NO(\Delta v=1)$, $H_2O(v_2)$
3	6.0 - 8.8	$H_2O(v_2)$, $O_3(v_1)$, $CH_4(v_4)$
FP 2	2.6 - 3.3	$OH(\Delta v=1)$, CO_2, aerosols
5	11.1 - 12.8	CO_2, $O_3(v_3)$, HNO_3
6	17.9 - 23	$H_2O(Rot)$
7	8.0 - 11.8	$O_3(v_3)$, CO_2
[a] 25% spectral response limits		

The detector response function for each bandpass is the product of a relative response function, normalized to a peak value of 1, and a scale factor. The detector responsivity values used in processing the raw data were determined from absolute calibrations with a blackbody source, assuming that the relative response functions were those of the filters alone. However, actual relative response functions were subsequently measured and found to be significantly different due to the non-uniform spectral response of the detectors. The scale factor, which serves to compensate for these differences, is the ratio of the integral of the blackbody-weighted filter response function to the integral of the equivalently weighted total response function. We performed approximate calculations of the scale factors, assuming a 300 K blackbody calibration source, and found them to agree to within 10-20% with results obtained from comparisons of radiometer and bandpass-integrated interferometer data taken simultaneously. Taking into account the likely uncertainties in the interferometer calibration and in the calculations, our best estimates for the scale factors are given in Table 4.

7

Table 4. Scale Factors for the CIRRIS-1A Radiometer Response Functions

Filter	Scale Factor	Uncertainty
0	1.1	30%
1	1.0	20%
2	1.3	20%
3	1.2	20%
FP 2	1.2	30%
5	1.1	20%
6	1.5	25%
7	1.0	20%

2.1.5 Spectral Radiance Computations

The comparisons of SAMM spectra with CIRRIS data for a specified field of view (FOV) take into account both the tangent height and the detector vertical footprint. CIRRIS spectra for tangent heights that lie between the pre-calculated values are logarithmically interpolated. The integration over the detector footprint, which on average is 16 km for the largest detector (number 3-2) in focal plane (FP) 3, is performed using a three-point average of interpolated spectra. Tests of this approach using an example of extreme altitude variation (a 2.5 km scale height, which occurs for O_3 and OH emissions in the lower thermosphere above 90 km) indicate a maximum error of 30%, which is comparable to the tangent height measurement uncertainty of about ± 1 km. Both the effect of the footprint size and the error in the computation decrease very rapidly as the scale height increases, and are typically less than 10%.

The CIRRIS interferometer spectra are 1.0-cm^{-1} resolution FWHM, output at approximately 0.5-cm^{-1} increments, whereas the SAMM calculated spectra are actually radiance sums for non-overlapping 1-cm^{-1}-wide bins. Thus, a quantitative comparison of the two data sets is possible only at a reduced spectral resolution. The CIRRIS and SAMM spectra were both degraded using the same resolution function. The resolution FWHM was chosen based on the desired final resolution, assuming that the resolution FWHM and the intrinsic 1-cm^{-1} resolution of the undegraded spectra add in quadrature, as would be the case for Gaussian resolution functions. For example, nominal 3-cm^{-1} resolution spectra were calculated using a resolution FWHM of $\sqrt{(3^2-1^2)} = 2.83$ cm^{-1}.

8

Several different resolution functions were tried, including square, triangular, Gaussian, and sech (=1/cosh) functions. Of these, the last two gave the smoothest line shapes. The spectral comparisons plots in the data base were calculated using the sech function.

Typically, a modest spectral degradation resulted in a very good match between the observed and calculated spectral shapes. An exception to this is when the spectrum consists of a series of evenly spaced lines, such as are found in the CO and NO bands. The depths of the valleys between the lines are sensitive to the valley widths, which in turn depend on the particular bins into which the lines fall. For certain line spacings, SAMM's relatively coarse binning can result in artificial oscillatory structure in the degraded spectrum, even at a resolution sufficient to wipe out the genuine line structure. The sech resolution function, which has less steep wings than a Gaussian, provides some reduction in this artificial structure and was therefore used for the final calculations. For the calculations in the database, the final FWHM ranged from 2.5 to 4 cm^{-1} and the degraded spectra were generated at 1-cm^{-1} intervals.

2.2 CIRRIS DATA

2.2.1 Radiometer Profiles

Files of a representative subset of CIRRIS radiometer profiles were generated using the OPUS software package developed by Boston College [Hegblom, 1991]. The data were selected on the basis of both quality and coverage of the full range of atmospheric conditions. Generally, all six FP 1 detectors and two of the three FP 2 detectors (2-1 and 2-3) were sampled. Only four of the FP 1 detectors (1-1, 1-2, 1-3, and 1-5) were sampled with filter 6, since the other two detectors, 1-4 and 1-6, showed much higher background contamination levels with that filter.

Many of the profiles used in the database comparisons were obtained from the "staircase" scanning modes which feature rapid vertical jumps in between constant-altitude stares. Therefore, frequent sampling of the radiometers was required for the in-between altitudes. This resulted in very large data files, typically 2 Mb each. To keep the total database manageable while maintaining the overall integrity of the data, an altitude-dependent algorithm was implemented for thinning the number of data points in each scan. The data were placed in 1-km bins and every $\sqrt{N}$-th point was retained, where N is the number of points in the bin. In addition, data falling below a minimum

9

radiance threshold (in the 10^{-9} W/cm^2/sr range) were eliminated, since these data are potentially affected by near-field shuttle contamination or off-axis telescope leakage.

2.2.2 Spectra

Using OPUS, files of spectral radiance versus wavenumber were generated from measurements taken with an individual FP 3 detector during a full-length interferometer scan at a constant tangent height or angle to the nadir. The FWHM resolution of the full-length scans is 1.0 cm^{-1} with Kaiser-Bessel apodization (α=2). The corresponding spectral noise files were also compiled, and were used to flag spectral regions of poor signal-to-noise for exclusion from the plotting routine. The noise level is calculated by OPUS from signal fluctuations in the uncalibrated spectrum at wavelengths where the detectivity is negligible.

Representative CIRRIS-1A data were selected primarily from the "staircase" altitude-scanning modes of data blocks PC12A and PC12B, which sampled the atmospheric radiance in approximately 12-km tangent height steps during mid-latitude nighttime and high-latitude daytime conditions. Different staircase scans used different bandpass filters in order to isolate a particular spectral region from much stronger interfering emissions, such as from CO_2 (v_2) and O_3 (v_3), that can generate photon noise and harmonic distortion components. The approximate filter bandpasses are listed in Table 5. For a given staircase scan, a spectrum was selected every 1 or 2 altitude steps or, equivalently, about every 12 to 24 km. Typically, the data from the largest and most sensitive detector, 3-2, were chosen. When detector 3-2 was saturated or when a smaller vertical footprint was desired, data taken by one of the smaller, less-sensitive detectors (3-3 to 3-5) were used. The vertical footprint, which is tangent height-dependent, is about 13 to 18 km for detector 3-2 and about 2 to 3 km for detectors 3-3, 3-4, and 3-5. The downward-looking measurements were performed in a horizontal stare mode during block PC51; a few representative spectra from detector 3-2 were chosen to include nadir views in the database.

Table 5. Nominal CIRRIS-1A Interferometer Bandpasses

Filter No.	Bandpass (μm)	Major Radiators
0	All (no filter)	$CO_2(v_2)$, $O_3(v_3)$
1	< 4.9	$CO_2(v_3)$, $CO(\Delta v=1)$, O_3
2	< 3.7	$OH(\Delta v=1)$, CO_2, aerosols
3	4.8 - 13	$H_2O(v_2)$, $O_3(v_1)$, $NO(\Delta v=1)$
5	11 - 13	O_3, OH(Rot), CO_2
6	> 17	H_2O(Rot)
7	8 - 13	O_3, OH(Rot), CO_2

2.3 RESULTS AND DISCUSSION

2.3.1 Day and Night Comparisons

The CIRRIS-1A-SAMM database of in-band radiance profiles and spectra provides the first comprehensive and systematic comparisons of real-world upper atmospheric IR background data with code calculations for a wide range of molecular bands and geographic and atmospheric conditions. This is significant because the database provides the basis for assessing and enhancing the predictive capabilities of atmospheric radiance and transmission codes required by systems engineers to optimize system design and operability. The major results of the in-band radiance profiles and spectra comparisons, particularly absolute radiance comparisons, are summarized below according to wavelength region.

Radiance profile and altitude dependent spectral plots comparing CIRRIS data with SAMM were generated using the SAG model atmospheres "m01" (1.92 hrs local time, mean Ap, 27° S latitude) and "m10" (10.37 hrs local time, mean Ap, 67°N latitude), which are described in detail in Tables 1 and 2. The major uncertainties in the radiometer data are 20-30% in the absolute radiances, reflecting the instrument calibrations, and ~2 km in the tangent height determinations. To avoid plotting very noisy spectral data, the spectral noise file from OPUS was compared with the radiance file, and when the RMS signal-to-noise ratio was less than a pre-defined value (in this case, 4), the data were replaced with a non-plottable (negative) number.

<u>Longer than 17 μm (below 600 cm^{-1})</u> The main source of emission at wavelengths longer than 17 μm is pure rotation transitions of H_2O. Representative night and day radiance profiles are shown in Figures 2 and 3, respectively. The measured and calculated in-band radiance profiles (filter 6) agree to within a factor of two or better up to 80 km. Below about 60 km the emission is very optically thick and thus fairly insensitive to the H_2O concentration. Above 80 km, a quantitative comparison is more difficult due to the rapid falloff in atmospheric radiance and the presence of near-field contamination from H_2O outgassing from the shuttle [Zhou *et al.*, 1993].

<u>13-17 μm (600-800 cm^{-1})</u> Radiation in the 13-17 μm spectral region dominates the 1-20 μm IR region at most altitudes and originates from several CO_2 v_2-type bands. Over most of the altitude range from 0 to 240 km, the agreement between the radiance measurements and calculations is good (see Figures 4-6), and the systematics of the observed variations in the radiometer data (filter 0) near 140 km are reasonably well reproduced by the calculations [Wise *et al.*, 1993]. However, near the mesopause (80-100 km) there is typically more fine structure in the radiance profile than is calculated. While the structure is quite variable, often there is a narrow layer of enhanced radiance near 85 km, especially between midnight and dawn in the southern hemisphere, as shown in Figures 4-6. This shows up in spectra from the smaller focal plane 3 detectors as well as in the radiometer profiles, but not in the spectra from the large detector 3-2. Since the CO_2 bands are at or near thermal equilibrium and the mixing ratio is well known at 85 km, vertical structure in the temperature profile which is not modeled by SAMM/SAG is the best explanation for the observed radiance layering. This would be consistent with recent LIDAR data [Chanin, 1992] that often show a "double mesopause"-shaped temperature profile that is considerably different from the MSIS model profiles used by SAG.

The spectral features of $CO_2(v_2)$ under daytime conditions are illustrated in Figures 7 and 8 for tangent altitudes of 13 km and 59 km, respectively, while Figures 9 and 10 show $CO_2(v_2)$ at night for tangent altitudes of 13 and 67 km, respectively. Again, the agreement between the CIRRIS-1A data and SAMM is quite remarkable.

Figure 2. Comparisons of the Nighttime CIRRIS-1A Radiance Profile in the 18-23 μm Bandpass with SAMM Calculations at a Latitude of -43°

Figure 3. Comparisons of the Daytime CIRRIS-1A Radiance Profile in the 18-23 μm Bandpass with SAMM Calculations at a Latitude of 65°

Figure 4. Comparisons of the Nighttime CIRRIS-1A Radiance Profile in the 8-18 μm Bandpass with SAMM Calculations at a Latitude of -29°

Figure 5. Comparisons of the Terminator CIRRIS-1A Radiance Profile in the 8-18 μm Bandpass with SAMM Calculations at a Latitude of 10°

14

Figure 6. Comparisons of the Daytime CIRRIS-1A Radiance Profile in the 8-18 μm Bandpass with SAMM Calculations at a Latitude of 28°

Figure 7. Daytime Comparisons of CIRRIS-1A Data in the 8-25 μm Spectral Region with SAMM Calculations at a Tangent Height of 13 km and a Latitude of 63°

Figure 8. Daytime Comparisons of CIRRIS-1A Data in the 8-25 μm Spectral Region with SAMM Calculations at a Tangent Height of 59 km and a Latitude of 65°

Figure 9. Nighttime Comparisons of CIRRIS-1A Data in the 8-25 μm Spectral Region with SAMM Calculations at a Tangent Height of 13 km and a Latitude of -42°

Figure 10. Nighttime Comparisons of CIRRIS-1A Data in the 8-25 μm Spectral Region with SAMM Calculations at a Tangent Height of 67 km and a Latitude of -43°

11-13 μm (800-900 cm⁻¹) In the 11 - 13 μm atmospheric window region, the major upper atmospheric emissions are from O_3 hot bands and solar-pumped CO_2 laser bands. Chemiluminescent emissions from OH rotation lines [Smith et al., 1992; Dodd et al., 1994] which are not currently modeled by SAMM, have also been observed by the CIRRIS-1A experiment in the mesopause region, primarily at night. The O_3 hot band intensities tend to be overpredicted by SAMM, especially near 800 cm⁻¹; this is primarily due to uncertainties in the spectroscopy and kinetics of high vibrational states of O_3. Nevertheless, the in-band radiance profiles calculated using SAMM for filter 5 are typically within a factor of two of the CIRRIS radiometer data at most altitudes, as shown in Figures 11 and 12. In the lower mesosphere, the largest differences occur during the daytime (see Figure 12)

Below about 30 km tangent height, the CIRRIS spectra show emission bands near 880 cm⁻¹ due to HNO_3 and near 850 cm⁻¹ due to CFC-11 [Bingham et al., 1993], see Figures 7-10. The HNO_3 band is prominent in the calculated spectra up to about 40 km but only up to about 30 km in the CIRRIS data. CFC's are not modeled currently by the SAMM code but have recently been added to MODTRAN.

17

Figure 11. Comparisons of the Nighttime CIRRIS-1A Radiance Profile in the 11-13 μm Bandpass with SAMM Calculations at a Latitude of -39°

Figure 12. Comparisons of the Daytime CIRRIS-1A Radiance Profile in the 11-13 μm Bandpass with SAMM Calculations at a Latitude of 68°

18

8-11 μm (900-1200 cm^{-1}) The major emissions in the 8-11 μm wavelength region are from the O_3 v_1 and v_3 fundamental modes and solar-pumped CO_2 bands. Representative radiance profiles at day and night are shown in Figures 13 and 14. Spectral features are again illustrated in Figures 7-10. As seen in the filter 7 radiometer data, near 80 km the SAMM code consistently overpredicts the ozone emission by about a factor of two, which is likely due to an overestimation of the O_3 concentration by SAG. At other altitudes, the average agreement is good, and the diurnal variability is realistically modeled by the calculations. Below 30 km tangent height, an emission band due to CFC-12 [Bingham *et al.*, 1993] can also be seen in the CIRRIS spectra near 920 cm^{-1}.

Figure 13. Comparisons of the Nighttime CIRRIS-1A Radiance Profile in the 8-12 μm Bandpass with SAMM Calculations at a Latitude of -29°

19

Figure 14. Comparisons of the Daytime CIRRIS-1A Radiance Profile in the 8-12 μm Bandpass with SAMM Calculations at a Latitude of 50°

5-8 μm (1200-2000 cm⁻¹) The major emitters between 5 and 8 μm are $H_2O(v_2)$, $CH_4(v_4)$ near 1311 cm⁻¹, and $NO(\Delta v=1)$. For the H_2O band, the measurement and model comparison is consistent with that of the rotation line emission. The spectral data comparisons also show that the methane emission is overpredicted in the upper mesosphere but predicted well at lower tangent heights. The source of the upper mesosphere discrepancy is under investigation and may be due to an error in a SAMM spectral parameter file that has since been corrected. In the mesopause region, the CIRRIS radiometer data for filters 2 and 3 typically show emission layers similar to those in the filter 0 data, which cover the 15 μm-region CO_2 bands. The presence of this feature is consistent with the explanation of temperature structure. Below the mesopause, the radiance profiles for filters 2 and 3 are dominated by $H_2O(v_2)$ (see Figures 15-18).

20

Figure 15. Comparisons of the Nighttime CIRRIS-1A Radiance Profile in the 5-7 μm Bandpass with SAMM Calculations at a Latitude of -28°

Figure 16. Comparisons of the Daytime CIRRIS-1A Radiance Profile in the 5-7 μm Bandpass with SAMM Calculations at a Latitude of 38°

Figure 17. Comparisons of the Nighttime CIRRIS-1A Radiance Profile in the 6-9 μm Bandpass with SAMM Calculations at a Latitude of -42°

Figure 18. Comparisons of the Daytime CIRRIS-1A Radiance Profile in the 6-9 μm Bandpass with SAMM Calculations at a Latitude of 64°

The 5-8 μm emission above the mesopause is dominated by NO(Δv=1), see Figures 15, 16, and 19. Both the measurements and calculations of the v=1 band emission vary by over an order of magnitude due mainly to the dependence of NO concentration on solar angle, latitude, and geomagnetic activity. Due to these atmospheric variations, the measurement and model agreement is erratic. The largest differences are found for the nighttime data, where there have been few measurements for the development of an empirical NO concentration model [Smith *et al.*, 1993] for use in SAG and other model atmosphere climatologies.
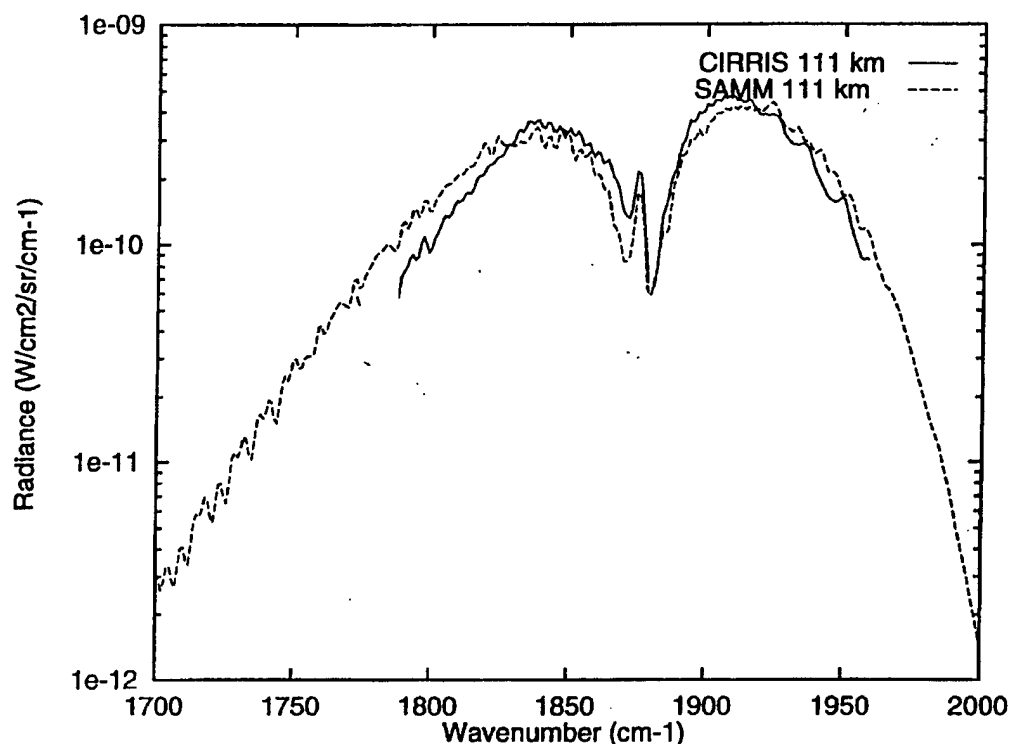
Figure 19. Nighttime Comparisons of CIRRIS-1A Data in the 5-6 μm Spectral Region with SAMM Calculations at a Tangent Height of 111 km and a Latitude of -44°

The daytime CIRRIS spectra show a contribution from high-v,J states of NO in the 1200-1700 cm^{-1} (6-8 μm) region [Armstrong *et al.*, 1993; *Smith and Ahmadjian*, 1993]. The source of this emission is believed to be primarily the reaction of fast N(^{4}S) atoms with O$_2$ [Duff *et al.*, 1994; *Sharma et al.*, 1998] and a model upgrade incorporating this mechanism is planned for AFRL radiance models.

<u>4-5 μm (2000-2500 cm^{-1})</u> The radiation in the 4-5 μm wavelength region is dominated by the CO_2 v_3-type bands, with smaller contributions from $CO(\Delta v=1)$ emissions and $NO^+(\Delta v=1)$ chemiluminescence at high altitudes during the day time [Winick *et al.*, 1992]. The in-band radiance profile (filter 1) and the CO_2 spectral radiance are modeled well by the SAMM Code for both nighttime (Figure 20) and daytime (Figure 21) conditions, typically to within better than a factor of two. Nighttime and Daytime spectral comparisons are shown in Figures 22 and 23 at 62 km and 59 km, respectively. The emission from NO^+ is not accounted for in these non-auroral SAMM calculations. Detailed analysis [Winick *et al.*, 1992] of the CIRRIS-1A data has made the first identification of non-auroral NO^+ emissions, which are an additional new source of radiation in the 4-5 μm spectral region for certain atmospheric conditions.
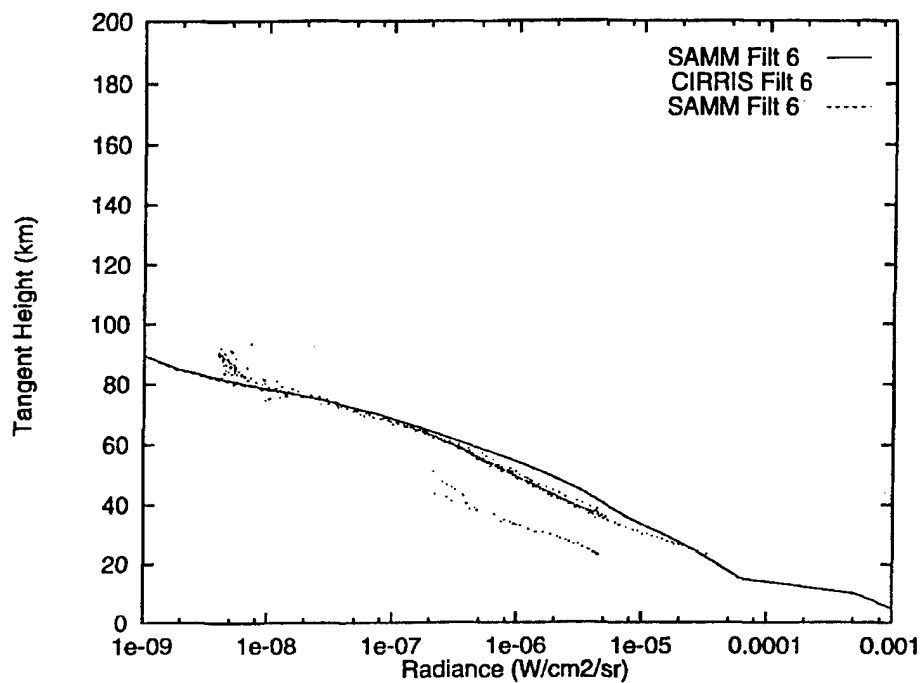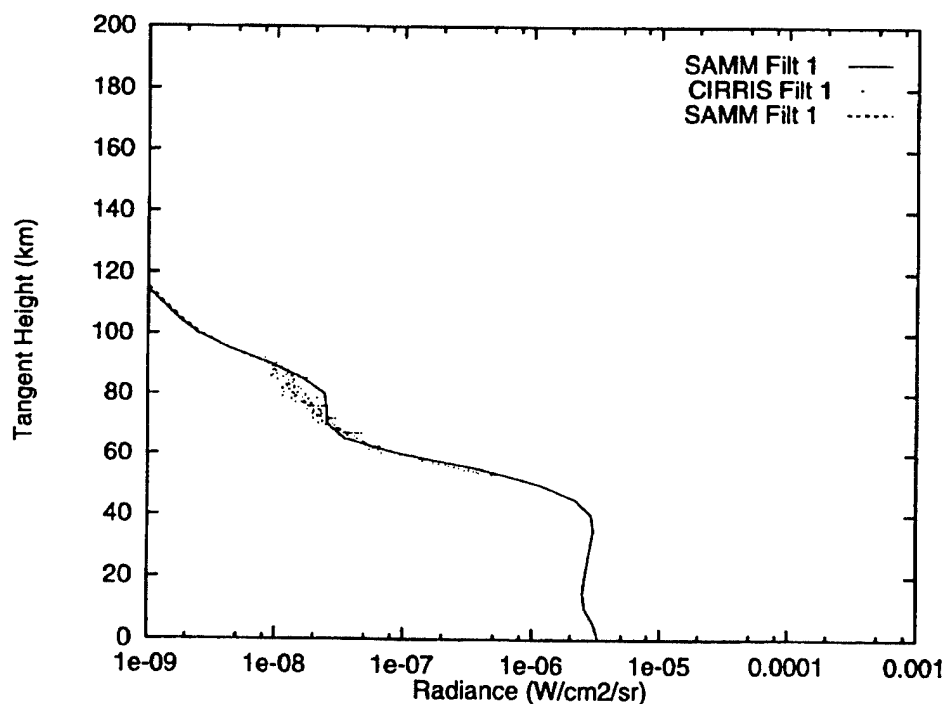

Figure 20. Comparisons of the Nighttime CIRRIS-1A Radiance Profile in the 4.1-4.5 μm Bandpass with SAMM Calculations at a Latitude of -13°
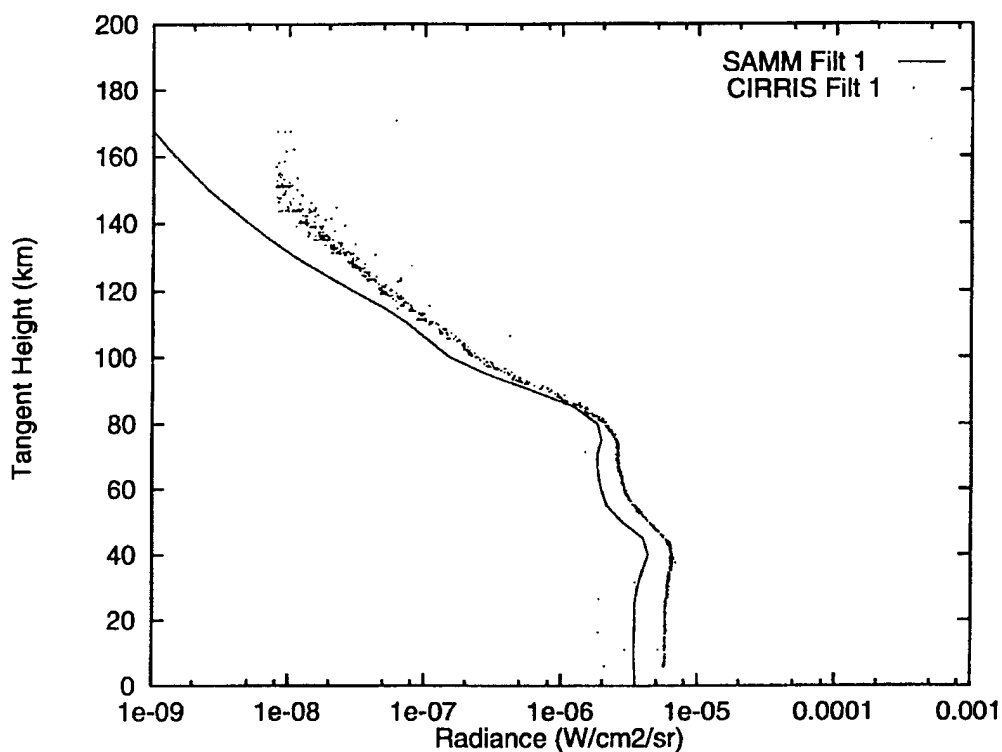
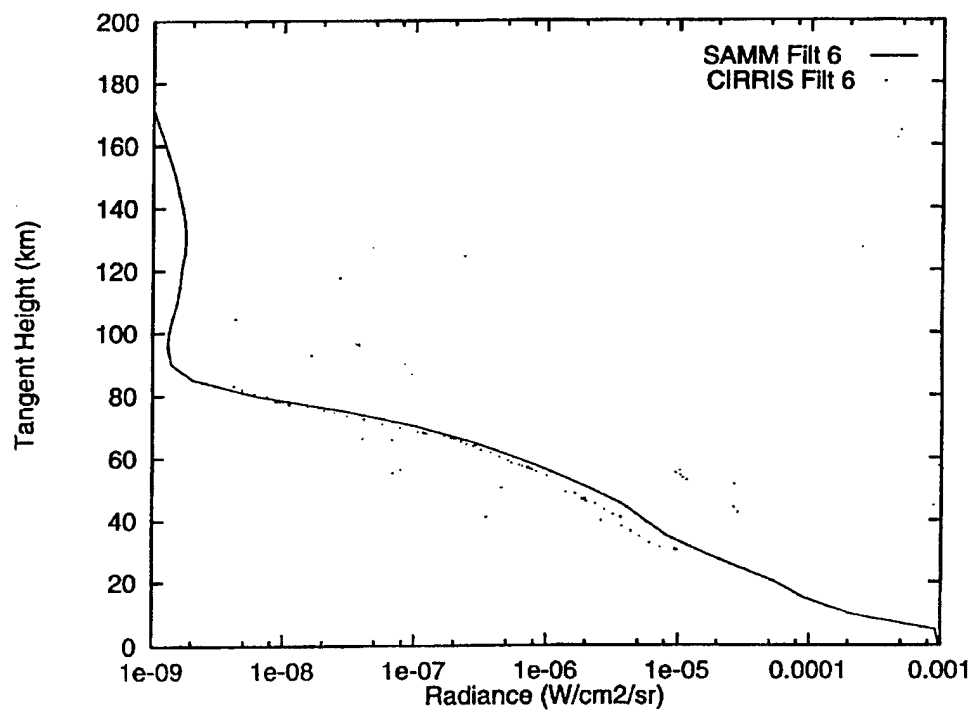**Figure 21. Comparisons of the Daytime CIRRIS-1A Radiance Profile in the 4.1-4.5 μm Bandpass with SAMM Calculations at a Latitude of 69°**
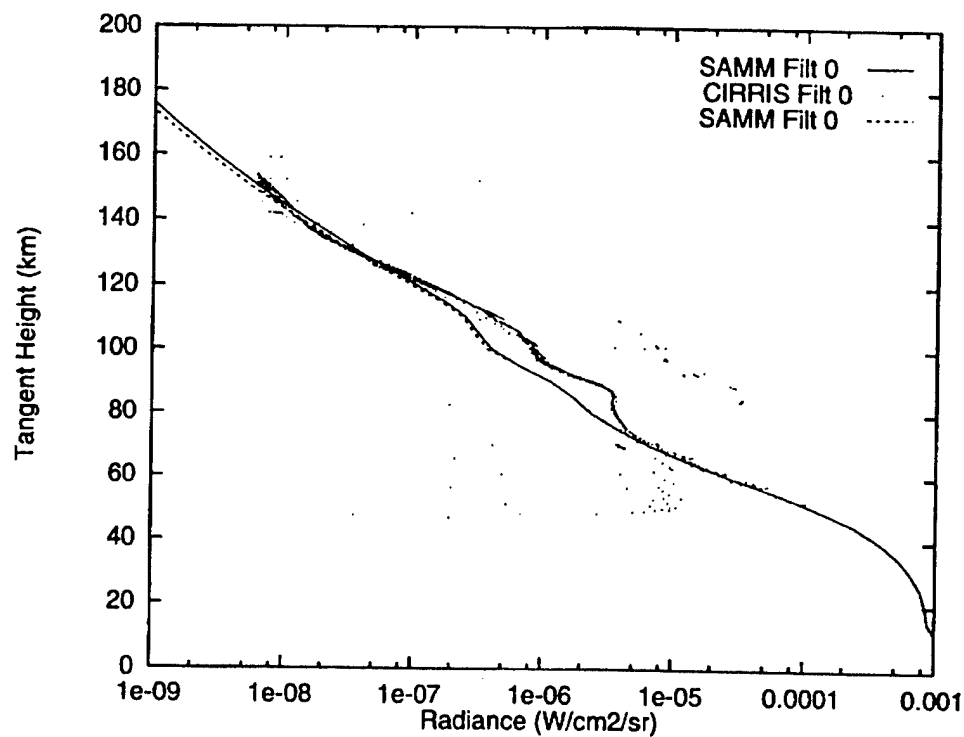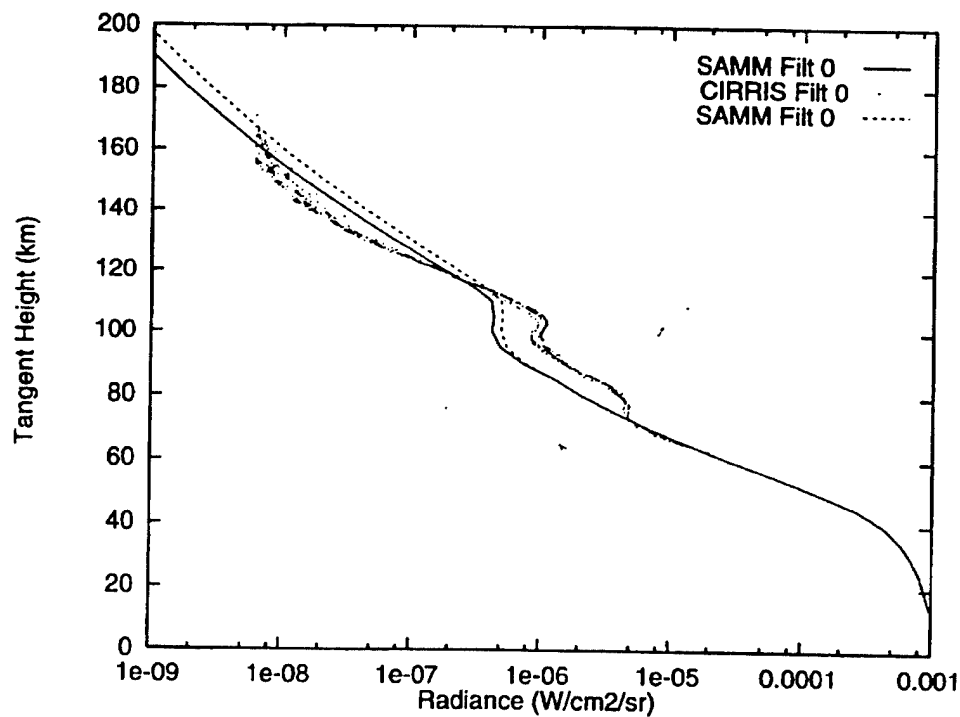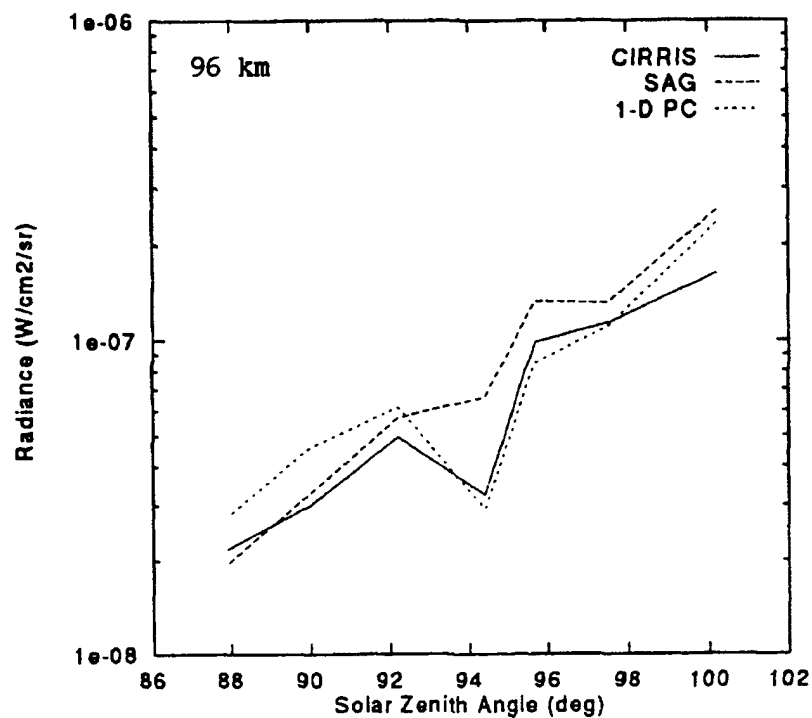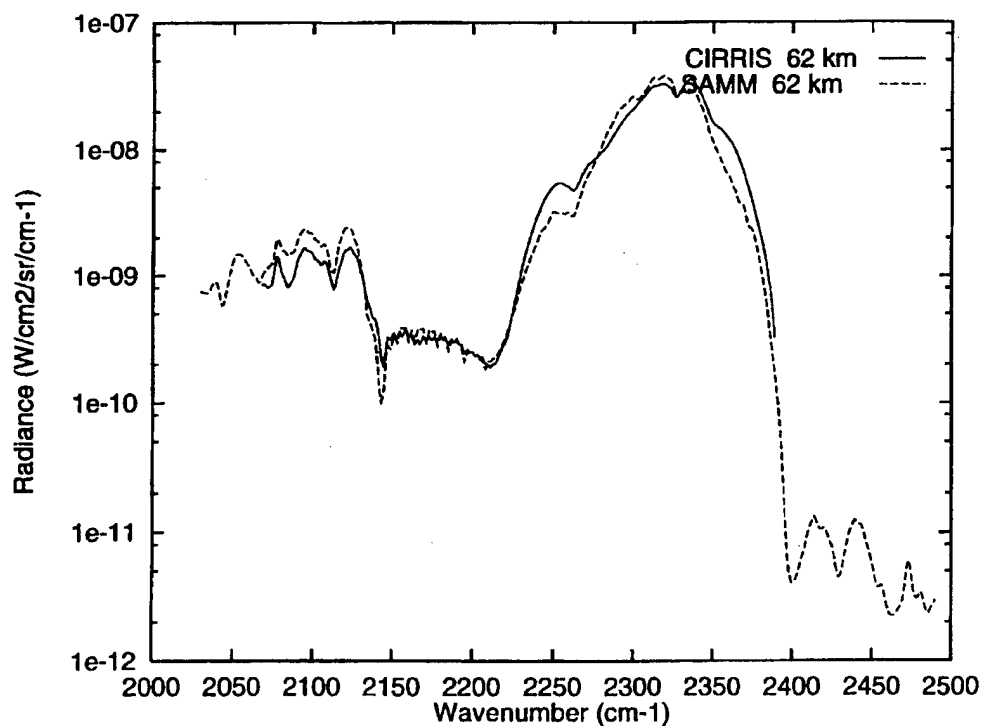

Figure 22. Daytime Comparisons of CIRRIS-1A Data in the 4-5 μm Spectral Region with SAMM Calculations at a Tangent Height of 62 km and a Latitude of 70°
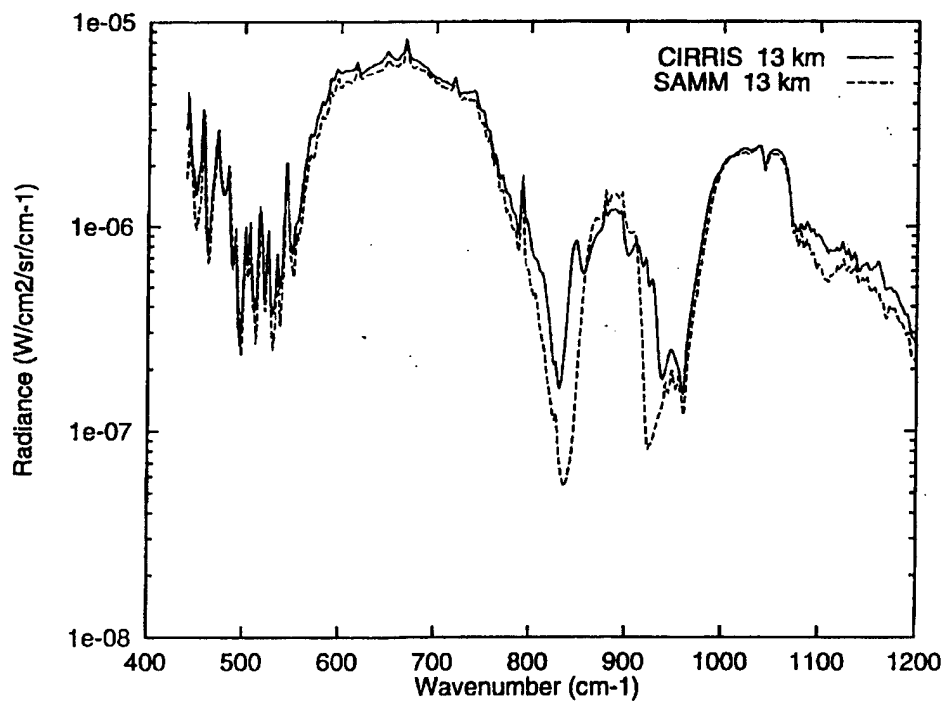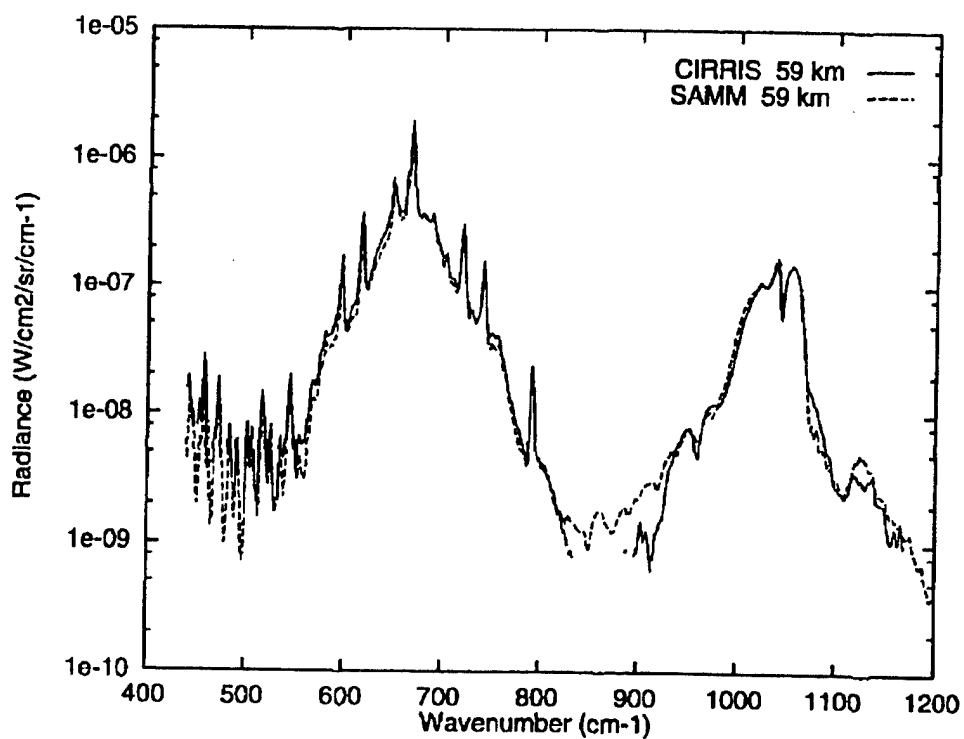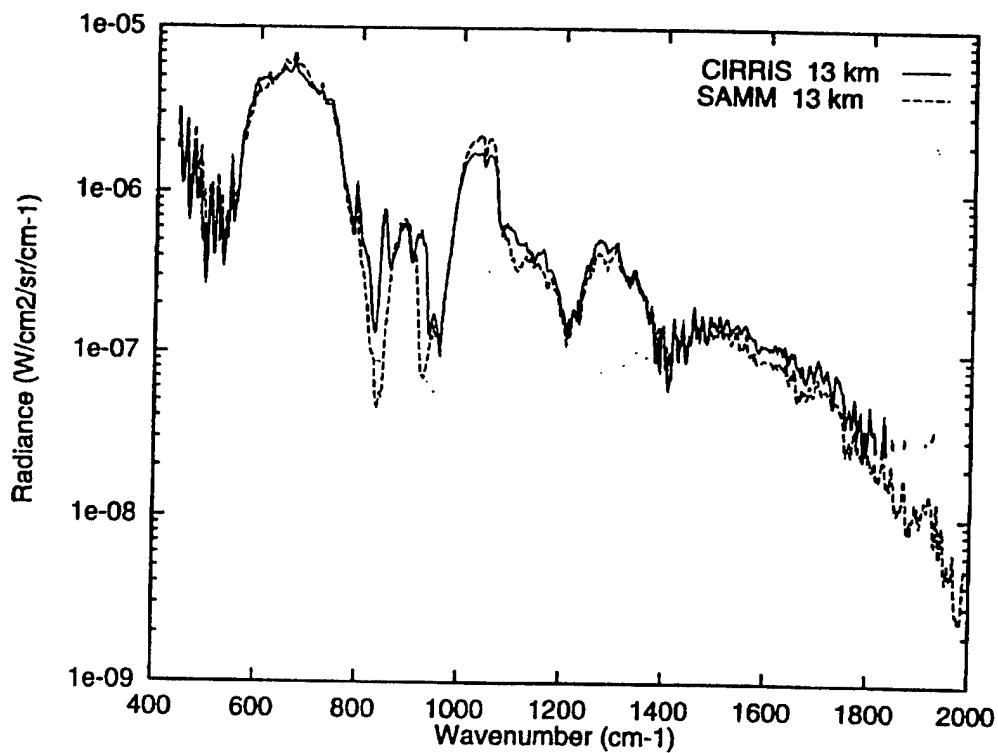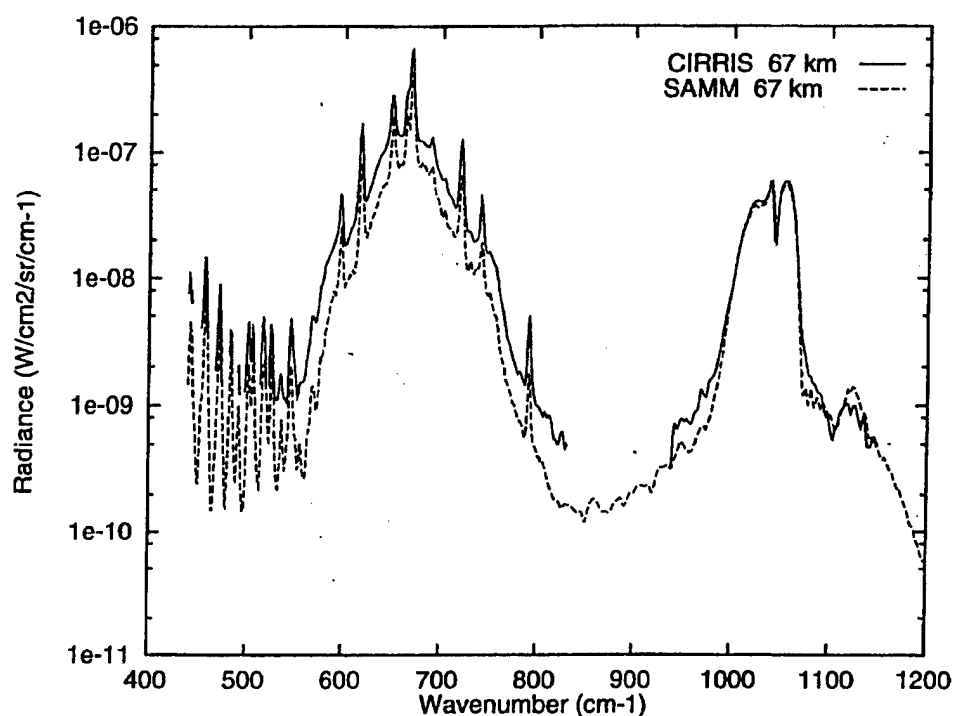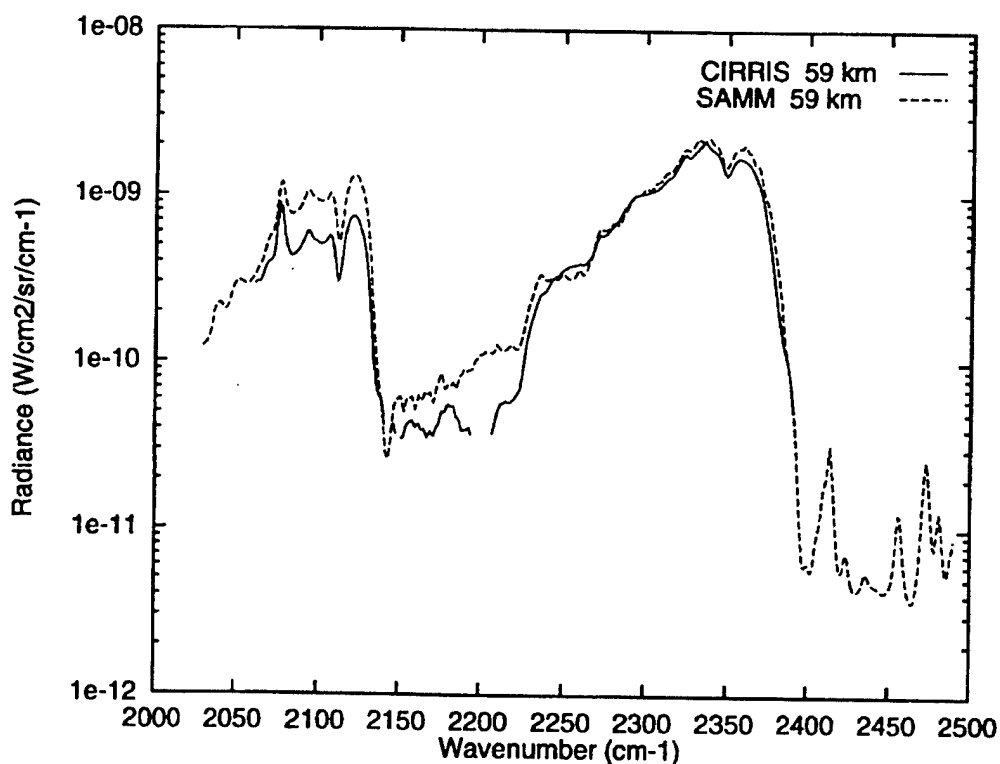
Figure 23. Nighttime Comparisons of CIRRIS-1A Data in the 8-25 μm Spectral Region with SAMM Calculations at a Tangent Height of 59 km and a Latitude of -40°

The downward-looking spectra, taken with interferometer filter 1, are dominated by $CO_2(v_3)$ emissions as well as blackbody emission and solar scattering from the earth's surface and from clouds. A considerable portion of the CO_2 emission is from above 30 km due to optical opacity effects and is characterized by a non-thermal vibrational state distribution. The total radiance level varies considerably from one CIRRIS scan to another. The major differences between the CIRRIS data and the SAMM calculations are likely due to uncertainties in the modeling of the earth surface temperature and the lack of cloud cover in the calculation.

Below 4 μm (above 2500 cm^{-1}) The radiometer data below 4 μm, from FP 2, contain contributions from solar-pumped CO_2 bands, the $\Delta v=1$ Meinel bands of OH, and, at the lowest altitudes, solar scattering from aerosols and/or clouds. The OH Meinel bands arise from the $H+O_3$ reaction and are a more prominent at night when the O_3 concentration is larger. At a 14 to 15 km tangent height, there is evidence of scattering from clouds, which are not modeled in these calculations, in the daytime CIRRIS spectra between 2600 and 2900 cm^{-1}. At higher wavenumbers, the spectra have

26

poor signal-to-noise, and only the strongest OH lines are identifiable. The limb radiance profiles (see Figures 24 and 25), which have good signal-to-noise, are generally modeled reasonably well by SAMM, although there is more variability in the data than predicted. Spectral data of higher S/N would be required to the separate the radiance contributions from each individual IR emitter.

2.3.2 Solar Terminator Comparisons

IR atmospheric background radiance varies substantially over the diurnal cycle. In many spectral regions, abrupt changes that can occur at the solar terminator (earth shadow edge) can seriously impact the performance of many sensing systems. These terminator radiance variations arise from several different phenomena. One is a photochemically-induced change in molecular number density caused by photochemical reactions. This occurs with both ozone (O_3), which is photolyzed at dawn and regenerated at dusk, and OH, which is formed from the reaction of O_3 with H atoms. O_3 emits strongly in the 8-12 μm region, and OH chemiluminescence is prominent around the mesopause at wavelengths below 3.7 μm. Another important source of terminator radiance variation is a change in the vibrational excitation of the molecule with solar illumination. This non-LTE effect occurs in a number of species including CO_2, and dramatically affects the 4.3 μm and 2.7 μm bands throughout the mesosphere and thermosphere. Data-model comparisons indicate that solar pumping of CO_2 is noticeable in the 4.3 μm region even in nadir views, which typically sense only the lower atmosphere.

Both the SHARC-3 and SAMM codes permit accurate modeling of limb radiance at the solar terminator. They allow the LOS to pass through multiple atmospheric regions, corresponding to different solar zenith angles (SZAs), in which complete, first-principles calculations of the non-LTE kinetics and radiation transport (including layer-layer radiative excitation effects) are performed. In a preliminary demonstration of terminator modeling capability [Adler-Golden and Matthew, 1993], SHARC-3 was used to model CO_2 4.3 μm data from the SPIRE rocket experiment as well as limited CIRRIS-1A dusk terminator data on O_3 in the 8-12 μm region and OH in the fundamental band region (below 3.7 μm). Good overall agreement was found.
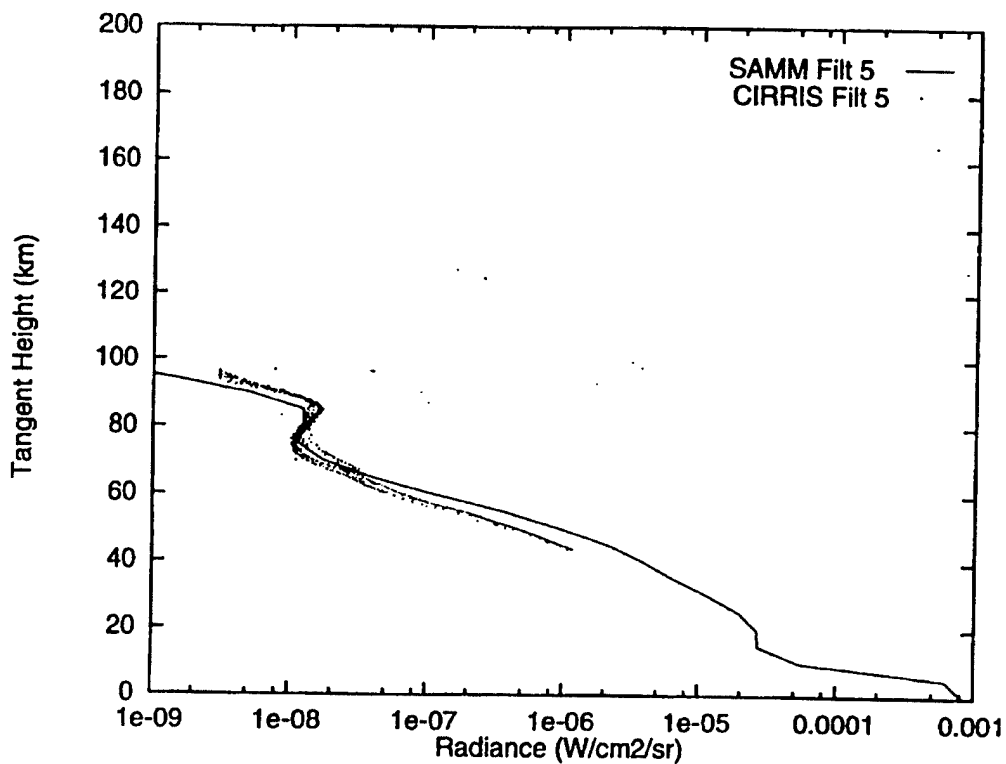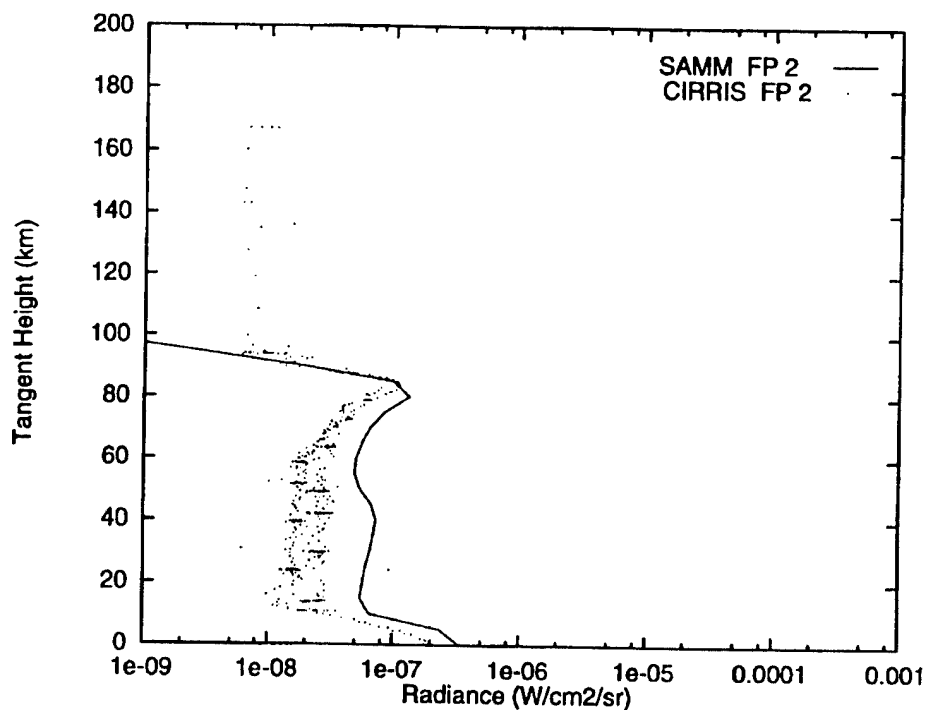
Figure 24. Comparisons of the Nighttime CIRRIS-1A Radiance Profile in the 2.6-3.3 μm Bandpass with SAMM Calculations at a Latitude of -36°
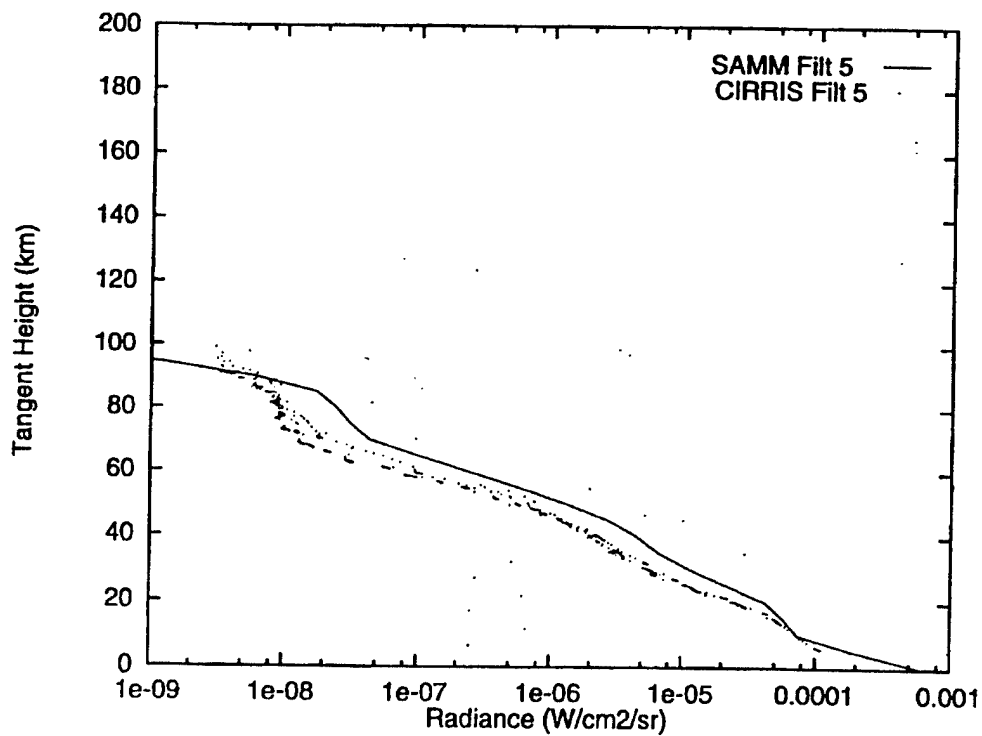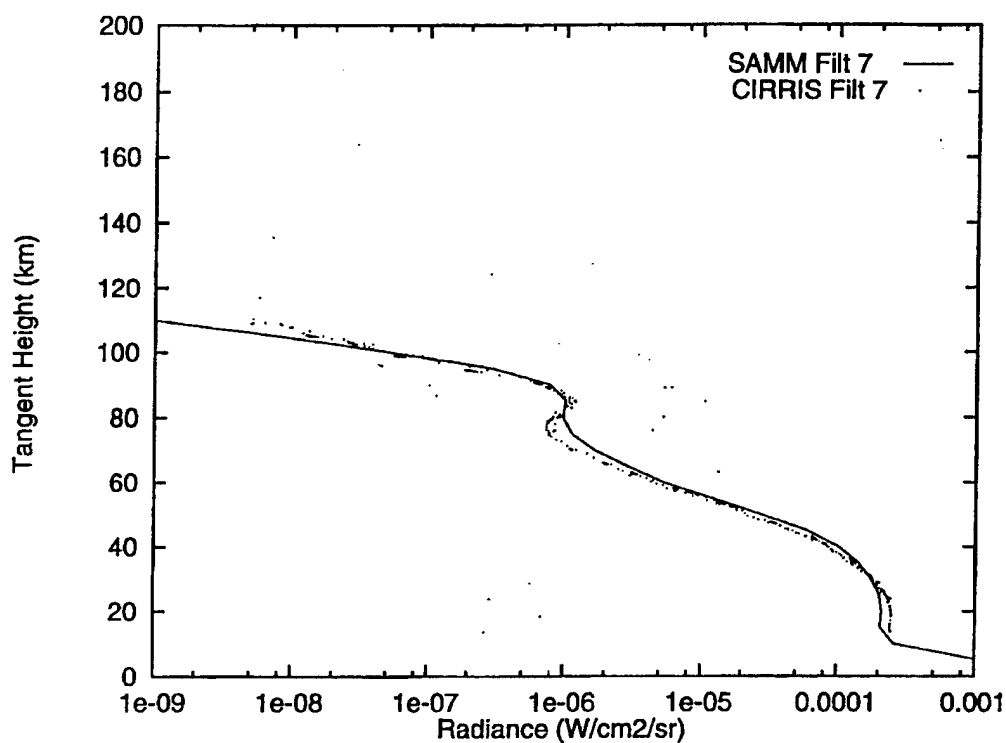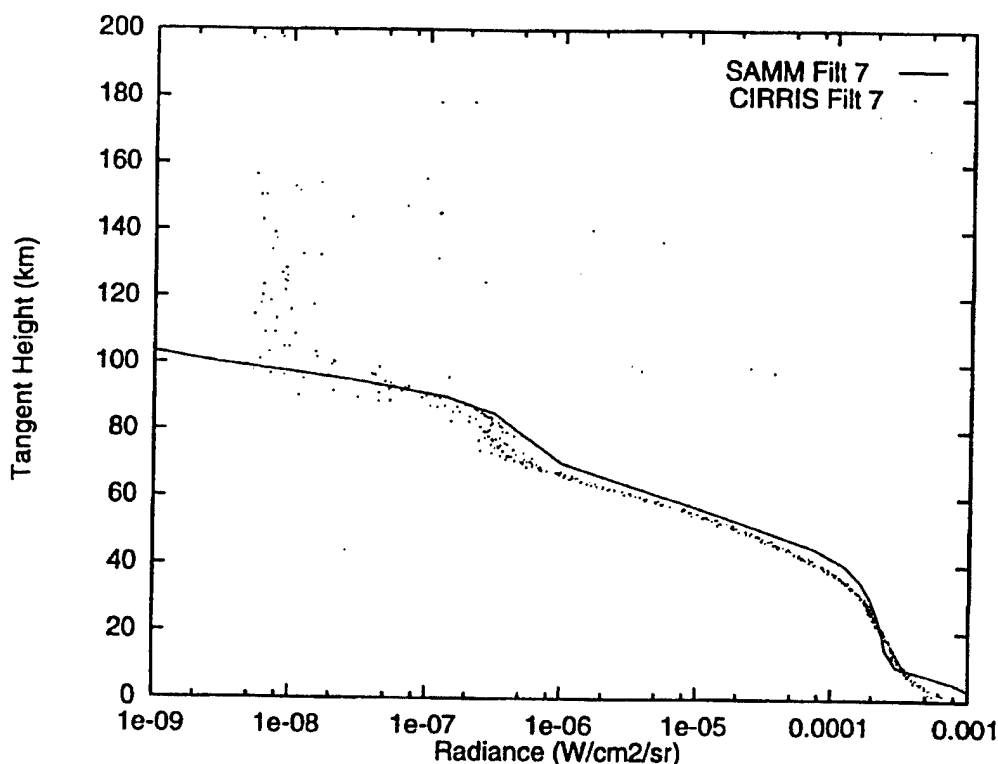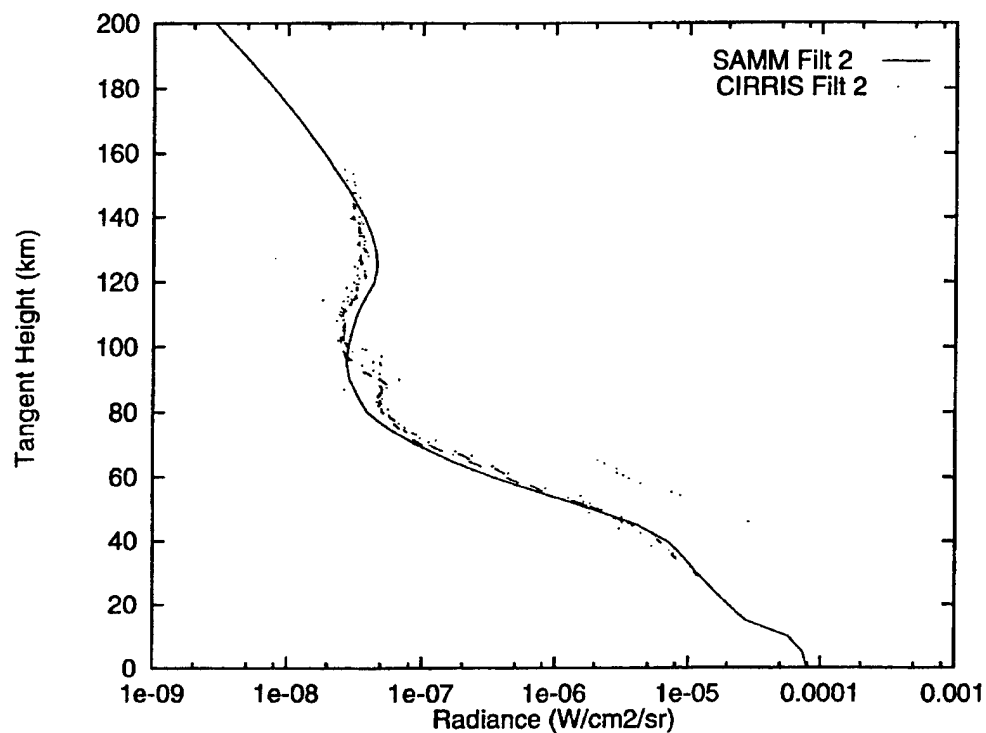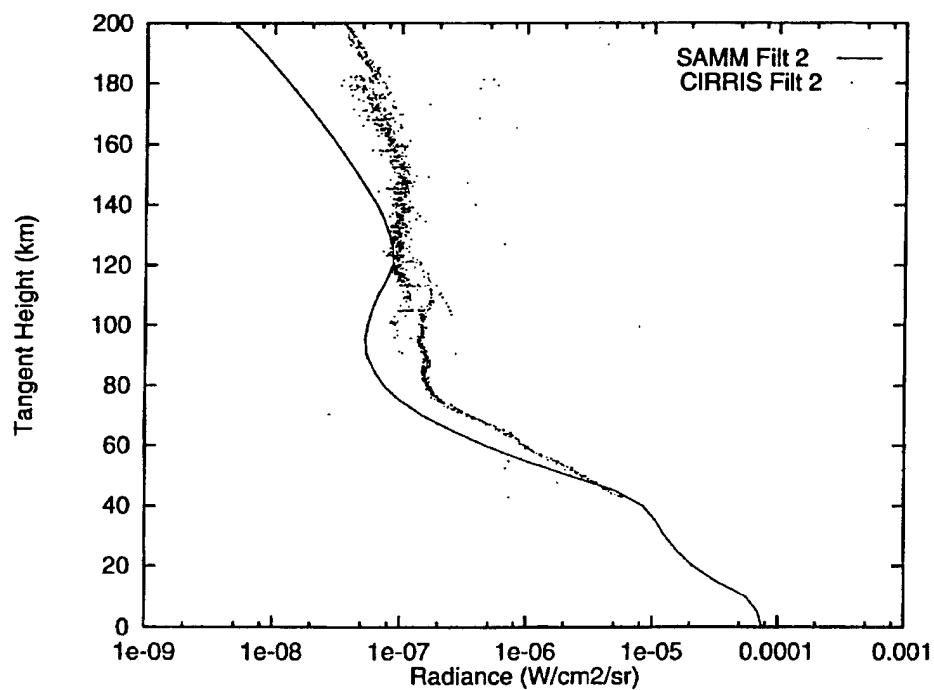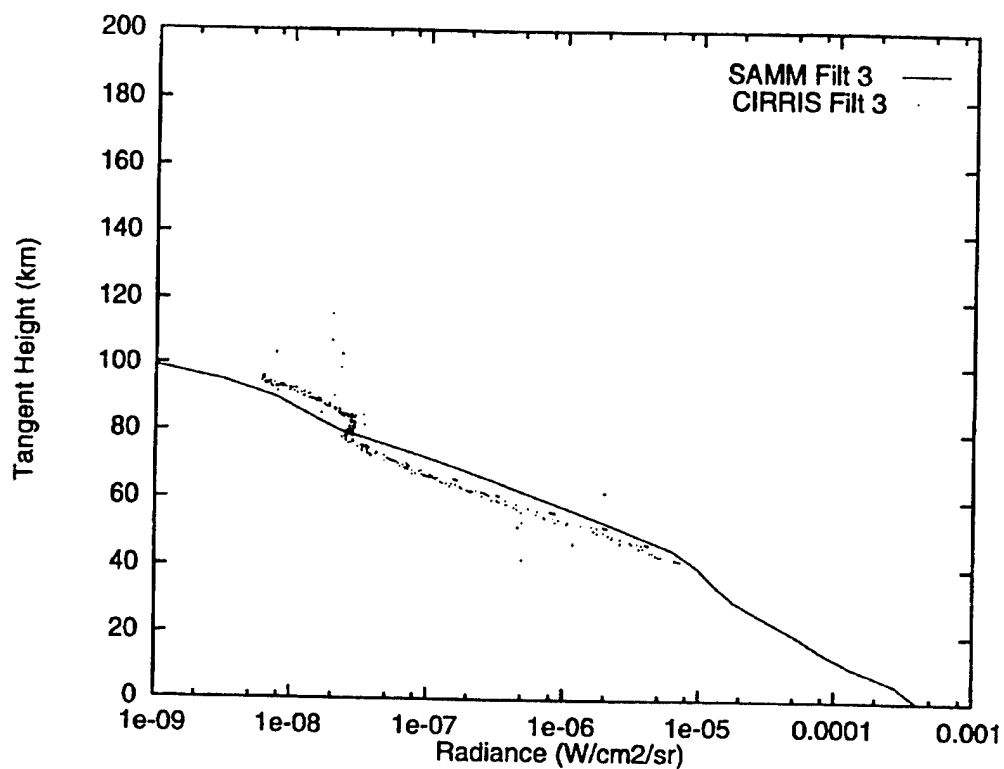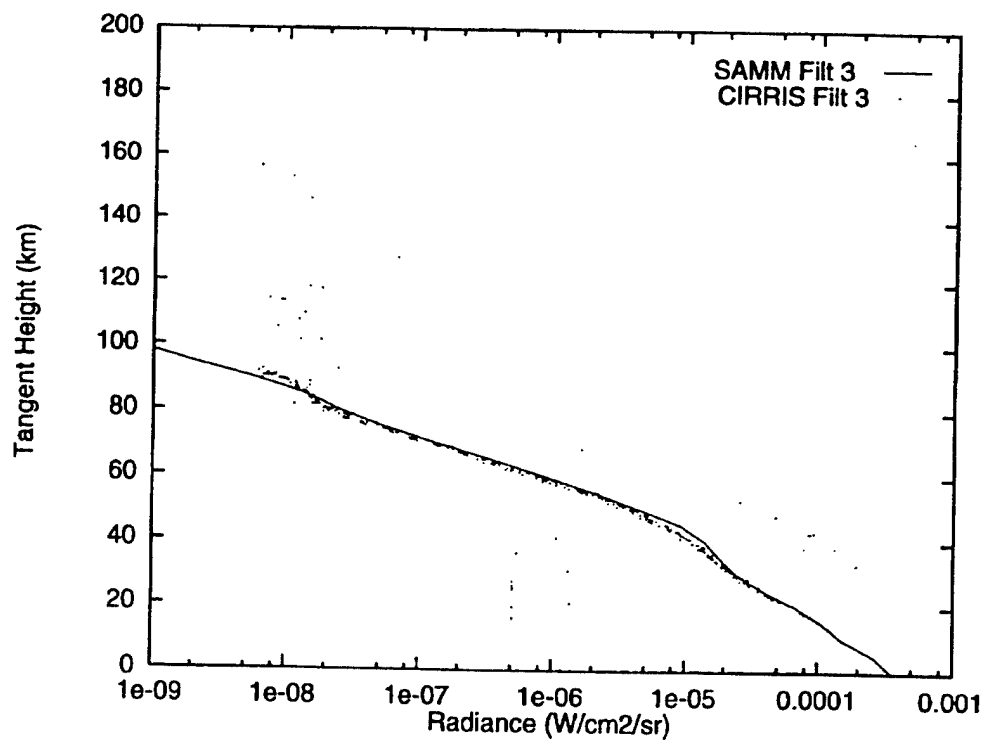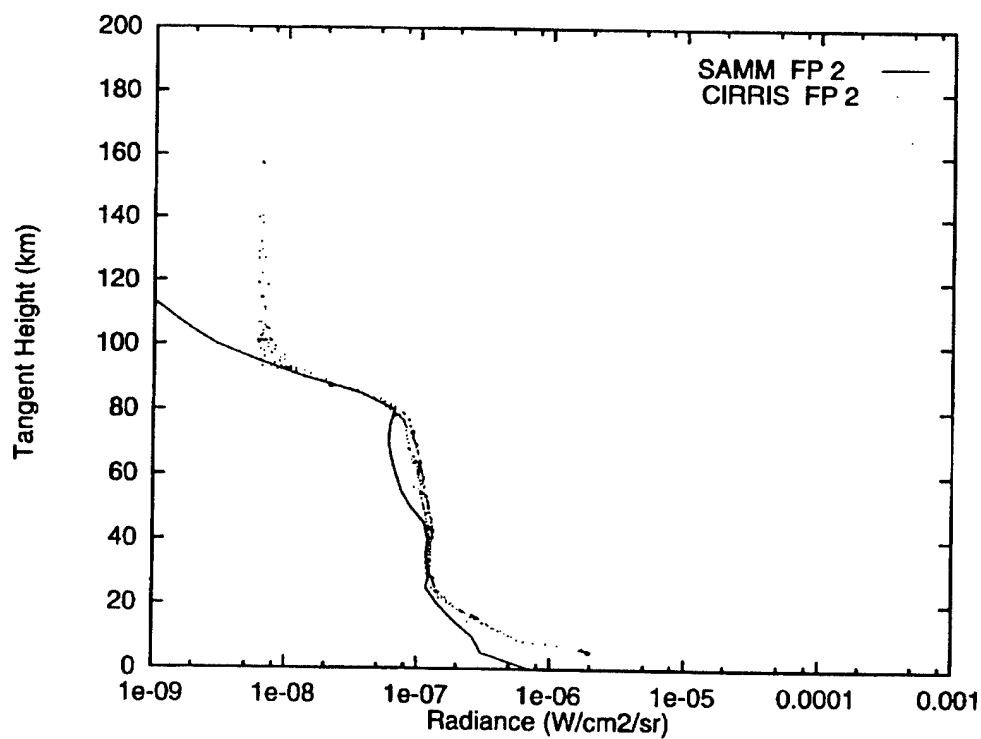

Figure 25. Comparisons of the Daytime CIRRIS-1A Radiance Profile in the 2.6-3.3 μm Bandpass with SAMM Calculations at a Latitude of 69°

The current investigation presents a more comprehensive set of terminator data-model radiance comparisons using results from the CIRRIS-1A experiment. Comparisons of representative CIRRIS-1A data with SAMM code predictions are presented for the altitude and wavelength ranges with the largest terminator variations and the greatest importance for sensing systems. The comparisons include in-band and/or spectral radiances for the 8-12 μm, $\lambda < 3.7$ μm, and 4.3 μm regions in the ~50-100 km altitude range.

The basic comparisons were performed using model atmospheres from the SHARC/SAMM atmosphere generator (SAG) as inputs to the SAMM code. In addition, for emissions from the odd-oxygen species O_3 and OH further SAMM calculations were performed using theoretical profiles from a one-dimensional photochemical model (1-D PC) [Makhlouf et al., 1994]. These profiles were found to yield better agreement with the CIRRIS data.

CIRRIS terminator data also exist for other spectral regions, including 5-7 μm and 18-23 μm. These data have been examined for solar excitation-related variations and are discussed briefly in Section 2.4.2.3.

2.3.2.1 8-12 μm and $\lambda < 3.7$ μm Regions

The 8-12 μm region and the region below 3.7 μm contain the major IR emissions of the odd-oxygen species, O_3 and OH. Since OH(v) is formed directly from O_3 (via reaction with H atoms), the O_3 and OH emissions track each other across the terminator. Dawn and dusk must be distinguished since the concentrations and hence emissions are not equivalent functions of solar angle in the two cases. Solar-excited bands from CO_2 also appear in these regions, but are generally much smaller contributors to the in-band radiance in the CIRRIS data.

2.3.2.1.1 *In-Band Radiances (FP3 Filter 7 and FP2)*

2.3.2.1.1.1 *Methodology*

CIRRIS-1A radiometer data from focal plane 3, filter 7 (8-12 μm) and focal plane 2 ($\lambda < 3.7$ μm) were obtained from the near-horizontal dawn terminator scan in Block PC12B, Mode 24-2. The filter 7 emissions are from the O_3 v_1 and v_3 bands and solar-excited CO_2 laser bands. The FP2 radiance derives from the OH($\Delta v = 1$) and solar-excited 2.7 μm CO_2 bands. The views are due west

across the terminator and the tangent heights range from approximately 74 km (detector 3-6) to 96 km (detector 3-1). Data were tabulated for specific times corresponding to approximately 2° increments in tangent point solar zenith angle (SZA) over a range of 100° to 88°. During this sequence of measurements the spacecraft traveled from approximately 28° N latitude to 41° N latitude.

The SAMM calculations were performed using a set of seven model atmospheres generated for a SZA range of 101-87°, a latitude range of 27-42° N, and a local time range of 4.58-5.34 hrs. These correspond to values for the tangent point viewed by the centers of the CIRRIS focal planes during the terminator traversal. In calculating the spectra and radiances for an individual detector on the focal plane, the actual tangent height and tangent point SZA for that detector were used; the latitudes and local times of the model atmospheres along the LOS differ slightly from the actual values. To exactly match the actual values, a separate set of atmospheres and vibrational state calculations would have been required for each location of the spacecraft. A direct comparison between the current approach and a calculation using the "exact" atmospheric conditions yielded only 1%-level LOS radiance differences.

2.3.2.1.1.2 Results

The data-model comparisons were made at tangent heights of 74 to 96 km. However, comparisons are shown in Figures 26 and 27 (FP3 filter 7) for the highest tangent heights (96 and 92 km) and Figures 28 and 29 (FP2) at tangent heights of 83 and 74 km. The initial SAMM calculations were based on model atmospheres from the SHARC/SAMM Atmosphere Generator (SAG) and are labeled "SAG". The radiance changes with SZA are superimposed on typically smaller fluctuations associated with ±2 km changes in the tangent point during the measurement period; the tangent altitude listed is the average for that detector.

In both bandpasses the largest changes in radiance with SZA occur at the highest altitudes; there the absolute agreement with the CIRRIS data is quite good. The location of the terminator edge and the radiance trend remain qualitatively reasonable at the lower altitudes; however, the absolute radiances are overpredicted by up to a factor of 4 (in filter 7 at 74 km).
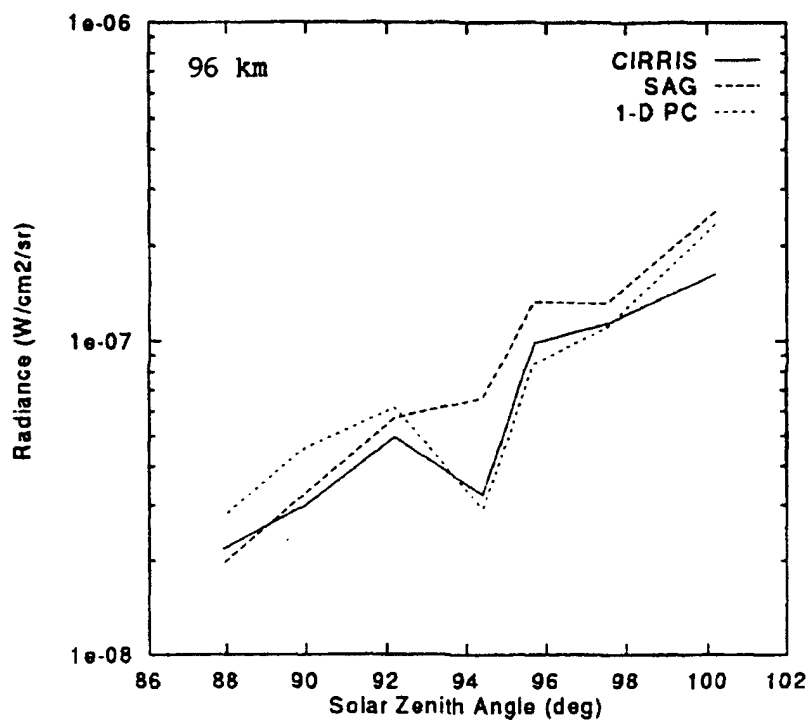
Figure 26. Dawn Terminator 8-12 μm Radiometric Comparisons for Average ±2 km) at a Tangent Height of 96 km. CIRRIS-1A Data are From Block PC12B Mode 24-2.
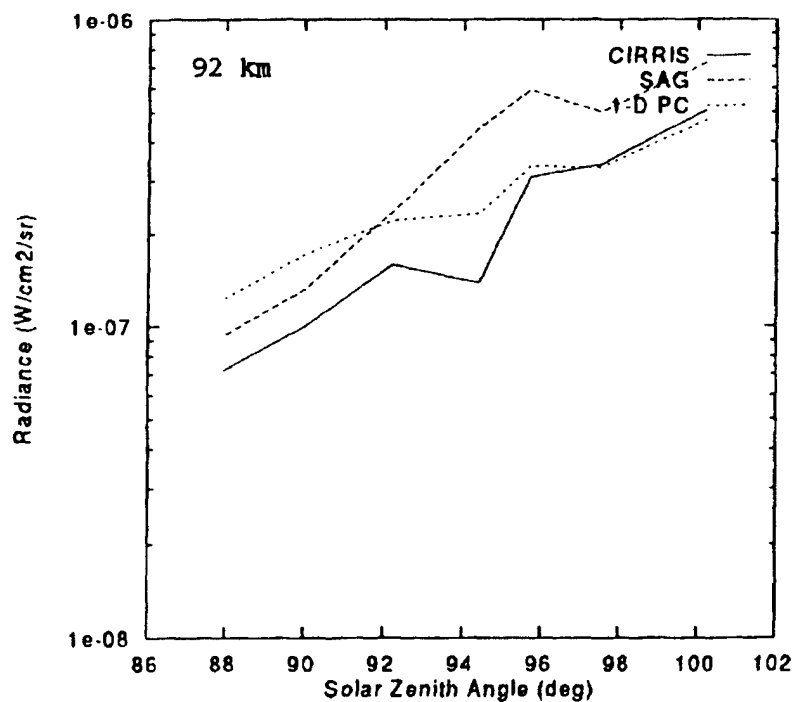
Figure 27. Dawn Terminator 8-12 μm Radiometric Comparisons for Average ±2 km) at a Tangent Height of 92 km. CIRRIS-1A Data are From Block PC12B Mode 24-2.

31
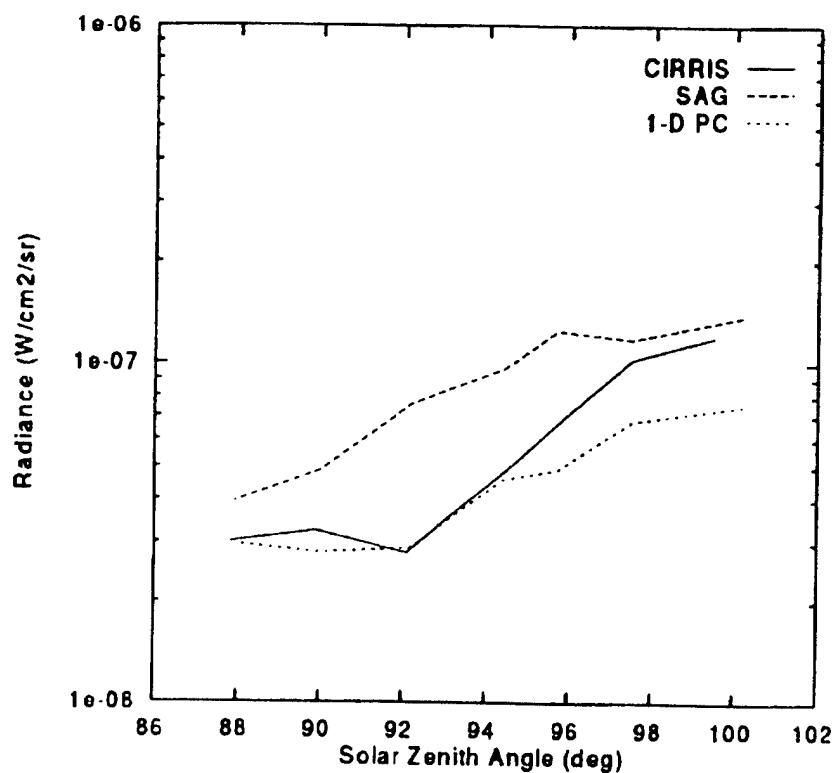
Figure 28. Dawn Terminator Radiometric Comparisons for Focal Plane 2 at at a Tangent Height of 83 km. Data were Taken Simultaneously with those in Figures 27 and 28.
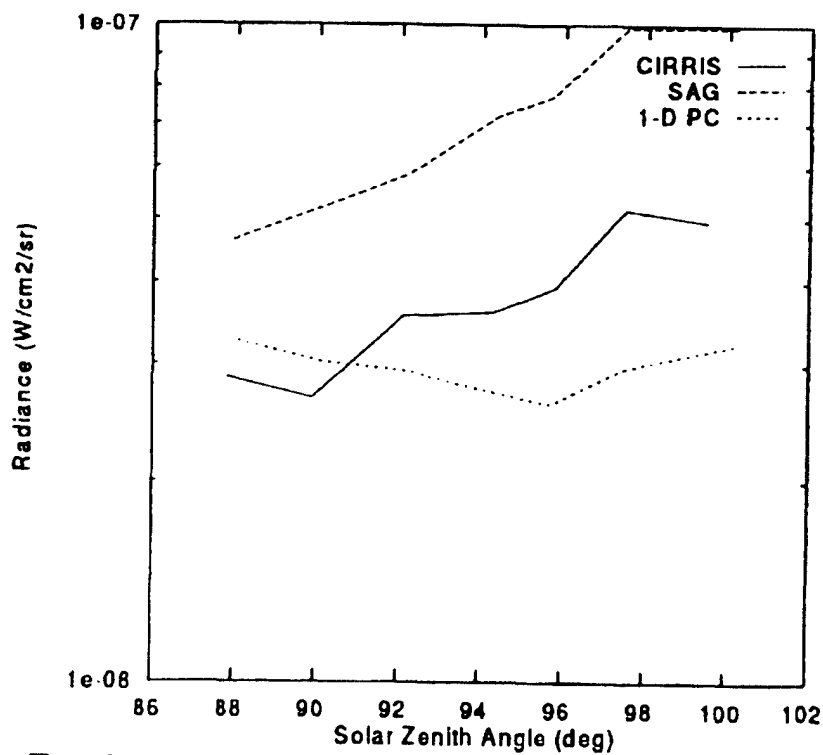
Figure 29. Dawn Terminator Radiometric Comparisons for Focal Plane 2 at at a Tangent Height of 74 km. Data were Taken Simultaneously with those in Figures 27 and 28.

As indicated earlier, the emissions at these wavelengths are dominated by OH and O_3, especially on the night side, and track each other across the terminator since both the OH(v) and O_3(v) concentrations are proportional to the O_3 number density. The radiance overpredictions by SAMM in the 74 to 83 km tangent height range are associated with excess O_3 in the SAG model atmospheres, which in turn is ascribed mainly to an overestimation of the atomic oxygen concentration at these altitudes, particularly at dawn. The atomic oxygen profile in SAG is approximate; as discussed in [Adler-Golden 1993], the profile is scaled from the MSISE-90 empirical model [Hedin, 1991] using a simple day/night ratio, an approach which does not accurately treat the time-dependence.

More quantitative modeling of OH and O_3 emissions in the 70-85 km altitude range requires an accurate simulation of the time-dependent concentration profiles for both the odd-oxygen and odd-hydrogen species. To demonstrate how improved species profiles can be used with SAMM for improved radiance predictions, a second set of calculations was performed using O_3, O, and H concentrations from a one-dimensional time-dependent photochemical model that has been developed at AFRL [Makhlouf et al., 1994]. The results are labeled "1-D PC" in Figures 26-29. The CIRRIS-SAMM agreement is seen to be very good in both the FP3 Filter 7 and FP2 bandpasses over the full altitude range.

It is concluded that in order to provide the most accurate terminator simulations for systems applications, results from this or similar time-dependent photochemical calculations should be incorporated in the model atmosphere. A simple but somewhat less accurate alternative would be to systematically scale back the O atom profile in SAG near 80 km, to yield reduced O_3 and OH.

2.3.2.1.2 *Spectra*

2.3.2.1.2.1 *Methodology*

Terminator spectra from the CIRRIS-1A interferometer in the wavelength region of Focal Plane 2 are rather limited, and the declining response of the interferometer detectors makes their signal-to-noise insufficient for separating the daytime CO_2 2.7 μm and OH(Δv=1) contributions without signal averaging. A detailed analysis of the nighttime OH data has recently been published [Dodd et al., 1994]. No spectral analysis of this wavelength region has therefore been attempted for this report.

Spectra of the dawn terminator in the 8-12 μm region were taken in CIRRIS during Blocks 11G, 16, and 42B with medium (3 cm⁻¹ FWHM) resolution. Similar data were taken in the dusk terminator during Block 12B. For the current comparisons, we selected a subset of 14 dawn spectra at tangent heights near 70 km, 78 km, and 86 km covering SZA's from 87°to 101°.

The SAMM simulations were performed using model atmospheres calculated for the specific times and locations along the LOS using the 1-D photochemical model for odd-O species and SAG for the remaining species and temperature profiles. The SAMM spectra were degraded to match the CIRRIS resolution. Unlike the spectral calculations illustrated in Section 2.4.1, these calculations do not account for the detector footprint and therefore may underpredict the radiance by up to one-third at some wavelengths. This is not a major consideration in evaluating the overall data-model agreement, however.

2.3.2.1.2.2 Results

The data-model comparisons are shown in detail in [Adler-Golden *et al.*, 1994]. A representative comparison is shown in Figure 30 at a tangent height of 71.4 km for the dawn terminator. The bulk of the radiance at these wavelengths is from the O_3 v_3 (001)-(000) ("cold") band. The SAMM and CIRRIS intensities for this band usually agree to within a factor of two or better. Near 86 km (Block 16) the SAMM cold band radiance is somewhat high, while near 70 km (Block 42B) it is too low, especially on the day side. This agreement, while reasonable, is not as good as was found with the Block PC12B radiometer data (Figures 26-29).

The chemiluminescent O_3 "hot" v_3 bands are the major source of emissions between 800 and 1000 cm⁻¹. Although there are some problems in the SAMM O_3 hot band model which affect wavenumbers below around 870 cm⁻¹ (wavelengths above 11.5 μm), the overall agreement in both spectral shape and intensity is good over the full altitude and solar angle range in the two- to five-quantum hot band region (approximately 870-1000 cm⁻¹) that is not overlapped by the CO_2 laser band centered at 961 cm⁻¹. At the resolution shown, the non-LTE OH rotational emission is not very prominent in the CIRRIS data, and its omission in SAMM is not a major source of error.

On the day side of the terminator, the CO_2 (00011)-(10001) and (00011)-(10002) laser bands, centered at respectively 961 cm⁻¹ and 1064 cm⁻¹, are underpredicted by SAMM by a factor of 2 to 3,

34

even accounting for the footprint effect. The same conclusion can be drawn from the daytime Filter 3 and Filter 7 spectra in Section 2.4.1, which are footprint-corrected. This observation is also consistent with an underprediction of the 4.3 μm (00011)-(00001) band (see the following subsection), which has the same upper state.
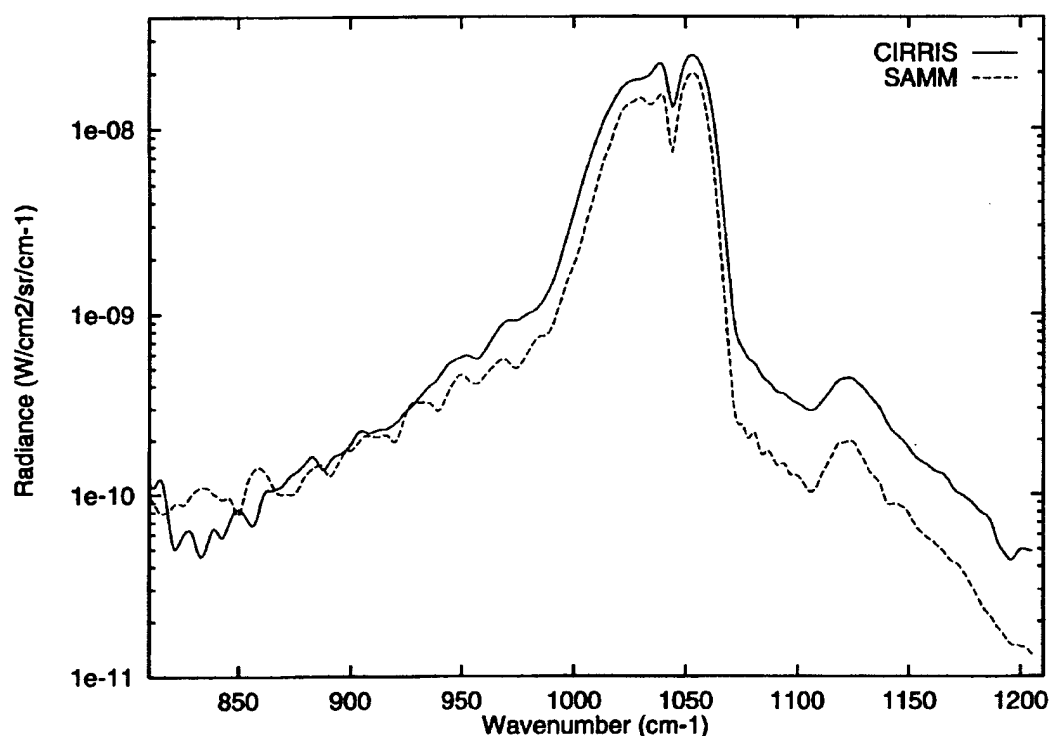
Figure 30. Dawn Terminator Comparisons of CIRRIS-1A Data in the 8-12 μm Region with SAMM Calculations at a Tangent Height of 71.4 km and a Solar Zenith Angle of 95.1°.

The greatest data-model differences occur on the high-wavenumber side of the spectrum at high altitudes, where the v_1 and $2v_2$-v_3 bands of ozone occur. Near 70 km the proportional differences are not much greater than for the cold band, and appear to be due mainly to an underprediction of O_3 concentration by the atmosphere model. However, at higher altitudes the CIRRIS data show significant excess radiances; this is more apparent on the day side of the terminator, where the predicted v_1 band contribution is smaller. The spectral shape of the excess radiance somewhat resembles that of the $2v_1$-v_3 ("crossover") band centered at 1159 cm^{-1}, although it seems to be broader and extended to higher wavenumbers. While we have no definitive explanation of this excess emission, we surmise that it is associated with ozone chemiluminescence, perhaps arising

35

from the crossover band in combination with other bands and possibly containing a rotationally hot component.

2.3.2.2 4.3 μm REGION

CIRRIS-1A-SAMM comparisons of 4.3 μm-region radiances near the terminator provide an excellent test of models for solar excitation of CO_2 and subsequent energy transfer processes giving rise to radiation from the v_3-type bands. In contrast to the O_3 and OH emissions, the uncertainty in the radiance associated with number density uncertainties is quite small due to the optical thickness of the bands, the uniform CO_2 mixing ratio over most of the altitude range of the 4.3 μm data, and the relative unimportance of other trace species in the excitation mechanisms.

Both the kinetics and radiation transport processes are extremely complex, and involve energy scrambling among a large number of CO_2 vibrational states (including minor isotopes), transfer to and from $N_2(v=1)$, multiple absorption and re-emission of photons within and between atmospheric layers, and other effects. Considering this complexity, the ability of SAMM to reproduce the two-order-of-magnitude variation of this radiation across the terminator to within typically a factor of two or better must be considered a major achievement of the code.

2.3.2.2.1 *4.3 μm In-Band Radiance (FP3 Filter 1)*

2.3.2.2.1.1 *Methodology*

The SAMM-CIRRIS database [Adler-Golden *et al.*, 1994] contains several 4.3 μm radiance profile comparisons for daytime and nighttime conditions; they show up to a two order-of-magnitude range of variation. Terminator data are available in CIRRIS only for a limited range of SZAs and altitudes. For this investigation we examined data from Block 10B, Mode 34, which provide the best overall, continuous SZA coverage. The tangent height range is 65-87 km and the views are southeast across the dawn terminator. The SZA range, approximately 92-95°, extends from the night side to around the middle of terminator and thus covers around half (one order of magnitude) of the day/night variation.

As in the O_3 and OH calculations, seven latitude-SZA-local time-correlated atmospheres were used to simulate all of the limb radiances measurements from the six CIRRIS FP3 detectors. The SZA range in the calculation is 100° to 87°.

36

2.3.2.2.1.2 Results

The measurement-model comparisons are shown in Figure 31. There is excellent agreement in the absolute radiance levels (within about 15%) on the night side of the terminator over the full tangent height range shown, as well as over the full SZA range up to 79 km. However, at the higher altitudes the CIRRIS data fall below the SAMM predictions by significant and increasing amounts (up to a factor of 1.6) in proceeding from the night towards the center of the terminator. The spectral analysis in the following section ascribes this discrepancy to CO_2 628 isotopic bands, which are selectively solar-pumped in the terminator. Interestingly, in the non-terminator profiles the CIRRIS-SAMM differences, while generally small, are in the opposite direction.

2.3.2.2.2 Spectra

2.3.2.2.2.1 Methodology

Since for the 4.3 μm region no single CIRRIS data block contains spectra for a wide range of SZAs and tangent heights, data were compiled from a number of different blocks and modes covering different mission times, local times, and latitudes corresponding to day, night, and mid-terminator. The terminator data are for the dawn and are from Block 10B, Mode 34. As before, the SAMM calculations were performed using a range of SAG model atmospheres that approximately match the latitudes and local times of the data and exactly match the SZAs and altitudes. The observed and calculated spectra are presented in detail in Adler-Golden *et al.* [1994]. Except for the ~66 km nighttime spectrum, from a medium-resolution scan, the spectra are high-resolution (1 cm^{-1}) and were degraded to 4 cm^{-1} FWHM with the sech function. The finite size of the detector footprint has been ignored in the calculations, but since at most altitudes and wavelengths the radiance does not fall off steeply with altitude this approximation should be satisfactory.

4.3 µm Terminator (CIRRIS)

Legend:
- 65 km
- 70 km
- 75 km
- 79 km
- 83 km
- 87 km

Radiance (W/cm²/sr) vs SZA (deg)

4.3 µm Terminator (SAMM)

Legend:
- 65 km
- 70 km
- 75 km
- 79 km
- 83 km
- 87 km

Radiance (W/cm²/sr) vs SZA (deg)
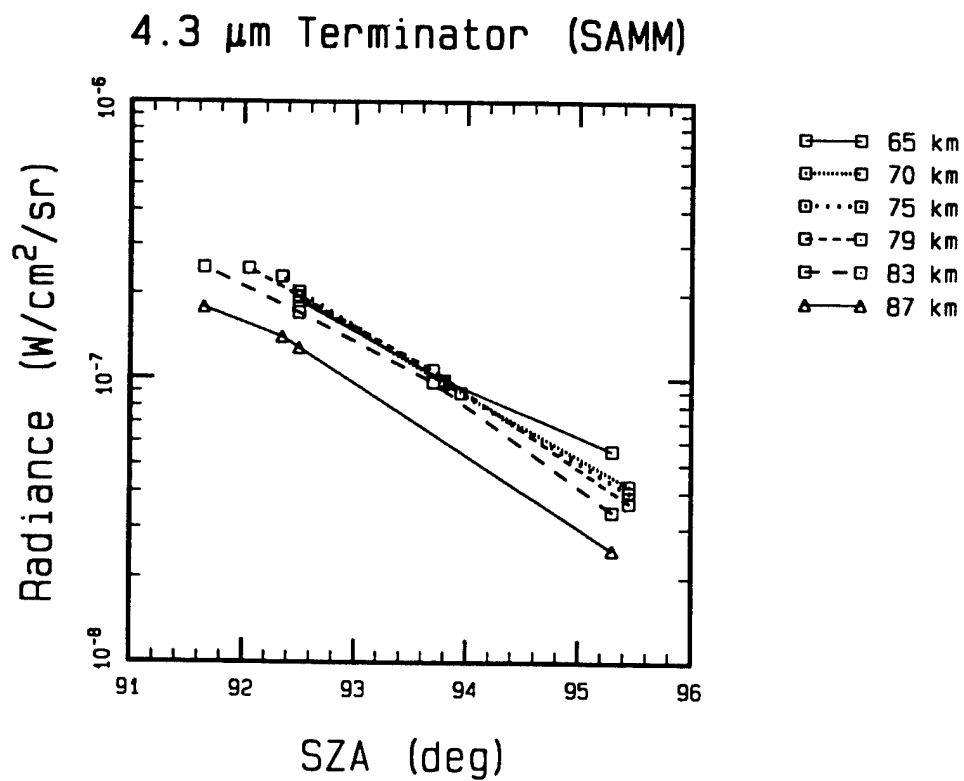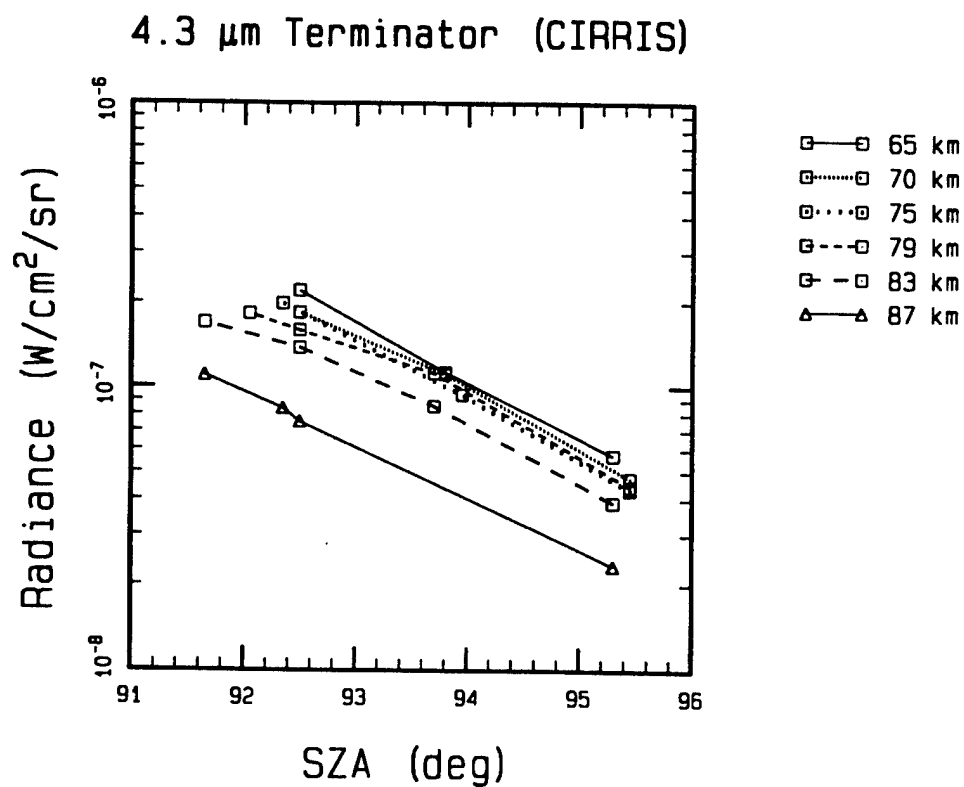
Figure 31. Dawn Terminator Radiometric Comparisons of CIRRIS-1A Data (Block 10B Mode 34) for the 4.3 µm Region (Filter 1) with SAMM Calculations.

2.3.2.2.2.2 Results

In general, the results indicate that the SAMM calculations match the CO_2 4.3 μm spectral radiance to within a factor of two or better at most wavelengths over the full two-order-of-magnitude range of diurnal variation; this represents a substantial modeling achievement. The overall agreement is best during the daytime. At night, the overall radiance is underpredicted by SAMM by up to a factor of three (at around 66 km), a small portion of which may be due to neglect of the detector footprint. At 47 km and at 72 km (see Figure 32) and above the nighttime agreement is excellent; this is in agreement with the bandpass radiance comparison discussed in the previous subsection.
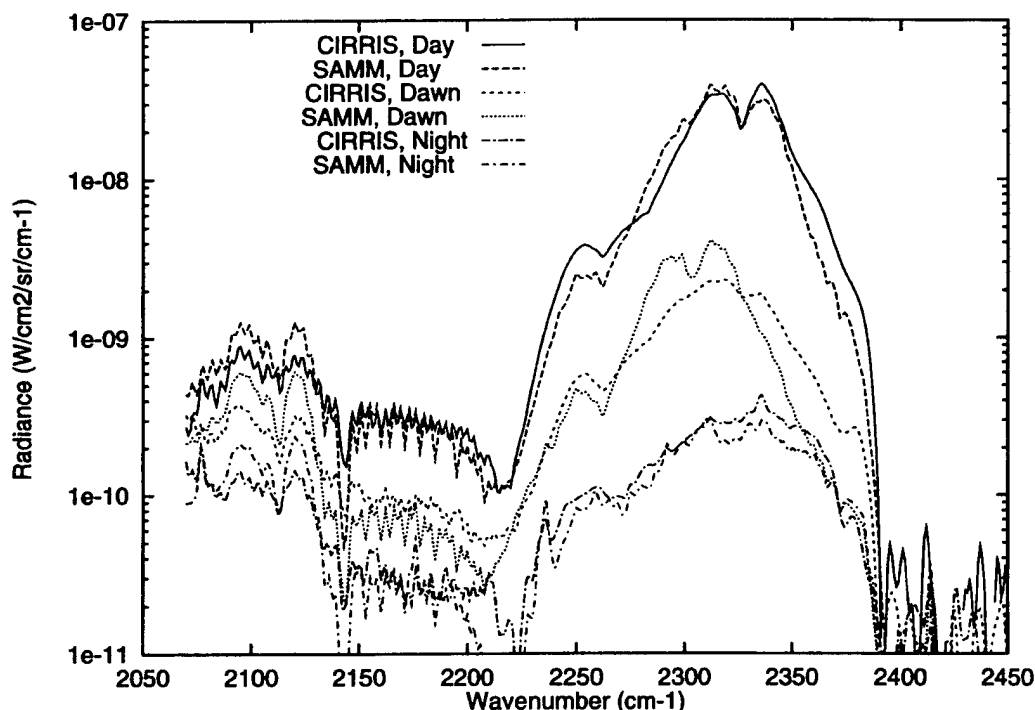
Figure 32. Diurnal Comparisons of CIRRIS-1A Data in the 4.3 μm Region with SAMM Calculations at a Tangent Height of ~72 km.

The comparisons show some data-model discrepancies in the shape of the 4.3 μm CO_2 spectrum. The terminator radiance overprediction by SAMM at high altitudes (see the previous subsection) is seen to originate from the region around 2300 cm^{-1}. The bands in this region are mainly from the 628 isotope, which remains sunlit further towards the night side than the main isotope and thus is

preferentially excited at the terminator. In addition, the high-wavenumber edge of the spectrum, where the (00011)-(00001) ("cold") band of the main isotope is found, is underpredicted by SAMM. This is consistent with the underprediction of the CO_2 laser bands in the 8-12 μm region, which have the same upper state. At the present time we have no explanations for these data-model differences.

2.3.2.3 Other Wavelength Regions

In addition to the CIRRIS-1A terminator data discussed in Sections 2.4.2.1 and 2.4.2.2, in-band radiances are also available for FP3 filters 2 (4.9-7.0 μm), 5 (11.1-12.8 μm), and 6 (17.9-23 μm), and were briefly examined. Filter 2 data were taken on the day side of the dawn terminator at thermospheric altitudes near the peak of the NO profile; they show a strong but gradual trend of increasing radiance with decreasing SZA, as previously reported by *Smith et al.* [1992]. According to the NO concentration model in SAG, the observed variation is only partly a solar terminator effect *per se*; the bulk of the increase is due to the movement of the spacecraft towards higher latitudes (where the NO concentration is greater) as the sun rose.

The filter 5 terminator data cover a spectral region within interferometer filter 7, the data from which are discussed in Section 2.4.2.1.2. Near the mesopause this bandpass is dominated by non-LTE emission from O_3 hot bands, which does not vary across the terminator, and OH rotational emissions, which does. Neither of these radiation sources are completely understood, and a model for the OH rotational emission is not currently available in SAMM. The lower altitudes can be modeled reasonably by SAMM, but there the terminator variation is relatively small and is probably due mainly to solar scattering by clouds and aerosols, which would need to be specified correctly in the model atmosphere.

The filter 6 bandpass contains almost exclusively H_2O emissions; the contribution from non-LTE OH rotation lines is small and confined to altitudes above around 80 km. Neither the CIRRIS radiance profiles nor SAMM simulations show any evidence of a solar terminator-related variation in this bandpass.

2.4 Conclusions And Future Work

The CIRRIS-1A-SAMM comparison data base has identified many categories of IR emission processes which are remarkably well modeled by the DoD standard radiance and transmission codes.

However, the results also indicate significant areas of uncertainty in IR background code predictions requiring new enhanced simulation capabilities to support the optimization of space-based optical sensor systems. In addition, the database comparisons demonstrate the need for additional field measurements of wider global and wavelength coverage to address the important issues of atmospheric and radiance variability.

Several chemistry and atmosphere model upgrades are indicated by both previous investigations and the current CIRRIS-1A data and SAMM code comparisons. The first major category of model upgrade is based on the discovery of a new class of important rotational emission processes. New $NO(v,J)$ and $OH(v,N)$ models are required to account for the non-equilibrium rotational population distributions producing substantial radiance enhancements in SWIR and LWIR bands. Other upgrades include a new non-auroral NO^+ model for accurate calculations of radiance levels in the important 4.3 micron band used to support optical sensor element design and optimization. The comparisons of CIRRIS-1A and SAMM data for the 8-11 micron wavelength region indicate upgrades are required to the kinetics and spectroscopy models used to calculate O_3 hot band emissions. Future SAMM code releases will also incorporate CFC's and other trace species which are important IR radiators along ATH and BTH sensor lines-of-sight. Lastly, to support the technology transition of earthlimb and down-looking data from upcoming experiments, including the MSX program, to validated optical background code simulations for a wide range of atmospheric conditions, a higher spectral resolution code capability is required.

A major recurring result of the CIRRIS-1A-SAMM data comparisons is the uncertainty in global, seasonal, and other atmospheric background radiance variations. Specifically for thermospheric IR radiances, the NO concentration profile used in the present work is in need of improvement, particularly for nighttime conditions and for low latitude locations. Although a simple model is unlikely to completely account for the relatively large variability associated with NO, an enhanced capability is required to credibly bound the variability excursions. In addition, upgrades to the O_3 and HNO_3 atmospheric profiles calculated using the SHARC/SAMM Atmosphere Generator would significantly improve the agreement between measured and predicted radiances at altitudes below the thermosphere. An improved temperature model is also required for the mesopause region to reduce radiance uncertainties in this altitude regime. These upgrades and others indicated by this study are

required to provide accurate, validated atmospheric IR background radiance codes for selecting sensor filter bandpasses to optimize surveillance, tracking, and interceptor system operability.

The CIRRIS-1A-SAMM solar terminator comparisons have examined variations in atmospheric limb radiance in a number of important IR bandpasses across the earth's shadow edge at tangent heights between 50 and 100 km. The results, together with those of an earlier study [Adler-Golden and Matthew, 1993], provide a reasonably comprehensive assessment of the ability of SAMM and other DoD standard radiation codes to simulate these radiance variations, a capability that is required for the optimization of space-based optical sensor systems. The comparisons indicate areas of good agreement, required code upgrades, and needs for additional field measurements.

The SAMM calculations yield reasonable qualitative predictions of the major variations in MWIR to LWIR limb radiance across the solar terminator. SAMM achieves quantitative accuracy, typically within a factor of two or better, in the strategically important 4.3 μm region, where the in-band radiance can change by a factor of 1.5 with only a 1°change in solar angle (i.e., a 1°change in latitude at the equator). While the overall description of CO_2 4.3 μm emission is good, certain states and bands are overpredicted (e.g., CO_2 628 bands at the terminator) or underpredicted (e.g., the solar-excited (00011) state) by the SAMM kinetic models by up to a factor of three. Reducing these errors will require a re-examination of the energy-transfer kinetics of the CO_2 vibrational states.

For O_3 v_3 and OH fundamental band emissions, which occur in the CIRRIS 8-12 μm and $\lambda < 3.7$ μm bandpasses, good in-band radiance accuracy (within a factor of two or better) is obtained at all solar angles using model atmospheres based on a 1-D photochemical model. Poorer agreement is obtained between 70 and 85 km using atmospheres generated with the current version of the SAG code, due to differences in the O_3 concentrations. The factor-of-four maximum errors may still be acceptable for many systems applications, however. It is recommended that an upgraded version of SAG be developed with an improved description of atmospheric odd-oxygen and odd-hydrogen photochemistry. In addition, since the bulk of the CIRRIS-1A terminator data at these wavelengths are for the dawn, it is recommended that additional measurements be performed at dusk to verify the accuracy of 1-D photochemical model calculations.

42

Comparatively poor data-model agreement is obtained in the most transparent (lowest background radiance) portions of the 8-12 μm region. This applies both near 12 μm where non-LTE O_3 and OH emissions contribute and in the 8-9 μm region above 70 km where significant excess radiance relative to SAMM is observed that is yet to be assigned. These conclusions are based on both the terminator comparisons and the non-terminator comparisons presented previously. Further analysis of the CIRRIS data and possibly additional measurements will be required to identify the source of the unknown emissions near 8 μm.

In the 4.9-7.0 μm, 11.1-12.8 μm, and 17.9-23 μm bandpasses, in-band radiance variations across the terminator are either gradual or absent in both the data and models. Development of a model for rotationally excited, chemiluminescent OH will be required to simulate the terminator variation in the 11-12 μm region. The 5.3 μm NO fundamental band radiance is consistent with known NO production and loss processes; variations can be large but are slow compared to the solar variation across the terminator. Latitude-related variations in NO, predicted qualitatively by the SAG concentration model, can mask these temporal changes for a rapidly moving sensor. Aurorally-induced fluctuations in NO density and radiation are also known to be quite large but have not been systematically studied with the CIRRIS-1A database. This is clearly an important area for future investigation.

3.0 ADDITION OF A CORRELATED-*k* CAPABILITY TO MODTRAN

3.1 Introduction

This section describes the approach used to add a Correlated-*k* (CK) capability to the MODTRAN (Berk *et al.*, 1998) atmospheric transmission/radiance computer code. The overall objective of the effort is to provide an accurate and fast means for evaluation of the effects of volcanic aerosols and clouds on atmospheric radiative heating/cooling and on retrievals of species concentration profiles. These radiative transfer computations require coupling the effects of gaseous molecular absorption due primarily to water vapor and carbon dioxide and particulate multiple scattering due to aerosols, ice crystals, and water droplets. The molecular absorption band model used in MODTRAN is not suitable for interfacing with standard multiple scattering algorithms. This is because the scattering models are based on a Beer's law description of the molecular absorption/transmission (i.e. T=exp(-ku)) whereas molecular band models exhibit different and more complex dependencies on the absorption coefficient k and absorber amount u. In order to adapt a band model approach for use in scattering calculations it is necessary to express the band model transmission function in terms of a weighted sum of Beer's law exponential terms. Thus, one of the fundamental problems addressed in this work is the development of a method for determining the weighting factors and monochromatic absorption coefficients corresponding to the MODTRAN band model.

3.2 Overview of CK Method

For simplicity, consider the problem of determining the average transmittance for a homogeneous path over a finite spectral interval. The generalization to inhomogeneous paths is straightforward and is also described below. The path transmittance can be exactly determined through evaluation of

$$T(u) = \frac{1}{\omega_2 - \omega_1} \int_{\omega_1}^{\omega_2} d\omega \, \exp(-k(\omega)u), \tag{1}$$

where ω is frequency and $k(\omega)$ is the monochromatic absorption coefficient. The basis of the CK approach is that evaluation of T(u) by integration over frequency can be replaced by an equivalent integration over the distribution of absorption coefficient values f(k) in the spectral interval

$$T(u) = \int_0^\infty dk \; f(k) \exp(-ku). \qquad (2)$$

The difficulty in evaluation of $T(u)$ via Equation (2) is the necessity of first determining $f(k)$; the advantage is that $k(\omega)$ is typically a highly repetitive function of ω (i.e. there are many nearly equivalent values of a given k in a spectral interval) and thus numerical evaluation of Equation (2) requires far fewer grid points than Equation (1). Note that $f(k)=0$ above the maximum k_{max} and below the minimum k_{min} absorption coefficients in the spectral interval. Several methods are available for determining $f(k)$. It can be determined directly from $k(\omega)$ by binning the k's into selected Δk sub-intervals. Another method takes advantage of the fact that Equation (2) is in the form of a Laplace transform; thus, $f(k)$ can be determined from the inverse Laplace transform of $T(u)$

$$f(k) = L^{-1}(T(u)). \qquad (3)$$

The utility of Equation (3) is it requires that only $T(u)$ and not $k(\omega)$ be known *a priori* and therefore can be applied to any transmittance model, both line-by-line and band model. The distribution function $f(k)$ is not smooth or monotonic; it generally consists of a series of sharp spikes which reflects the sharp line structure of $k(\omega)$. It is computationally more convenient to work with the smooth and monotonic cumulative probability distribution function

$$g(k) = \int_0^k d'k \; f(k'). \qquad (4)$$

Physically, $g(k)$ corresponds to a monotonic re-ordering of $k(\omega)$ within the finite spectral interval ω_1 to ω_2. It assumes the values $g=0$ at $k=k_{min}$ and $g=1$ at $k=k_{max}$. The transmittance is related to g by

$$T(u) = \int_0^1 dg \; \exp(-k(g)u), \qquad (5)$$

where $k(g)$ is given by the inverse of $g(k)$, $k(g) = g^{-1}(k)$. In practice, the evaluation of Equation (5) proceeds via summation according to

$$T(u) = \sum_{i=1}^{imax} \Delta g_i \exp(-\bar{k}_i u), \qquad (6)$$

where the Δg_i's and $\bar{k}_i$'s are the sub-interval weighting factors and effective absorption coefficients we seek to define for the MODTRAN band model. The maximum number of intervals i_{max} and the specific selection of Δg_i interval boundaries (g_i, g_{i+1}) are chosen based on consideration of a number of factors including computational speed and accuracy, and the altitude and spectral ranges of interest. For multi-layer paths it assumed that there is perfect spectral correlation among the sub-intervals of each layer, resulting in a total path transmittance given by

$$T(u) = \sum_{i=1}^{imax} \Delta g_i \exp(-\sum_{j=1}^{jmax} \bar{k}_{ij} u), \qquad (7)$$

where j denotes the sum over layers.

3.3 MODTRAN k-Distributions

The MODTRAN band model for a single species (multiple species are discussed later) is based on four parameters: (1) the integrated line strength S in a spectral interval $\Delta \omega$ ($\Delta \omega = 1$ cm^{-1} in MODTRAN), (2) the effective number of equivalent lines n (non-integer values of n are acceptable) in the interval, (3) the average pressure broadening Lorentz line width γ_L, and (3) the Doppler line width γ_D. These parameters are determined directly from the HITRAN (*Rothman et. al.*, 1998) line parameter compilation. The molecular transmittance model is given by

$$T(u) = (1 - \frac{W(S_{sl} u, \gamma_L, \gamma_D)}{\Delta \omega})^n, \qquad (8)$$

where $S_{sl} = S/n$ is the strength for a single effective line, and W is the Voigt equivalent width of the line taking into consideration only the portion of the line shape which falls within the spectral interval. This functional form for the band model transmittance derives from the assumption that all the lines in the spectral interval are positionally uncorrelated and thus accounts for line overlap in a statistically average sense. The transmittance contribution due to the tails of lines which originate from outside the spectral interval are included as a single multiplicative Beer's law term.

46

Detailed formulas for the equivalent width W are available elsewhere (*Berk et. al.*, 1998). As discussed earlier the k-distribution f(k) for the band model could be determined directly from the inverse Laplace transform of T(u) given by Equation (8). Alternatively, and the method applied here, it can be determined from line-by-line (LBL) simulations which are physically constrained by the same assumptions used to derive Equation (8). The use of real time LBL simulation or inverse Laplace transformation to derive f(k) during a MODTRAN run is much too slow to be of practical value; however, the approach adopted here is to use LBL simulation off-line to pre-compute a table of k-distributions which can be rapidly accessed and interpolated during a MODTRAN run.

3.3.1 Monte Carlo Line-by-Line Simulation of f(k)

For a given choice of n, γ_L, γ_D, and S=1 cm^{-2} atm^{-1} (f(k) is directly proportional to S so any convenient reference value can be used) a series of LBL absorption coefficient spectra are generated. The positions of the n lines for each spectrum are selected at random with uniform probability over the spectral interval. The f(k) for each spectrum is determined and all the f(k)'s are averaged with equal weighting to determine the final band model equivalent k-distribution. The final f(k) is then transformed into the more conveniently used k(g) distribution as discussed earlier. The procedure is illustrated in Figures 33-34 for an example using n=5 lines. Figure 33 shows several of the many LBL spectra used to determine f(k). In determining the f(k) distribution, each trial spectrum is interrogated over a fine grid of equally spaced frequency points $\delta\omega$ and the k value at each point is binned into a logarithmic sequence of k-bins

$$k_j = k_{min} 10^{\alpha j}, \qquad (9)$$

where α controls the spacing of adjacent k-bins. In this study α=0.005 was used which results in a spacing of $10^{0.005}$=1.012. The Monte Carlo averaged k(g) distribution is then calculated from

$$\Delta g_j = \frac{n_j}{n_{MC}} \frac{\delta\omega}{\Delta\omega}, \qquad (10)$$

where n_j is the number of binned k values between k_j and k_{j+1}, and n_{MC} is the number of Monte Carlo trial spectra. The function $g_j(k_j)$ is constructed from the Δg_j's by

$$g_j = \sum_{i=1}^{j} \Delta g_i, \qquad (11)$$

47

which also defines the final desired distribution function $k_j(g_j)$.
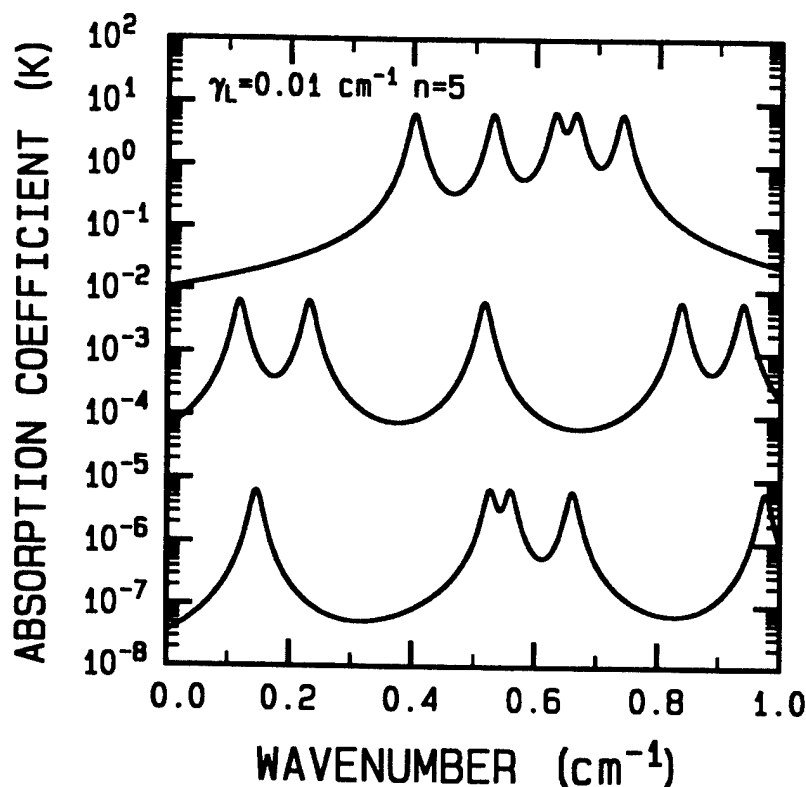
Figure 33. Sample Monte Carlo Trial Spectral Calculations. The bottom spectra are offset by factors of 10^{-3} and 10^{-6} from the top spectrum for display purposes

The convergence of the $k(g)$ distribution as a function of the number of Monte Carlo trial spectra is shown in Figure 34. Reasonable convergence is obtained after 20 trials, although some differences are noted between 20 and 100 trials. The number of trials needed to obtain a good distribution depends on the number of lines n; as a general rule of thumb at least $n_{MC}=100/n$ trials are required to obtain a useful result. It is difficult to see the convergence of $k(g)$ in the region of $g=1$ in Figure 34; this region is shown in an expanded scale in Figure 35. It is seen that the peak value of k approximately doubles when 20 or more trials are considered. This reflects the probability that any two of the n=5 lines will closely overlap for a given trial spectrum. If enough trials were considered, eventually overlaps of 3, 4, and 5 lines would be observed; however, the cumulative probability interval Δg associated with these cases would be insignificant and would have an inconsequential impact on radiative transfer calculations.

48
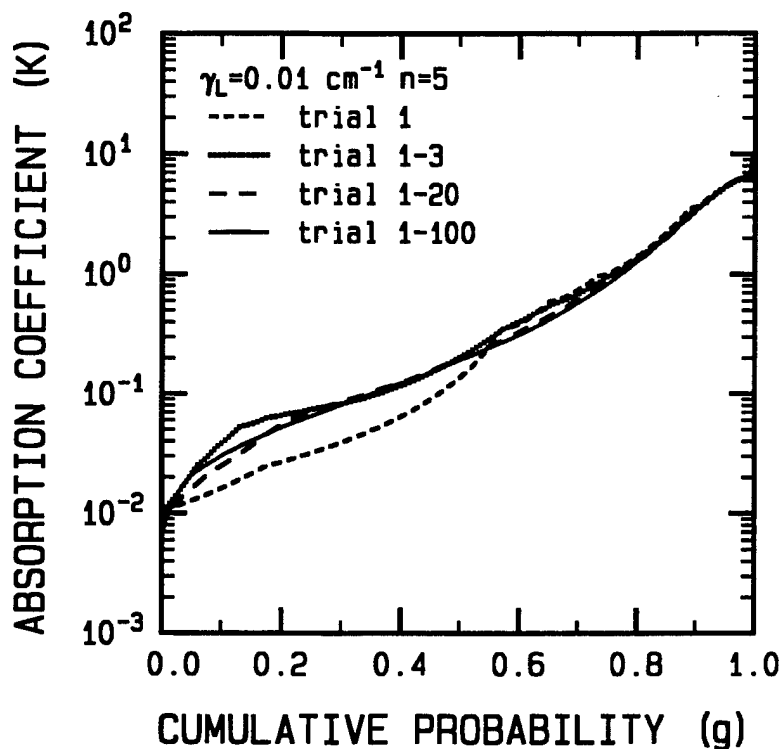
Figure 34. Convergence of the k(g) Distribution as a Function of the Number of Monte Carlo Trial Spectra
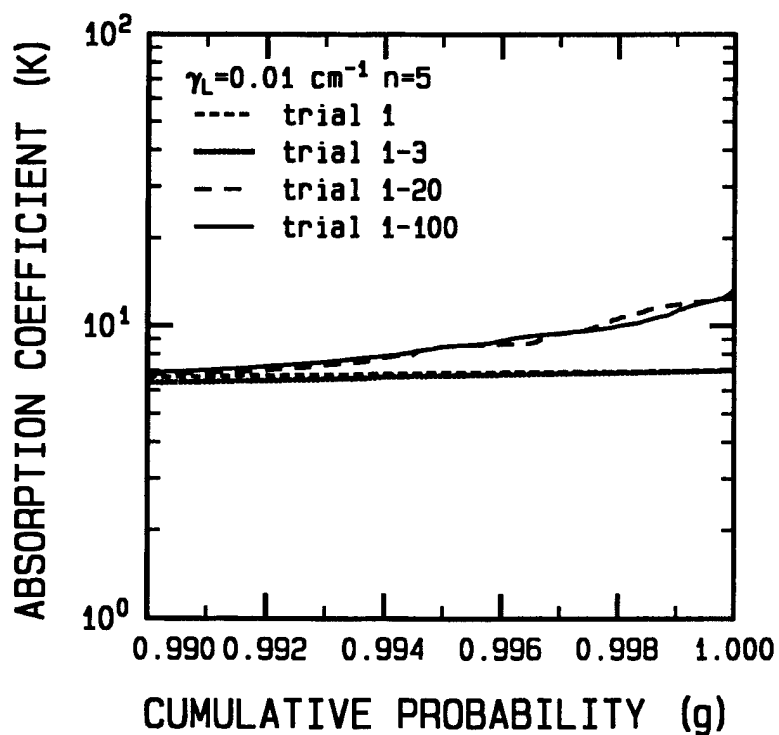
Figure 35. Same as Figure 33 But Showing the Convergence in the Region of g=1 in More Detail

Several examples of k-distributions and their variability with n, γ_L, and γ_D are shown in Figures 36-38. Figure 36 shows the variation with the Lorentz line width where it is seen that the line wing absorption coefficients (i.e. g<0.8) are proportional to γ_L. Figure 37 shows that in the limit of a very large number of lines the absorption coefficients asymptote to a constant value for the entire spectral interval. Figure 38 illustrates the changes in the k-distribution when Doppler broadening is added to a pure Lorentz broadened line. Only the region near the peak absorption coefficients is shown (i.e. near g=1.0) since the line tail absorption coefficient distribution is unaffected by the inclusion of Doppler broadening.

A non-integer number of lines n.x (x denotes a fractional line) is treated by consideration of a distribution consisting of n lines of strength S_1 and a single line of strength S_2. The strengths are constrained to both preserve the total interval strength (i.e. $S=S_1+S_2$) and the effective number of lines n.x. These lines are used in the Monte Carlo simulation described above to determine f(k) for a non-integer number of lines.
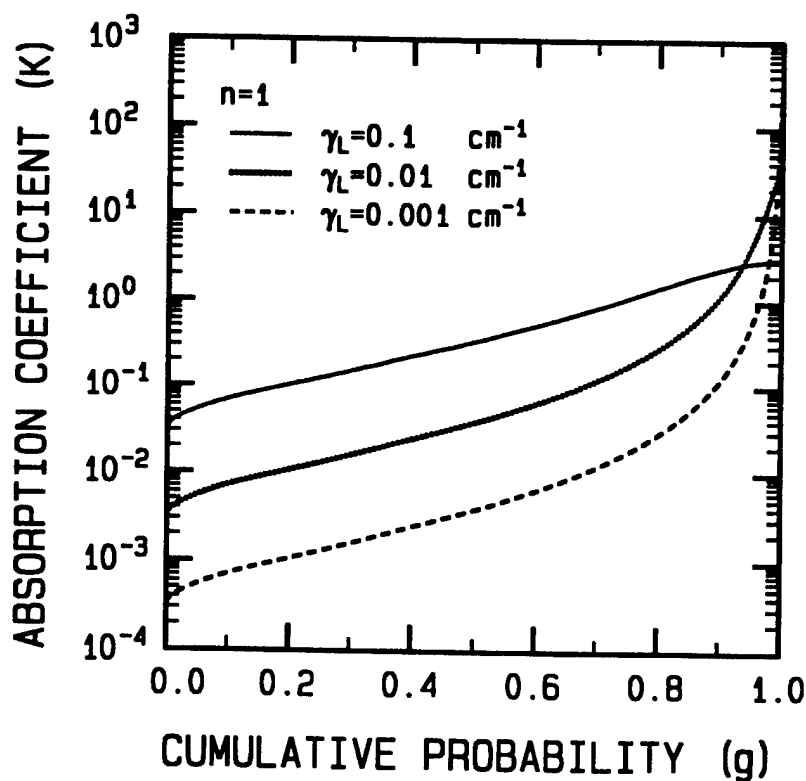
Figure 36. Dependence of k(g) on the Lorentz Line Width γ_L for γ_D=0.0 cm^{-1} and n=1
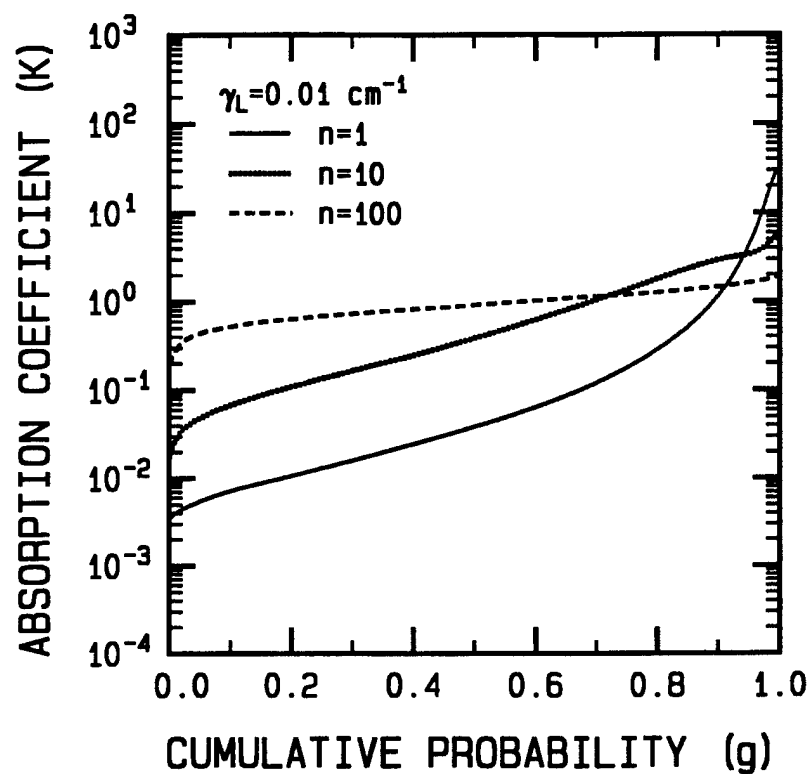
Figure 37. Dependence of k(g) on the Number of Lines n for γ_L =0.01 cm^{-1} and $\gamma_{D\,L}$ =0.0 cm^{-1}
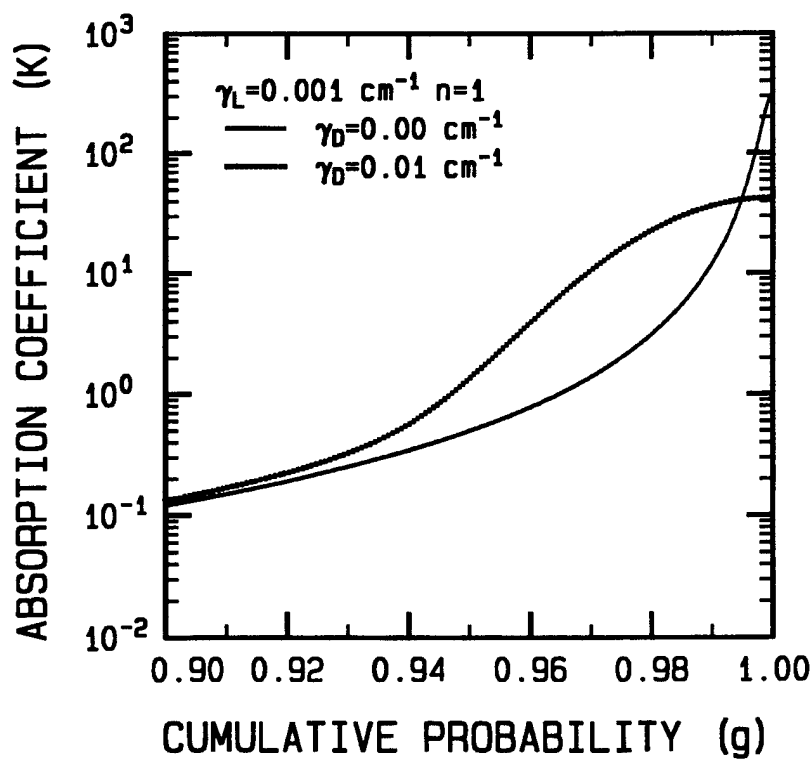
Figure 38. Effect on k(g) for Inclusion of Doppler Broadening for n=1 and γ_L =0.001 cm^{-1}

3.3.2 Determination of the MODTRAN k(g) Table

A table of $k(g)$ distributions was constructed for real time use during a MODTRAN run. Each tabulated $k(g)$ distribution corresponds to a specific set of values for n, γ_L, and γ_D and a reference interval strength of $S=1$ cm^{-2} atm^{-1}. The ranges of values considered for these parameters were chosen to be compatible with radiative transfer calculations covering the altitude range 0-70 km, the spectral range 10-10,000 cm^{-1}, and including all the MODTRAN atmospheric species. This translated into the ranges of $0.2-10^{-6}$ cm^{-1} for γ_L, $0.02-10^{-5}$ cm^{-1} for γ_D, and 1-90 for n. Each of these ranges was spanned by a logarithmic scale of values with a spacing factor of $2^{1/2}$. This resulted in approximately 10,000 tabulated distributions where each distribution was represented at 33 g values. The overall size of the $k(g)$ data base is 1.4 mbytes. The g values were selected so that the $k(g)$ distribution with the largest dynamic range in k values would have each decade of k values covered by approximately 3 (k_i, g_i) points. It would be preferable from a computational speed point of view to span each decade with fewer points; however, as shown later 3 points per decade is a reasonable trade off between computational speed and accuracy. The largest dynamic range occurs for n=1, $\gamma_L=10^{-6}$ cm^{-1}, and $\gamma_D=10^{-5}$ cm^{-1}. Most of the g_i points were selected based on the logarithmic scale

$$g_i = 1 - 10^{-5}(1.46780)^i, \tag{12}$$

where i ranged from 1 to 30. Three additional points were added, g=1 for the peak, and g=0.05 and g=0.1 to resolve structure near g=0.0. The selection of g values for this stressing case is illustrated in Figure 39 which shows that the distribution spans 12 orders of magnitude, and in Figures 40-42 which provide a more detailed look at various portions of the distribution. Each (n, γ_L, γ_D) distribution is tabulated at the same g_i grid points as indicated in these figures. During a MODTRAN calculation the (k_i, g_i) points for each atmospheric layer are found by a three dimensional linear interpolation over n, γ_L, and γ_D.
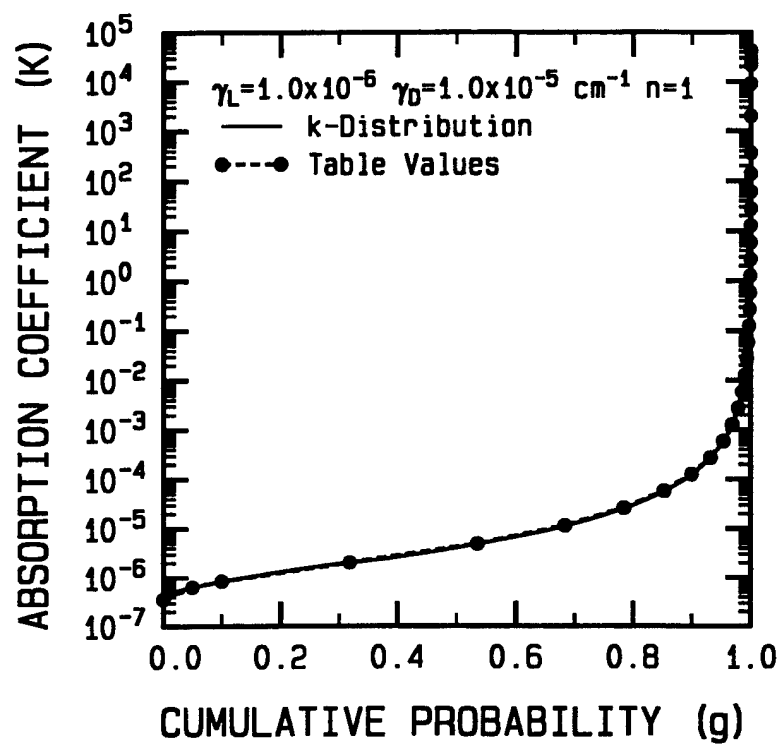
Figure 39. Selection of gi Table Values for the k(g) Distribution with the Largest Dynamic Range of k Values
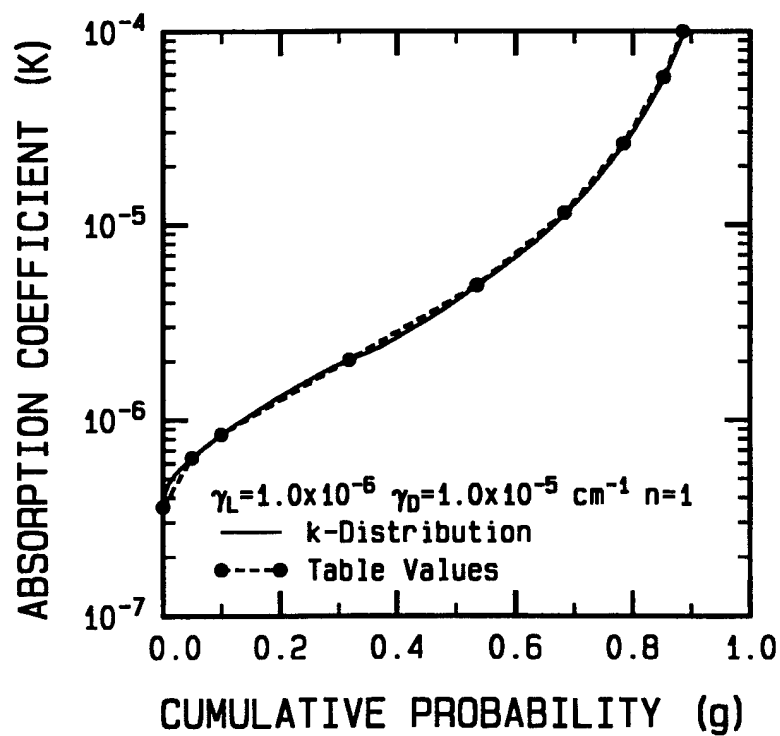
Figure 40. Same as Figure 39 But Showing an Expanded k range near k_{min}
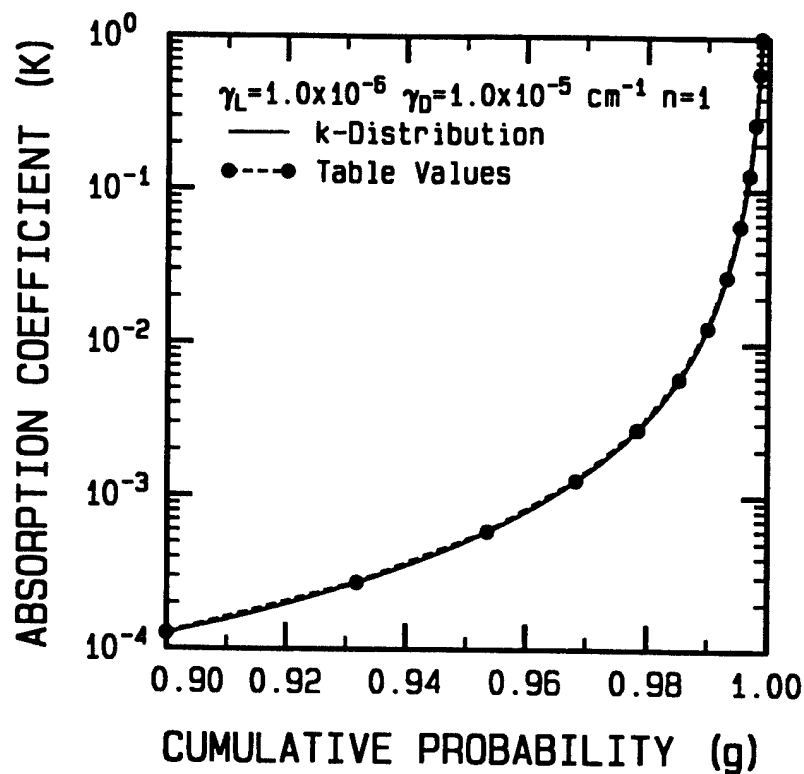
Figure 41. Same as Figure 39 But Showing an Expanded k and g Scales
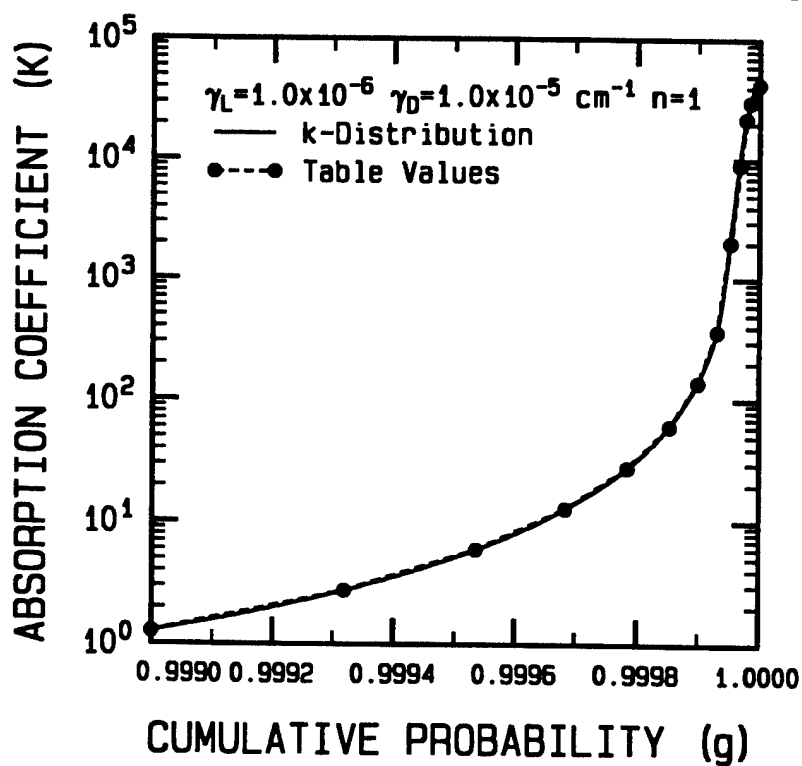
Figure 42. Same as Figure 39 But Showing an Expanded k and g Scales

54

3.3.3 Determination of Effective Sub-interval Absorption Coefficients

We adopt the approach of Lacis and Oinas (*Lacis and Oinas*, 1991) for determining an effective absorption coefficient $\overline{k}_i$ for the sub-interval $\Delta g_i = g_{i+1} - g_i$ which preserves the average transmittance for each atmospheric layer. It is given by

$$\exp(-\overline{k}_i u) = \frac{1}{\Delta g_i} \int_{g_i}^{g_{i+1}} dg \, \exp(-k(g)u). \tag{13}$$

Since we have tabulated the k(g) distribution over a relatively coarse grid, an assumed functional form for the k variation over Δg is required in order to evaluate Equation (13). An exponential variation is assumed

$$k = k_i \exp(b(g - g_i)), \tag{14}$$

where b is given by

$$b = \frac{\ln(k_{i+1}/k_i)}{\Delta g_i}. \tag{15}$$

This variation is a reasonable representation of k(g) as can be seen in Figures 40-42 where the tabulated points are connected with straight lines (i.e. this is equivalent to Equation (14)). There are differences of several percent with the actual k(g) in some places; however, this case is the most stressing one. When eqs.(14) and (15) are substituted into Equation (16) the final expression for $\overline{k}_i$ becomes

$$\overline{k}_i = -\frac{1}{u} \ln(\frac{E_1(k_i u) - E_1(k_{i+1} u)}{b \Delta g_i}), \tag{16}$$

where E_1 is a first order exponential integral. From Equation (16) it is clear that the effective absorption coefficient is a function of the absorption column density u. While this approach preserves the average transmittance for each layer in a multi-layer calculation, it does not preserve the total path transmittance.

55

In general, the CK transmittance T_{CK} and the bandmodel transmittance T_{BM} for the same values of S, γ_L, γ_D, and n will not be identical. This is illustrated in Figure 43 for a 500 km horizontal path at 15 km altitude; differences in the model transmittances as large as approximately $\forall$ 10% are evident. Although both transmittance formulations are based on the same underlying physical assumptions (i.e. equal strength positionally uncorrelated lines), the implementation of each involves different numerical approaches and approximations. In order to maintain internal consistency in MODTRAN between the two approaches, the CK absorption coefficients are adjusted to exactly preserve the bandmodel transmittance for each layer. This is achieved by determining the fractional change in the $\overline{k}_i$'s from Equation (16) required to change T_{CK} into T_{BM}. It can be shown that the fractional change δ can be related to the transmittance difference $\Delta T = T_{CK} - T_{BM}$ through a Taylor expansion of the CK transmittance function Equation (6) and is given by

$$\Delta T = -\delta \sum_{i=1}^{imax} \Delta g_i \overline{k_i} u \exp(-\overline{k_{iu}}) + \frac{\delta^2}{2} \sum_{i=1}^{imax} \Delta g_i \overline{k_i^2} u^2 \exp(-\overline{k_i} u), \tag{17}$$

where the value of δ of interest corresponds to the negative root of this quadratic equation. This approach does not preserve the total path transmittance for multi-layer paths as is evident in Figure 44 for a vertical path from 5 km to space; the largest differences are approximately $\pm 7\%$.

In summary, a new CK approach has been developed and integrated into MODTRAN. We are currently using this new capability to analyze infrared observations of clouds in the thermal and solar multiple scattering regimes.
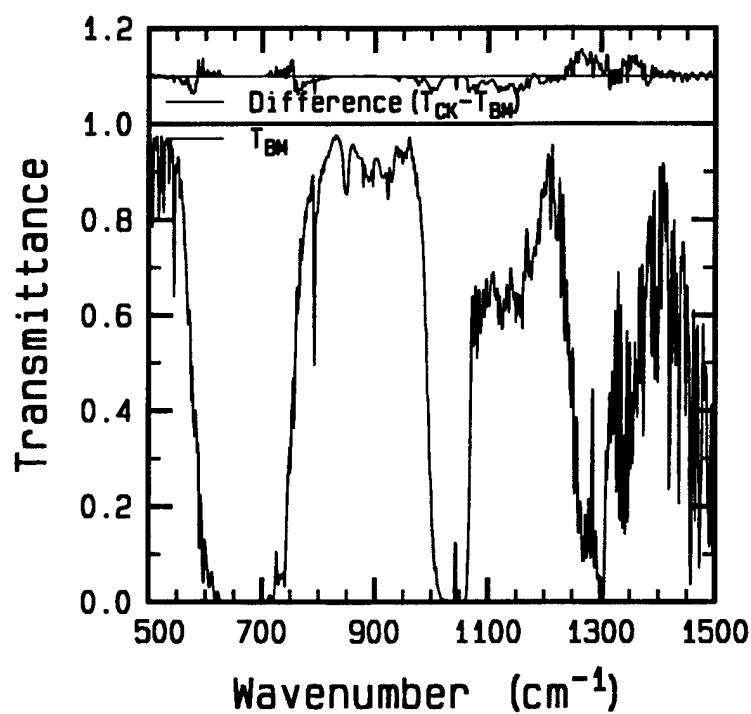
Figure 43. Comparison of Computed Transmittances for the Correlated-k (CK) and bandmodel (BM) Approaches for a 500 km Horizontal Path at 15 km Altitude
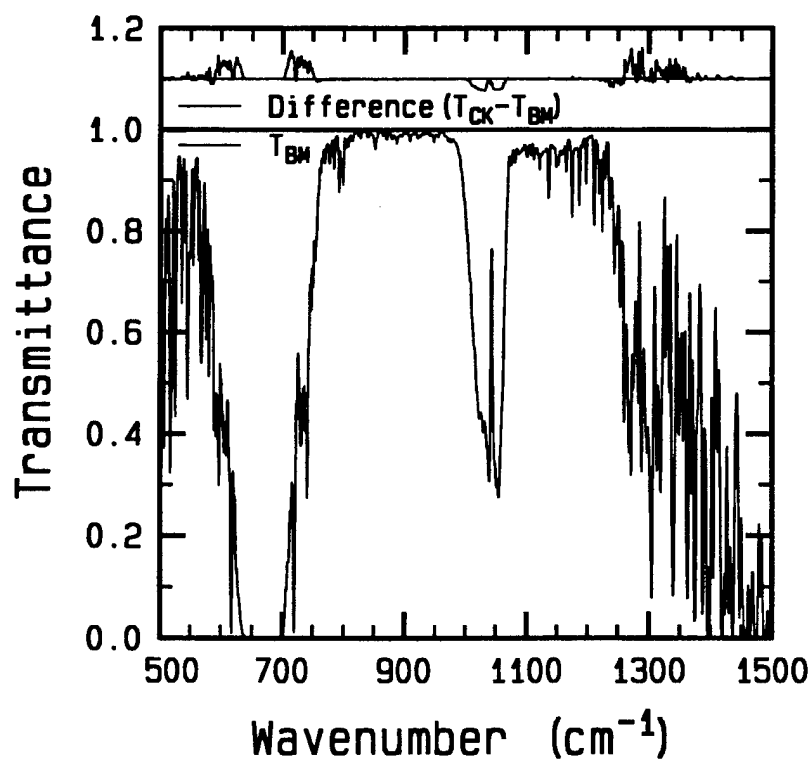
Figure 44. Same as Figure 43 Except for a vertical Path from 5 km to Space

4.0 VERY NARROW BAND MODEL CALCULATIONS OF ATMOSPHERIC FLUXES AND COOLING RATES

Because of the large computational speed advantage afforded by band models over line-by-line(LBL) models the development and application of band models to the calculation of atmospheric radiative fluxes and cooling rates continues to be an active area of research. A wide variety of narrow band model(NBM) and wide band model(WBM) approaches have been developed. Typically the calculational spectral resolution, $\Delta\omega$, of the NBMs falls within the $5 \leq \Delta\omega \leq 20$ cm^{-1} range, while for the WBMs $\Delta\omega \geq 100$ cm^{-1}. Most of the band model approaches are based on one of just a few simple analytical functions that approximately represent the average transmission of a finite spectral interval for a homogeneous path. Application of these functions to the atmospheric problem requires further approximations in order to handle the inhomogeneous atmospheric path properties as well as the effects of spectrally overlapping bands from different species. Direct application of these band models to the calculation of atmospheric fluxes and cooling rates usually results in poor to only fair agreement with LBL calculations. In order to circumvent this problem the band models are treated as parameterizations rather than as first principles models. One or more model parameters are then adjusted to yield a best fit to LBL reference transmittance or atmospheric flux calculations. These tuned band models can yield atmospheric flux and cooling rate predictions of LBL-like quality.

A new very narrow band model(VNBM)approach [Bernstein *et al.*, 1996] has been developed which yields atmospheric flux and cooling rate predictions of near LBL quality without the necessity of tuning the VNBM to a specific set of LBL reference calculations. The VNBM is incorporated in the Phillips Laboratory MODTRAN [*Berk et. al.*, 1998] atmospheric transmittance-radiance code which enables general specification of the atmospheric species, concentration and thermodynamic profiles, calculational spectral interval, and path geometry. and incorporated into the MODTRAN atmospheric transmittance-radiance code. The VNBM approach includes a computational spectral resolution of 1 cm^{-1}, a single-line Voigt equivalent width formalism based on the Rodgers-Williams approximation which accounts for the finite spectral width of the interval, explicit consideration of line tails, a statistical line overlap correction, a new sub-layer integration approach which treats the effect of the sub-layer temperature gradient on the path radiance, and the Curtis-Godson(CG) approximation for inhomogeneous paths. An additional and new correction for exact and near-exact line overlap is introduced as a modification to the determination of the band model line density parameter, $1/d$. The

standard two parameter CG approximation is used for H_2O and CO_2, while the Goody three parameter CG approximation is used for O_3. Atmospheric flux and cooling rate predictions using MODTRAN are presented for H_2O (with and without the continuum), CO_2, and O_3 for several model atmospheres. The effect of doubling the CO_2 concentration is also considered. These calculations are compared to line-by-line(LBL) model calculations using the AER, GLA, GFDL, and GISS codes.

The availability of these LBL calculations is an outgrowth of the Intercomparison of Radiation Codes used in Climate Models (ICRCCM) study. The results from the ICRCCM study indicated that band model calculations of atmospheric fluxes and cooling rates which included all the atmospheric species demonstrated the best overall agreement with LBL calculations. However, the agreement was much poorer when only single species were considered and also when calculations of the sensitivities of the fluxes and cooling rates to changes in species concentrations were performed. The focus of this study is on the individual species H_2O (with and without continuum), CO_2, and O_3. Several model atmospheres are considered as well as the sensitivity to a doubling of the CO_2 mixing ratio. Each of these molecules challenge different aspects of an atmospheric radiative transfer model. H_2O dominates the clear sky tropospheric atmospheric cooling and its concentration can vary extremely rapidly with altitude. CO_2 dominates the cooling above the tropopause and thus requires that the effects due to the Voigt line shape function be reflected in the model. O_3 is of interest because its mixing ratio increases strongly with increasing altitude. This is a troublesome behavior for the Curtis-Godson approximation often employed in band model codes to account for the non-uniform distribution of absorbers along the line of sight path.

The MODTRAN calculations are based on a 0-3,000 cm^{-1} spectral interval, a 60 layer atmosphere, and a two angle quadrature integration. It was demonstrated for H_2O, CO_2, and O_3 that the MODTRAN predictions fall within the spread of the LBL results. We estimate, based on previous comparisons of MODTRAN to FASCODE transmittance calculations, that the computational speed of MODTRAN is in the range of 10 to 100 times faster than that for the LBL models. The unique combination of computational speed, 1 cm^{-1} spectral resolution, wide spectral coverage, wide selection of and ease of adding new species, and near LBL accuracy afforded by MODTRAN makes it an attractive alternative to LBL models for applications in which absolute accuracy is not the sole criterion for code selection.

5.0 CREATION OF A MODTRAN INPUT FILE FROM RADIOSONDE MEASUREMENTS

Local radiosonde measurements of temperature, pressure and atmospheric absorbers such as water and ozone can be used in MODTRAN to model the local radiative environment. For this purpose MODTRAN must be run with the MODEL = 7 option, enabling it to read in radiosonde data from the input file, called TAPE5. This section describes the workings, requirements and I/O, of a program, called SNDTP5, which converts radiosonde measurements into a TAPE5 format.

The input to SNDTP5 consists of radiosonde measurements of pressure, temperature and water vapor content at various altitude levels. Typically, radiosonde measurements are performed at several thousand altitudes ranging from the surface of the earth to tens of kilometers. The number of atmospheric altitude levels acceptable to MODTRAN is currently 61. This number is set by a FORTRAN parameter and can be increased at will. However, if MODTRAN is to be executed repeatedly, there is a need for a program like SNDTP5 which "compresses" data at thousands of altitude levels into a reasonable number. This is also determined by a parameter, and currently set to MODTRAN's 61. It also can be increased at will; of course, all FORTRAN codes must be recompiled once a parameter is changed.

5.1 Summary of Important Features

- SNDTP5 can be executed interactively or in the batch mode.

- The radiosonde data can be in any arbitrary units permitted in MODTRAN. TAPE5 outputs are in millibars for water and pressure, and Kelvin, for temperature.

- MODTRAN default profile values are written out for altitudes beyond the highest sonde altitude. The MODTRAN default profiles are chosen based on a least-squares match of water and temperature values to data. Consequently, there are two TAPE5's written out, one corresponding to best-match temperature and the other, to H\2O. The user also has the choice of smoothly blending in MODTRAN default profiles with data at higher altitudes.

- The user may have up to 10 layers of data closest to the ground retained "as is" in TAPE5.

- The user may discard noisy/inaccurate layers of data both near the ground and at the top.

- In order to maximize the number of layers in the measurement region, the user has control over the highest MODTRAN altitude in TAPE5, in lieu of simply accepting the standard 100 km. Most users probably will set this altitude to 70 km. Of course, more altitudes in the sonde-region means fewer in the upper atmosphere, and vice versa.

5.2 General Description of the SNDTP5 Program

The SNDTP5 program incorporates and satisfies several common sense ideas and requirements.

PROGRAM EXECUTION

SNDTP5 is a rather general program. Therefore, it queries the user for several inputs to be described later. There are two ways to run this program, interactively or in the batch mode. Helpful information is displayed during interactive sessions. Two annotated sample batch input files are included for ease of editing. SNDTP5 can be executed in the batch mode on PC's and UNIX systems by typing: "SNDTP5 < batchfile".

ALTITUDE REGIONS

The radiosonde is often inaccurate at higher altitudes, typically above 20 km or so. The surface measurements also appear to be unstable for the first few altitude levels. Therefore, the program queries the user for two altitudes (SNDBOT and SNDTOP), below and above which the data are ignored. The region bounded by SNDBOT and SNDTOP is referred to as the sonde-region.

Below SNDBOT, there are several choices. Two of these are either to do nothing, in which case SNDBOT becomes the ground level, or to input surface meteorological information. The other choices are to use MODTRAN model profiles or to extrapolate (via interpolation) radiosonde data down to 0 km.

We have modified MODTRAN to accept negative ground altitudes for the atmosphere and lines-of-sight (LOS's) as the the radiosonde data can actually start from below the sea level.

Above SNDTOP, MODTRAN builtin profiles are used. The choice of the builtin MODTRAN profiles, of which there are six, is based on least-squares-matches of radiosonde data to MODTRAN profiles. Two separate TAPE5's are output based on best match to temperatures and to water values.

61

Depending on user inputs, the least-squares procedure does not necessarily match the entire sonde-region values to the MODTRAN models. The reason is that at higher altitudes, the radiosonde measurements (particularly, relative humidity) tend to be inaccurate. Also, close to the ground, the measurements probably reflect the local terrain, geography and weather characteristics. Therefore, a subregion of the region is used for matching against MODTRAN models which are essentially averages in time and space over large areas of the globe. The user is asked to supply the bottom (SUBBOT) and top (SUBTOP) of a subregion contained inside the sonde-region for the least-squares match.

As mentioned in the above paragraphs, MODTRAN model profiles are used at altitudes above SNDTOP. However, in order to avoid abrupt discontinuities in the atmospheric quantities, the user is queried to supply an intermediate value: SNDMID, SNDBOT $\leq$ SNDMID $\leq$ SNDTOP. From SNDMID to SNDTOP, a linear combination of radiosonde measurements and MODTRAN profiles are used. At SNDMID the linear combination coefficient is unity for the measured data and 0 for the MODTRAN values; at SNDTOP, the coefficients are reversed.

UNITS AND CONTENTS OF THE RADIOSONDE DATA FILE

Typically, radiosonde water measurements are in relative humidity. However, SNDTP5 can accept water content in any of these eight MODTRAN units: ppmv, cm^{-3}, g/kg, g/m^{-3}, dew point in K and C, and relative humidity in percent. Pressure values can be in mb, torr or atm. The temperature units can be in C or K. However, the TAPE5 outputs of SNDTP5 will be in units of K, mb and mb for temperature, pressure and water vapor.

It is assumed that radiosonde data are stored in a file each line of which is in this format: altitude, pressure, temperature, water content, ... The altitudes can be in either increasing or decreasing order. There must be one set of data per altitude per line. Any additional information present, for example, time, is ignored by SNDTP5. The numbers are read using list-directed, that is, unformatted read. Sometimes the balloon performing measurements bobs up-and-down near the highest altitude. Therefore, SNDTP5 stops reading data at the first sign of a decreasing altitude.

The SNDTP5 program uses data without any error correction. Bad data points in the sonde-region are not dropped. If the user suspect that a data point is bad, s/he can either edit that line out of the file or replace the bad data by a negative number less than or equal to -999.0. The SNDTP5

program will treat that entry as a "missing" value and will replace it by an interpolated value. The user has the choice of doing this automatically for the first 10 layers.

Throughout, SNDTP5 uses linear interpolation for temperature. Exponential interpolation of P/T and partial pressure divided by T is used for atmospheric pressure and water. Division by T converts these quantities to number densities.

FILE NAMES

The user is queried for a file root name, which for illustration purposes in this writeup is assumed to be ROOT. SNDTP5 assumes that the radiosonde data resides in a file called ROOT.SND. If these is no such file, SNDTP5 looks for a file called, simply, ROOT. The TAPE5 output files will

be called ROOT.TP5T and ROOT.TP5W. ROOT.TP5T is the TAPE5 which has the MODTRAN built-in profile values based on the best least-squares-match to temperatures; ROOT.TP5W has values based on best match to water values. Miscellaneous information is output to a file called

ROOT.OUT. Information for plotting purposes is contained in the file ROOT.DAT. It has both the radiosonde data (in TAPE5 units) and the TAPE5 information, separated by a blank line.

CONSERVATION OF COLUMN DENSITIES AND TAPE5 ALTITUDES

The most important quantities that determine transmittance and radiance are the column densities of species along the LOS. Therefore, it is important how both the TAPE5 altitudes and the species concentrations at these altitudes are chosen to represent the radiosonde data.

How the TAPE5 altitudes are chosen is described later. Once these altitudes are chosen, the species concentrations cannot simply be chosen by interpolating radiosonde measurements. If the number of TAPE5 layers were not restricted to 61 or so, interpolation may actually preserve column densities. But 61 layers is not sufficient for this purpose. So the TAPE5 concentrations and altitudes are a compromise between conservation of vertical column density and reproduction of the detailed humidity and temperature profiles.

The water concentration at a TAPE5 altitude is determined from the cumulative water amount which is computed by adding up the layer amounts in data. The adding process starts from the top as it is much less error prone that starting from the bottom. At certain altitudes, this method may result

in a TAPE5 concentration which differs significantly from the radiosonde data. This is particularly true if the data changes sharply in a very thin interval. If this occurs, we set the TAPE5 value to the interpolated value.

Pressure can be calculated similarly. However, experience suggests that simple exponential interpolation of P/T is sufficient to conserve column density of air, and the more elaborate scheme is not necessary.

Temperature is determined by assuming linear variation at all altitudes.

DETERMINATION OF ALTITUDES FOR TAPE5

SNDTP5 selects TAPE5 altitudes based on one of three schemes. The MODTRAN code has a FORTRAN parameter LAYDIM which can be set to accommodate arbitrary number of altitudes; the code must be recompiled if LAYDIM is changed. LAYDIM is also used in SNDTP5 and set to the current MODTRAN value. If any of the schemes comes up with a number of altitudes which exceeds LAYDIM, the program will stop with an appropriate message.

SCHEME 1 The TAPE5 altitudes (in kilometers) are individually read from a file. The altitudes must be in the file one per line and in increasing or decreasing order. The SNDBOT and SNDTOP will be inserted in the altitude grid if they differ from grid points. Altitudes below SNDBOT are ignored.

SCHEME 2 The TAPE5 altitudes (in km) will be computed from a file containing: EndPt1, EndPt2, Delta1, EndPt3, Delta2, ..., EndPtN, DeltaN-1

EndPt1 is the earth surface and EndPtN is the top of the atmosphere (TOA). Delta1 is the altitude increment for the region from EndPt1 to EndPt2, Delta2 is the increment in the region from EndPt2 to EndPt3, ... The values must be one per line or in the following format:

EndPt1, EndPt2, Delta1
EndPt3, Delta2
...
EndPtN-1, DeltaN-2
EndPtN, DeltaN-1

The SNDBOT and SNDTOP will be inserted in the altitude grid if they differ from grid points. Altitudes below SNDBOT are ignored.

SCHEME 3 This is the most useful and automatic altitude scheme. Most users are expected to use this method.

Radiosonde pressure and water concentration (in practice in percent relative humidity) arrays are converted into mb (millibar) units. Temperature, pressure and H\2O arrays are then examined for local minima and maxima. In practice, pressure and temperature do not possess significant extrema points, only the water profile does. Finding extrema array in water is not an exact science. We have tried to detect L- and elbow-shaped extrema in addition to the usual ones. This involved some experimentation on using thresholds. The H_2O data usually has lot of bumps in it. Therefore prior to finding extrema, the data is averaged over an width of, say, 100 meters.

All the extrema are then combined to form an array of altitudes. The extrema points are candidates for TAPE5 altitudes. But there may not be enough of them. So, the user is queried for an increment (DELSND) which is then used to form an altitude grid in the sonde-region. By combining this grid with the extrema array, a new altitude grid is formed. Still there may not be enough altitudes in the sonde region. There SNDTP5 also requires an input for the minimum number of altitudes (NMNSND) acceptable in the sonde-region. The actual number of layers will exceed NMNSND if possible. The input NMNSND must equal or exceed {(SNDTOP-SNDBOT)/DELSND + 1}.

(As mentioned, the minima and maxima are found by using thresholds on smoothed raw data. The thresholds and smoothing windows are both gradually increased, if needed, until the total number altitudes in TAPE5 equals the MODTRAN limit.)

Next the altitudes from the top of the sonde-region to the TOA are chosen. For this purpose, the user can either choose the built-in MODTRAN altitudes or input individual altitudes explicitly.

The total number of MODTRAN input altitudes are now computed. The program will then output a MODTRAN input file if the total number of altitude does not exceed LAYDIM. If this condition is not met, the program will terminate with an appropriate message.

5.3 SUMMARY OF USER INPUTS

1. Radiosonde data units for altitudes, pressure, temperature and H\2O.
2. Root name of the radiosonde data file.

3. SNDBOT and SNDTOP (optional).

4. SUBBOT, SUBTOP and SNDMID (for matching radiosonde data with MODTRAN profiles, see comment below).

5. TAPE5 altitude scheme.

6. File names (optional for altitude schemes 1 and 2).

7. DELSND, NMNSND (for altitude scheme 3)

8. Options and data (optional) for action below SNDBOT.

All FORTRAN parameters reside in the file PARMS.H. These need not be changed often; the program must be recompiled if they are changed.

In addition to inputting SUBBOT, SUBTOP and SNDMID explicitly, there are two other choices. The user may input "1" which sets SUBBOT = SNDBOT, SUBTOP = SNDTOP and SNDMID = SNDTOP. An input of "2" is identical to "1" in all respects except that SNDMID is one-tenth of the way (one-tenth of the width of the sonde-region) below SNDTOP. An input of "3" requires all three inputs explicitly.

5.4 TWO ANNOTATED SAMPLE INPUT FILES

Both input files are for the altitude scheme 3 where the TAPE5 altitudes are selected by examining extrema of the radiosonde data.

The input file below drops data below 0.33 and above 22 km. Note that the input line containing "TAPE1" cannot be annotated as this line is read as a character string. See the previous section for understanding the input for defining the subregion for matching and blending with the MODTRAN internal profiles.

```
TAPE1
1       (1 KM,  2 M)
1       (1 MB,  2 ATM,  3 TORR)
2       (1 K,  2 C)
8       (1 PPMV,  2 CM-3,  3 G/KG,  4 G/M3,  5 MB,  6 DP  (K),  7 DP  (C),  8 RH)
1       (DROP DATA BELOW AN ALT?  1/0.  NEXT LINE:  ALT IF 1, NO. OF "AS IS" LYRS IF 0)
.33
1       (IGNORE DATA ABOVE AN ALTITUDE?  1=YES, 0=NO.  IF 1, NEED ALTITUDE BELOW)
22
3       (1, 2, 3 FOR ALTITUDE SCHEME, ISCHEM)
2.0     (DELSND, FOR ISCHEM=3)
32      (NMNSND, FOR ISCHEM=3)
1       (1, 2, 3 FOR ALTITUDES ABOVE THE SONDE-REGION, ITOP)
70.     (MAXIMUM TAPE5 ALT)
1       (1, 2, 3 FOR DEFINING SUBREGION FOR MATCHING AND BLENDING W/ MODTRAN MODEL)
1   (OPTION BELOW SONDE 1=DO NOTHING. 2=SURF DAT. 3=INTERP TO 0 KM. 4=MODTRAN MODEL)
```

This input file does not drop any data. It prints the three lowest layers "as is". Note that one cannot have any "as is" layers while at the same time ignore data below a certain altitude.

```
TAPE1
1       (1 KM, 2 M)
1       (1 MB, 2 ATM, 3 TORR)
2       (1 K, 2 C)
8       (1 PPMV, 2 CM-3, 3 G/KG, 4 G/M3, 5 MB, 6 DP (K), 7 DP (C), 8 RH)
0       (DROP DATA BELOW AN ALT?  1/0.  NEXT LINE:  ALT IF 1, NO. OF "AS IS" LYRS IF 0)
3
0       (IGNORE DATA ABOVE AN ALTITUDE?  1=YES, 0=NO.  IF 1, NEED ALTITUDE BELOW)
3       (1, 2, 3 FOR ALTITUDE SCHEME, ISCHEM)
2.0     (DELSND)
40      (NMNSND)
1       (1, 2, 3 FOR ALTITUDES ABOVE THE SONDE-REGION, ITOP)
70.     (MAXIMUM TAPE5 ALT)
1       (1, 2, 3 FOR DEFINING SUBREGION FOR MATCHING AND BLENDING W/ MODTRAN MODEL)
1       (OPTION BELOW SONDE 1=DO NOTHING, 2=SURF DAT, 3=INTERP TO 0 KM, 4=MODTRAN MODEL)
```

5.5 Example Calculations

Here we show several plots of radiosonde data and TAPE5 values for a typical set of radiosonde measurements. The abscissa values of the circles denote the TAPE5 altitudes. As can be seen from these figures, the SNDTP5 program captures the shape of the radiosonde data reasonably well. These were generated using the input files shown above. Note that in the radiosonde data P and T become zero (0 mb and 0 K) suddenly after 22.855 km. The relative humidity is also essentially zero beyond 22.855 km. The first three plots (Figures 45-47) process the entire sonde region in the data file, from 0.315 km to 68 km. The first three altitudes, at 0.315, 0.320 and 0.330 km, are retained "as is" in TAPE5. Notice the sharp drop in the H\2O value at 0.320 km.

In the second set of three plots (Figures 48-50), data below 0.33 km and above 22 km are dropped.
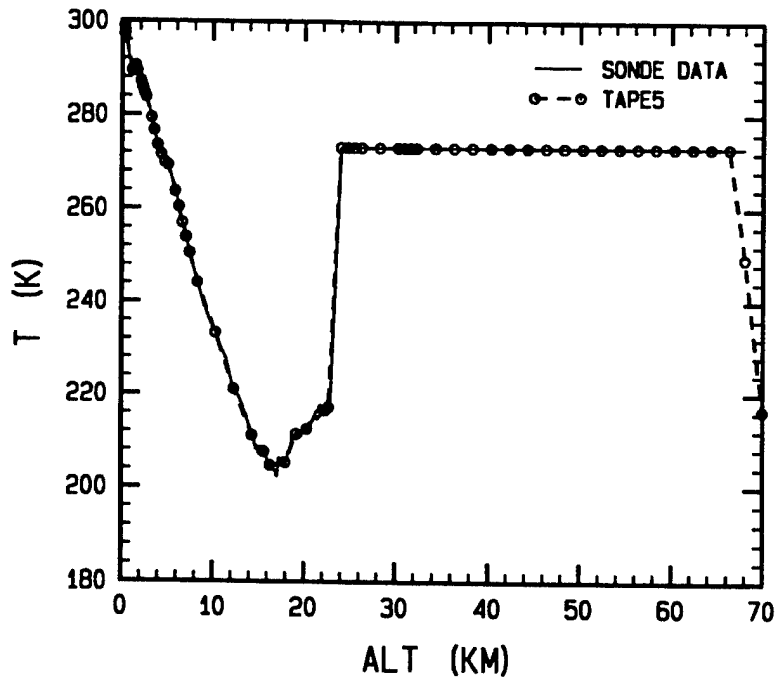
Figure 45. Comparison of Sonde Data and TAPE5 File for Temperature. No Data are Dropped, and the Number of "as is" Layers is 3. The Appropriate MODTRAN Model is Chosen by Matching the Entire Data. However, the Data Abruptly Become Zero (0 mb and 0 K) Above 22.855 km. This Figure is Generated by Using the Second Input File of the Preceding Section.
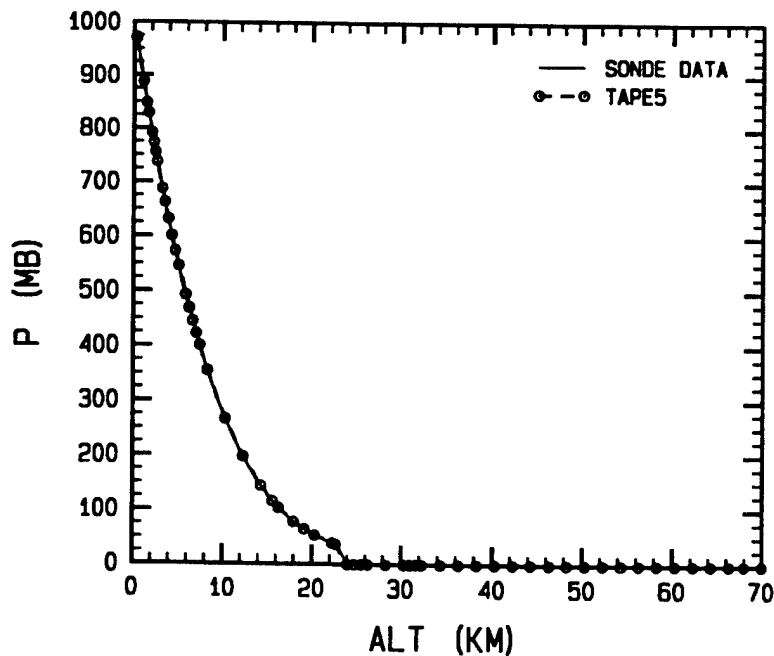
Figure 46. Comparison of TAPE5 vs. Data for Pressure, Generated as in Figure 45.

68
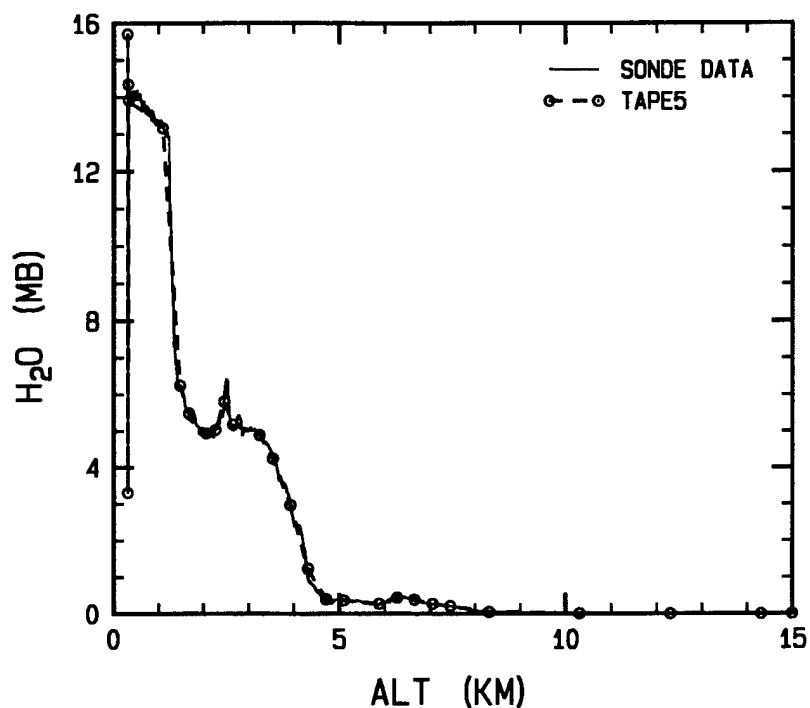
Figure 47. Comparison of TAPE5 vs. Data for Water Vapor, Generated as in Figure 45
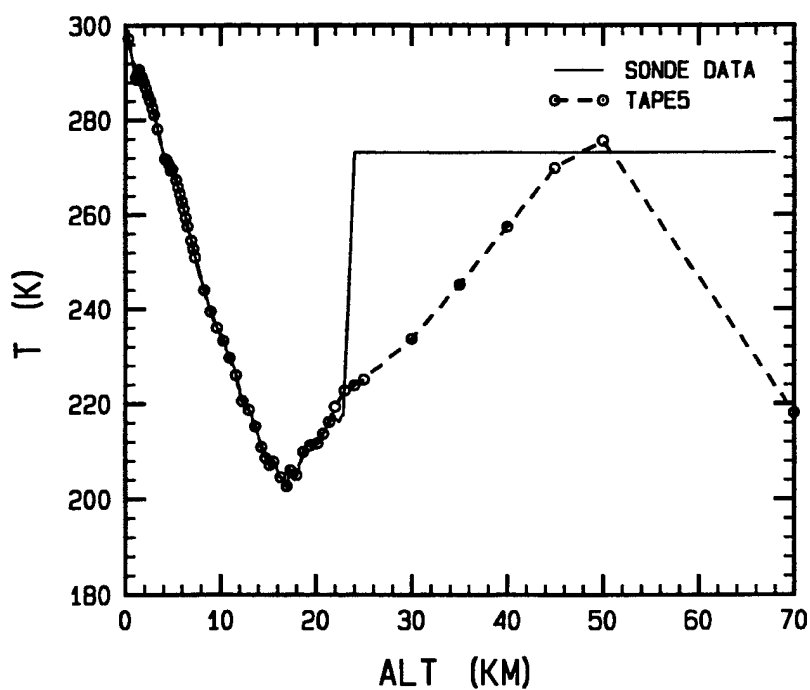
Figure 48. Comparison of Sonde Data and TAPE5 File for Temperature. Data Below 0.33 and 22 km are Dropped Because the Temperature Measurements Fluctuate for the First Few Measurements and All Measurements Become Abruptly Zero Above 22 km. This Figure is Generated by Using the First Input File of the Previous Section.
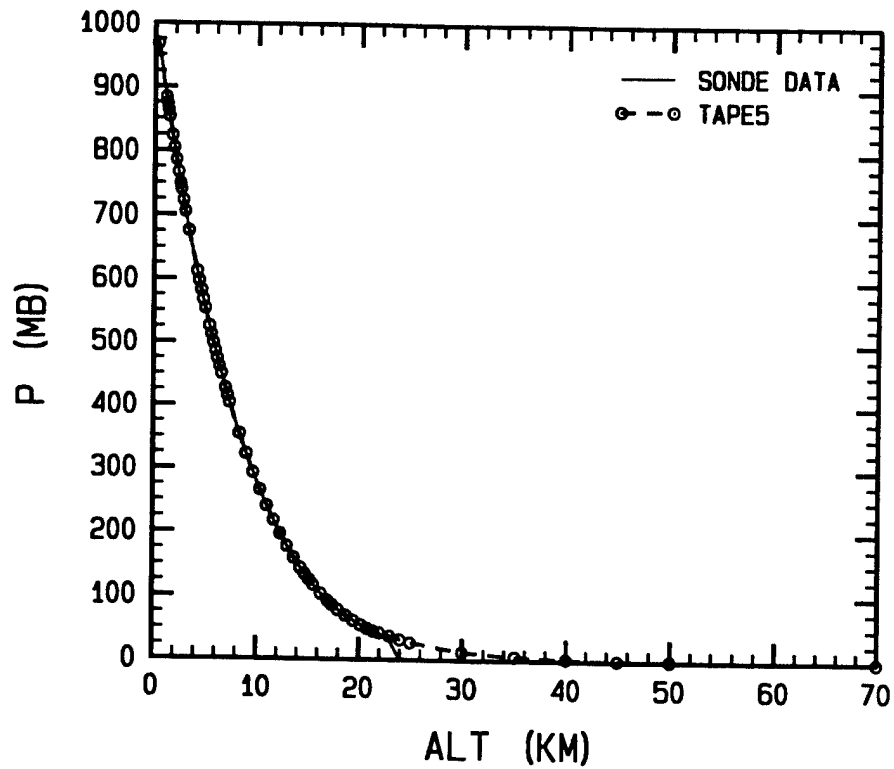
Figure 49. Comparison of TAPE5 vs. Data for Pressure, Generated as in Figure 48
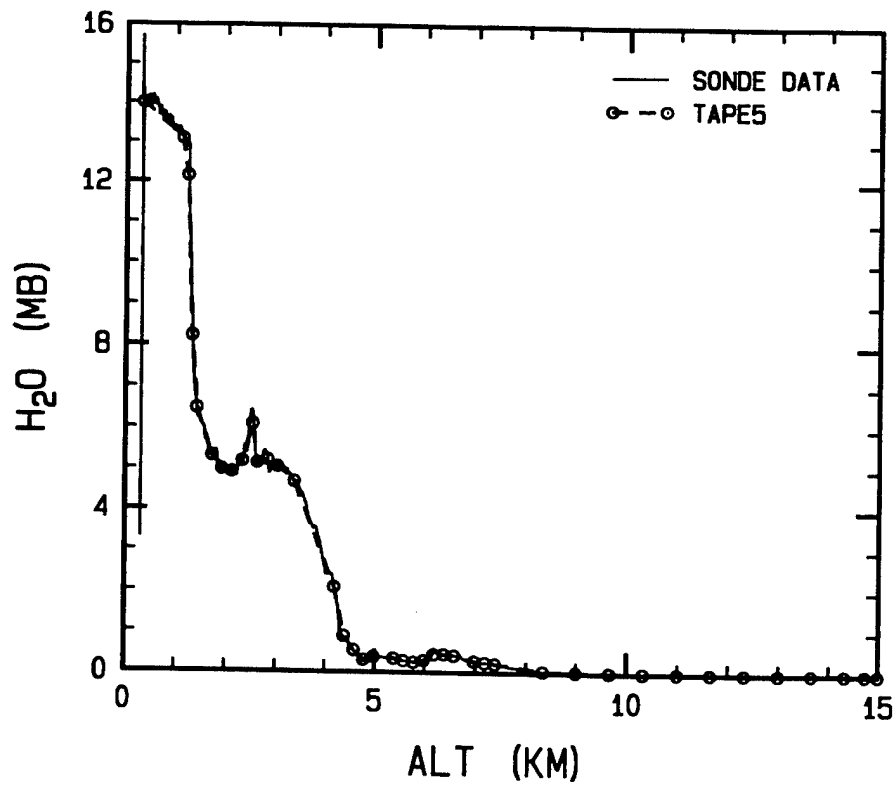
Figure 50. Comparison of TAPE5 vs. Data for Water Vapor, Generated as in Figure 48

6.0 IMPROVEMENTS TO MODTRAN ACCURACY FOR REMOTE SENSING

Real-time or near-real-time optical remote sensing of the atmosphere requires a fast yet accurate computer code for calculating transmittance and/or radiance at the spectral resolution of the sensor. MODTRAN [Berk et al., 1998], a moderate-resolution, band-model-based atmospheric radiation code, has proven valuable for a number of such applications, including remote sensing of temperature and humidity [Anderson et al., 1993] and the calculation of radiative heating and cooling rates [Bernstein et al., 1996].

In the current investigation, we compared MODTRAN3 with "exact" line-by-line calculations for several representative remote sensing applications. We also developed improvements to MODTRAN which provide increased accuracy. Most of the improvements have been incorporated in a new beta test code. Upgrades were made to the O_2 vibrational continuum, the collisional linewidths, the equivalent width formula, and the band model formalism. The band model has been revised to address three problem areas:

(1) Line strength distribution effects. A more sophisticated, 2-line-group model was developed which accounts for effects of a wide line strength dynamic range within a spectral bin. As discussed in this report, the improvements in accuracy are significant for molecules such as ozone that have both a high density of lines and a wide dynamic range of line strengths.

(2) Effects caused by non-random line locations within the spectral bins. Such positional correlation effects are noticeable in a limited number of spectral regions, such as in the NO_2 band near 1600 cm^{-1}. A practical and effective method for adjusting the band model parameters to compensate for these effects was developed and tested in a stand-alone code for uniform paths.

(3) The quasi-continuum representing the line tails that "leak" into or out of the 1-cm^{-1}-wide spectral bins. An improved method for calculating this continuum has been developed.

The results of this work are illustrated with transmittance and spectral radiance comparisons between MODTRAN3, the new beta code, and "exact" FASCODE [Clough et al., 1988] calculations for both horizontal and vertical atmospheric paths. The overall agreement between the spectra from all three codes is found to be quite good for resolutions down to several cm^{-1}.

6.1 Band Model Upgrade

6.1.1 Standard MODTRAN Approach

For the discrete line portion of the spectrum, MODTRAN's calculation of transmittance for a given species has been based on the simple power-law expression,

$$T = (1 - W/\Delta v)^{\Delta v/d} \ . \tag{18}$$

This equation assumes that the spectrum can be represented by a set of $n = \Delta v/d$ lines of identical strength, S, randomly located in the bin of width Δv ($= 1 \ cm^{-1}$); d represents the average line spacing and W the equivalent width of an individual line. W is based on standard formulas applicable to an infinitely wide bin; an approximate correction for the finite bin width is made. Following *Goody and Yung* [1989], the S and n values may be chosen by solving the simultaneous equations

$$nS^{1/2} = \Sigma S_i^{1/2} \tag{19}$$

$$nS = \Sigma S_i \tag{20}$$

where the S_i are the actual line strengths. This solution insures that the sum of the equivalent widths for the model lines matches the sum for the real lines in both the optically thin (linear curve of growth) and thick-Lorentzian (square-root curve of growth) limits. As a result, the correct transmittance is obtained in those same limits as long as the individual line equivalent widths are small compared to the width of the bin, Δv.

A basic problem with this approach is that there is usually a wide range of line strengths in a given bin, so it can be a poor approximation to represent the actual lines by equal-strength lines when the all of the lines are neither very thin nor very thick. The problem is most pronounced at high altitudes, where the lines are closer to Doppler than Lorentzian in shape and the limiting square-root regime for which the model was designed is reached only at extremely high optical depths that are not encountered in the atmosphere.

At lower altitudes, where the lines are nearly pure Lorentzian, the errors are smaller but still significant (up to several percent in transmittance) when the equivalent widths are intermediate between the thin and thick limits. To find the conditions under which this will occur, we examine the equivalent width expression for Lorentzian lines,

72

$$W = Su/(1 + 0.25Su/\alpha)^{1/2} \tag{21}$$

where u is the column density and α is the pressure-broadened half-width. Intermediate equivalent widths occur when the two terms in the denominator of Equation (21) are comparable in size. The effect of W errors on fractional transmittance is greatest when the transmittance is of order 1/e --that is, when W is approximately equal to the average spacing d. Setting $Su/4\alpha = 1$, $W = d$, and $\alpha = 0.07P$ where P is total pressure in atm leads to the condition $1/d = 5/P$ under which sizable transmittance errors are expected. Since P is always 1 atm or less, this occurs only for molecular bands having more than around 5 lines per wavenumber. Generally speaking, these are bands of O_3, N_2O, NO_2, and CH_4.

To reduce the overall errors, the 1/d values may be empirically reduced. In MODTRAN3 this is accomplished by combining lines within sub-bins. This does a reasonable job of accounting for the line density-dependence of the error and gives good results for the test case of a 500 km horizontal path at 15 km. However, no single 1/d value is correct at all optical depths, so substantial errors occur for certain atmospheric paths. For example, as shown in the following subsection MODTRAN3 can give up to a 10% transmittance error in the ozone fundamental band at 40 km altitude.

6.1.2 Modified Approach

To address these problems of the standard MODTRAN band model, we have developed a new model that uses two groups of lines of different strengths to better approximate the actual line strength distribution. The use of four parameters (S_1, S_2, n_1, and n_2) rather than two (e.g., S/d and 1/d) allows (and requires) the incorporation of two extra mathematical constraints. The drawback is that the data storage and computation requirements are increased by almost a factor of 2.

In the current investigation, the constraints on the parameters were taken as

$$n_1 S_1^{p/2} + n_2 S_2^{p/2} = \Sigma S_i^{p/2} \quad , \quad p = 1 - 4 \tag{22-25}$$

where the subscripts "1" and "2" label the line group and the subscript "i" labels the actual line strengths. The $p = 1$ and $p = 2$ equations correspond to Equations (19) and (20). The $p = 4$ equation

insures that the equivalent width sums for the actual and model line distributions are matched through second order terms in line strength. With the addition of the $p = 3$ equation there is a simple, analytical solution which is found to give good overall agreement with calculations that use the exact line strength distribution.

Figure 51 shows comparisons of MODTRAN3 and the new algorithm with FASCOD3 for a 500 km horizontal path at 15 km altitude. (For clarity, only the difference vs. FASCOD3 is shown for the new algorithm.) The agreement with FASCOD3 is quite good overall for both band model codes; the RMS transmittance errors are only 1.8%. It should be noted that these comparisons are superior to ones performed previously [Anderson et al., 1993]due to the O_2 continuum correction, discussed in Section 6.4. The new algorithm provides noticeable improvements in a few troublesome regions, such as on the red sides of the CO_2 and O_3 bands near 600 and 1000 cm^{-1}, respectively. The region near 600 cm^{-1} is significant for remote temperature sensing, and is discussed further in Section 6.5.

For a 1000 km path at 40 km altitude, MODTRAN3 gives good results at most wavelengths but produces up to 10% errors in the O_3 band near 1000 cm-1, as shown in Figure 52.

Initial calculations with the new algorithm gave a smaller but still sizable (around 5%) error in the O_3 band in the opposite direction from MODTRAN3. The sizable error indicates that at very low pressures even two line groups have difficulty in matching the curve of growth generated by the extremely wide range of ozone line strengths. The error is reduced when the range of S is artificially restricted by combining lines that are always optically thin in the atmosphere. To do this, ozone lines that are weaker than a certain cutoff strength are combined into a smaller number of lines that have approximately the cutoff strength; the sum of the strengths is preserved. A reasonable value for the cutoff strength is the Doppler half-width divided by a maximum column density of around 3 atm-cm. The band model parameters were recomputed using the combined lines and the result is shown in Figure 52. The agreement with FASCODE is now reasonable in the ozone band. The RMS error for the entire spectrum is around 20% smaller than with MODTRAN3. The introduction of the strength cutoff has no effect on the spectrum at 15 km altitude or below.

HORIZONTAL PATH, 15 KM ALT.
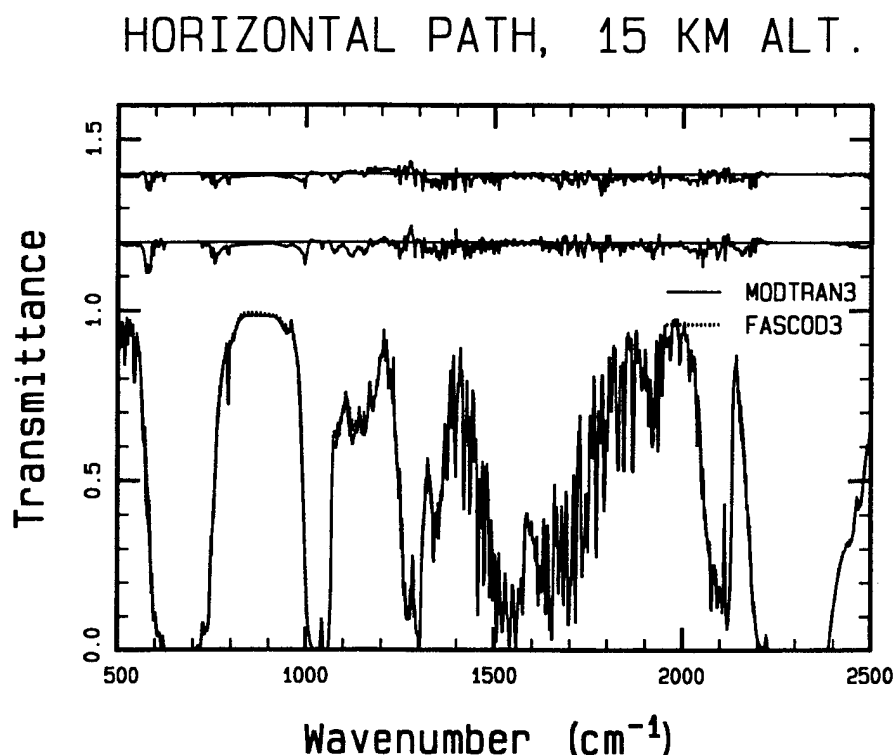
Figure 51. **Comparisons of MODTRAN3, the New Band Model, and "Exact" FASCOD3**
Transmittance Calculations for a 500 km Long Horizontal Path Through the US
Standard Atmosphere at 15 km Altitude. 1 cm^{-1} Spectra were Convolved with a 5
cm^{-1} Wide Slit. The Offset Traces at the Top Show the Difference vs. FASCOD3
for the New Model (Upper Trace) and MODTRAN3 (Lower Trace).

6.1.3 Path Averaging

For treating non-uniform paths, both MODTRAN and the new algorithm use Curtis-Godson averaging of the band model parameters over the varying temperatures and pressures along the path. Separate averages of all parameters, including the Doppler and pressure-broadened half-widths, are computed for each line group of each species. The averaging method implicitly assumes that the spectrum for a given species is comprised of the same actual lines over the entire path, an assumption which may not hold over a wide temperature range. To come closest to this ideal with the two-group algorithm, the most closely corresponding line groups should be averaged together. Since the two line group solutions generally do not correspond to actual lines, there is nothing to identify the groups except their n and S values. For the present, we identify corresponding groups by ranking them in order of their S values. This should be adequate for a small temperature range and when the lines in one group are consistently stronger than in the other.

HORIZONTAL PATH, 40 KM ALT.
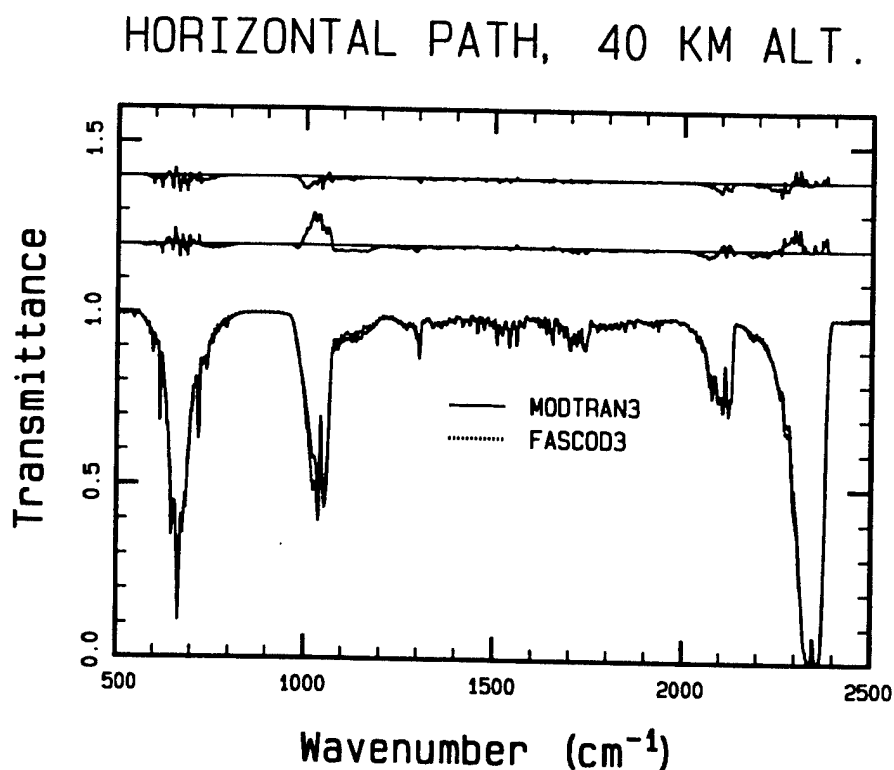
Figure 52. Comparisons of MODTRAN3, the New Band Model, and "Exact" FASCOD3 Transmittance Calculations for a 500 km Long Horizontal Path Through the US Standard Atmosphere at 15 km Altitude. 1 cm^{-1} Spectra were Convolved with a 5 cm^{-1} Wide Slit. The Offset Traces at the Top Show the Differences vs. FASCOD3 for the New Model (Upper Trace) and MODTRAN3 (Lower Trace)

If one set of actual lines dominates at low temperatures and another dominates at high temperatures, the s-ranking approach might not properly identify corresponding groups, causing the averaging method to break down. The single-group MODTRAN method as well as the correlated-k method would also break down in this situation because of the changing line identities. For a wide range of temperature along the path, we expect that the actual transmittance will be smaller than predicted due to reduced line position correlation. The best way to eliminate this problem would be to adopt a more time-consuming line-by-line equivalent width formulation, such as is used in the SHARC [Sundberg *et al.*, 1996] and SAMM [Sharma *et al.*, 1998].

Spectral calculations for a non-uniform, vertical path are presented and discussed in Section 6.5. In this example, the differences between MODTRAN and the 2-line-group algorithm turn out to be qualitatively the same as for a uniform path.

6.2 Compensation for Line Positional Correlation

Like many other band models, MODTRAN implicitly assumes that individual lines are positionally uncorrelated, so that the net transmittance can be approximated as a product of individual line transmittances. Positional correlation among the lines (e.g., due to spin-orbit near-degeneracies, band heads, Q branches, etc.) can increase or (occasionally) decrease line overlap and thereby alter the effective number of lines in the interval, $n = \Delta v/d$. Since the degree of overlap increases with the equivalent widths, correlation effects are more pronounced at low transmittances than at high transmittances. To some extent, at different transmittances different line spacings enter into play. However, in the important middle range of transmittance from around 0.3 to 0.7, where the transmittance is most sensitive to equivalent width errors, the line spacings of interest are on the order of the average line spacing, d.

Through extensive experimentation with simulated spectra, we have developed an efficient and reasonably accurate approach for compensating for line positional correlation. The basic approach was developed for the standard Goody (equal line strength) band model; it involves adjusting the 1/d value (which represents the effective number of lines in the spectral bin) by interpolating between the standard value, which is used for transmittances near unity, and a pre-calculated correlation-corrected value, which is used for transmittances of around 1/e and below. To perform this interpolation, an approximate transmittance must first be calculated using the uncorrected 1/d. A simpler alternative that avoids the transmittance iteration and 1/d interpolation is to use the correlation-corrected 1/d value at all times and accept the resulting errors at high transmittances. Since we have not yet decided on the optimal form for the interpolation function, for the present we shall discuss only the calculation of the correlation-corrected 1/d value, $1/d_c$. With the new 2-line-group algorithm, the same 1/d correction factor is applied to both the n_1 and n_2 values.

Ideally, $1/d_c$ should be determined for each spectral bin by (1) generating an exact spectrum with a transmittance of around 1/e using an optically thick Lorentzian line shape and the actual line strengths and locations, (2) comparing the resulting transmittance with that obtained using randomly positioned (but otherwise identical) lines, and finally (3) adjusting 1/d (at a constant line strength sum s/d) for the random case until the exact transmittance is matched. However, we have found that surprisingly good results can be obtained with the following, more computationally efficient procedure:

77

(1) Assign each line in the bin an equivalent width W_i that is proportional to $S_i^{1/2}$ and is scaled to give a net interval transmittance T of 1/e. The scaling factor may be found by using Equation (1) to solve for W, which is taken as the average equivalent width.

(2) Assuming that the transmittance line shapes $T_i(v)$ are square with equivalent width W_i and are centered on the actual line centers, evaluate the net transmittance in the bin. Since the line shapes are square, this can be accomplished using an exact, analytical method which is much faster than a line-by-line grid calculation.

(3) The 1/d correction factor ($1/d_c$ to $1/d$ ratio) equals the ratio of the logarithms of the transmittances calculated with the randomly located lines (i.e., T = 1/e) and with the actual line centers (Step 2).

At this time, we do not have a complete understanding of why this approach works as well as it does, but we have verified its success using a variety of actual and simulated molecular line distributions. In typical tests, the above definition of $1/d_c$ together with an empirical interpolation function were found to eliminate the bulk of the line correlation effects and reduce overall transmittance errors around a factor of 2 for the case of equal-strength lines. In addition, it is easy to show mathematically that accurate results (in some cases exact) are obtained for a set of equal-strength lines in which some or all of the lines are multiply degenerate.

Since there are many other sources of error in MODTRAN, positional correlation effects are usually noticeable in only a few spectral regions where there is very strong line clustering. The largest effect that we have observed is in the NO_2 band at around 1600 cm^{-1}, and leads to transmittance errors of up to around 10%. This would impact the 15 km horizontal spectrum if NO_2 were included in the species list for that test case.

Comparisons of the 2-line-group band model and "exact" line-by-line calculations for 0.1 atm-cm of NO_2 are shown in Figure 53. Without the correlation correction, the band model is very inaccurate. Results from MODTRAN3 are slightly better but still very poor. With the correlation correction, the errors are reduced by around a factor of 3, yielding reasonable agreement with the exact calculation.

At the present time, the correlation correction has not been incorporated into the beta test code; we plan to do at a future date.
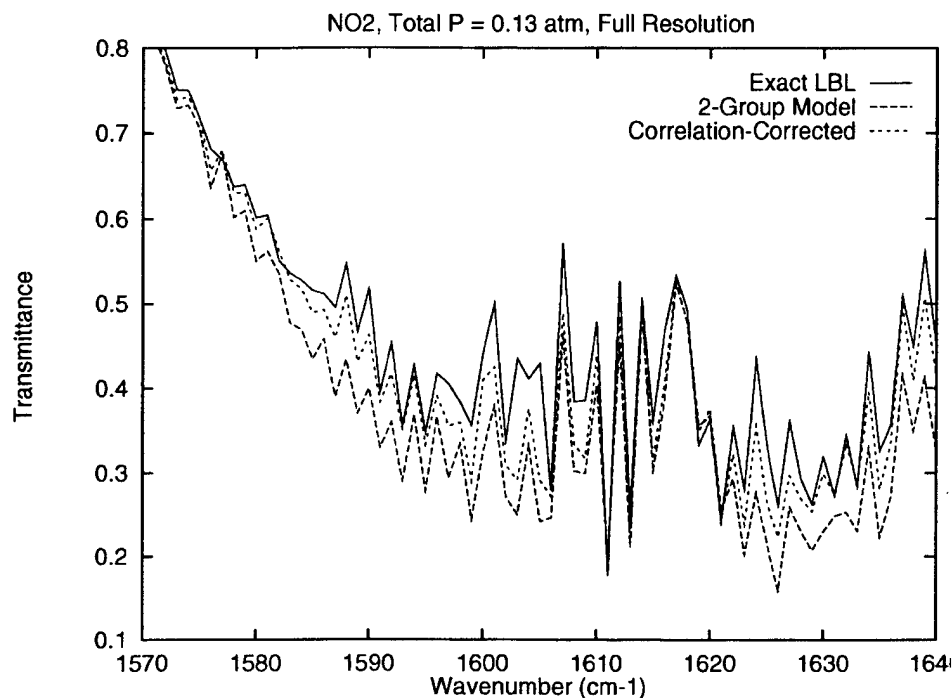
Figure 53. Comparisons of "Exact" and New Band Model (2-Group and 2-Group Correlation-Corrected) Transmittances for NO_2 at 1 cm^{-1} Spectral Resolution. Column Density is 2.5×10^{18} molec/cm^2, Pressure is 0.13 atm, Temperature is 296 K

6.3 Quasi-Continuum Treatment

MODTRAN uses a simple quasi-continuum treatment to account for the tail portions of the line that extend beyond the 1-cm^{-1}-wide spectral bin into which the line center falls. It is assumed that these tail portions are sufficiently flat that they may be represented by an average, continuum absorption coefficient. This is a good approximation for distant bins, and is adequate for the neighboring bins except when the line center is close to the bin edge and the optical depth is very large, leading to excess absorption. In this situation, it is sensible to shift the line towards the center of the bin in order to give a more accurate result for the equivalent width sum over all the bins.

To calculate the continuum and the center bin equivalent width, MODTRAN has traditionally assumed that each line center is at a standard location in the bin that is not too close to the edge, such as at the midpoint or, in a recent version, 1/4 of the way from one edge. The first-order continuum may be calculated by assuming a Lorentz line shape at 1 atm pressure. A correction to account for non-Lorentzian line tails is added for several species. In the radiation transport algorithm, this pre-calculated continuum is scaled by the column density and the total pressure.

In the current investigation, we used an alternative approach for the continuum calculation in which actual line center locations (within the limits discussed below) are used and the half-width term in the denominator of the lineshape expression is ignored (this gives the correct line shape in the zero pressure limit). To maintain consistency with the center bin equivalent width calculation, the center bin continuum is adjusted to account for the difference between the absorption coefficient calculated with the actual line location and that calculated with the standard line location, which is taken as 1/4 of the way from an edge. (Because of this adjustment, the continuum for a bin containing one or more strong lines can sometimes be negative; these values may be set to zero.) To prevent excessive absorption from lines that are close to the edge of the bin and from neglect of the half-width term, lines are relocated as needed to insure that the distance from the line center to the bin edges is a certain minimum value, d_{min}.

Comparisons with exact calculations using synthetic line distributions showed that with a d_{min} value of 0.15 to 0.20 cm^{-1} the new continuum definition improves the transmittance accuracy by a small amount, typically 2% or less in individual 1 cm^{-1} bins. The improvement is noticeable when the resolution and total pressure are both high (see Section 5.5). At low resolution, results are virtually identical to those obtained using the continuum from MODTRAN3, since both continua have nearly the same average values.

6.4 Other Upgrades

In addition to the band model improvements, the beta code incorporates three other upgrades. The first is a rescaling of the O_2 continuum (i.e., the pressure-induced component of the fundamental absorption band) to match that in FASCOD3. The coefficients are multiplied by 0.78 based on the work of *Rinsland et al.* [1989]. The omission of this factor in earlier versions of MODTRAN had been a major source of MODTRAN vs. FASCODE differences for the 15 km test case. The scale factor is included in the December, 1995 version of MODTRAN3 that was used in the current work.

The second upgrade is a more accurate temperature scaling of the collision-broadened half widths. The actual temperature exponents from the HITRAN line list rather than a preset value are now used to compute the 273 K half-widths. In addition, based on a survey of the exponent data we decided to replace the "standard" exponent value of 0.5 with the value 0.75, which was previously used only for CO_2.

The third upgrade is the replacement of the Lorentz equivalent width approximation, Equation (21), with a more accurate one, such as the expression from the NASA Handbook [Ludwig, 1973]

$$W = Su/(1 + 0.1768(Su/\alpha)^{1.25})^{0.4}. \tag{26}$$

The differences between the two expressions can amount to several percent.

6.5 Water Vapor and Temperature Sounding Simulations

To see what effects the various code upgrades might have on ground-based remote sensing of water vapor and temperature, we ran a spectral radiance case using MODTRAN3, the new algorithm (which includes all upgrades except the correlation correction), and FASCOD3 for a vertical line-of-sight through the US Standard atmosphere. The spectrum was convolved with a 3 cm^{-1} wide slit.

Results for the 1900 - 2300 cm^{-1} (4.3 - 5.3 μm) region, which has been studied by *Cipperly* [private communication], are shown in Figure 54. While the average error is 40% smaller with the new algorithm than with MODTRAN3, the agreement with FASCOD3 is very good for both band model codes. Most of the differences between MODTRAN3 and the new code are due to differences in the quasi-continuum from the water line tails. At 1 cm^{-1} resolution these line tail effects are more pronounced. At lower resolution they nearly disappear, and the main difference between the codes is in the N_2O band near 2200 cm^{-1}. The new algorithm is more accurate than MODTRAN3 on the low wavenumber side of the N_2O band but slightly less so on the high wavenumber side.

Figure 55 shows the corresponding calculations for the 500 - 900 cm^{-1} (11 - 20 μm) region, which has been studied for remote temperature sensing. Here the emission is dominated by CO_2 bands. As elsewhere, the agreement with FASCOD3 is good for both band model codes; the average error is 30% smaller with the new algorithm. The improvement in the 700 - 750 cm^{-1} region is due mainly to use of the 2-group band model, while the improvement in the 500 - 600 cm^{-1} region is due to the quasi-continuum upgrade.
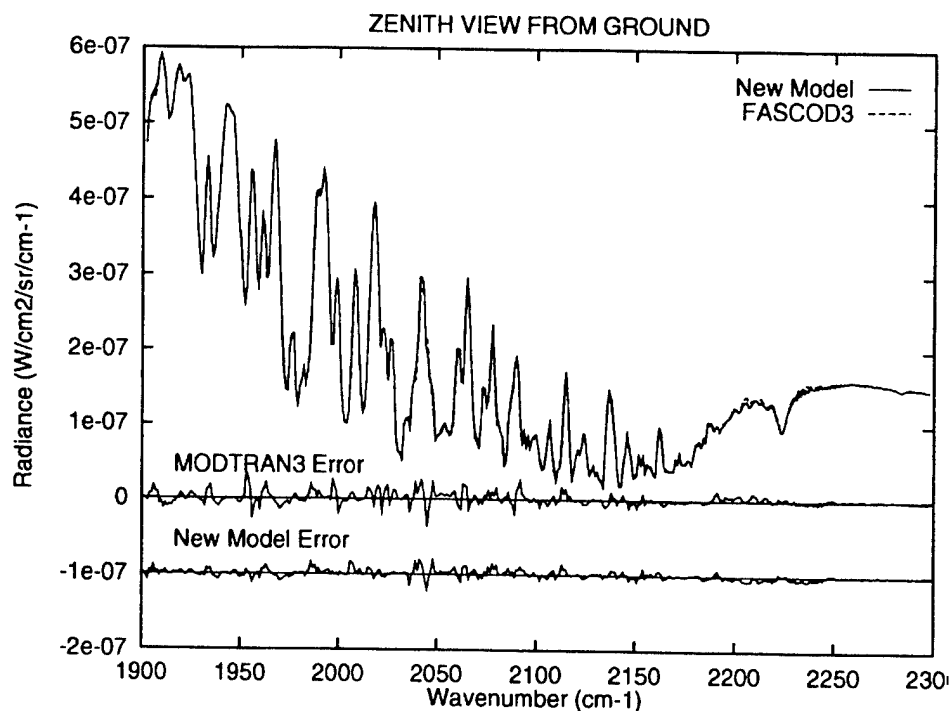
Figure 54. Comparisons of FASCOD3, New Band Model, and MODTRAN3 Spectral Radiances for a Vertical Ground-to-Space Path Through the US Standard Atmosphere. Spectra were Convolved with a 3 cm⁻¹ Wide Slit. The Offset Traces at the Bottom Show the Differences vs. FASCOD3.
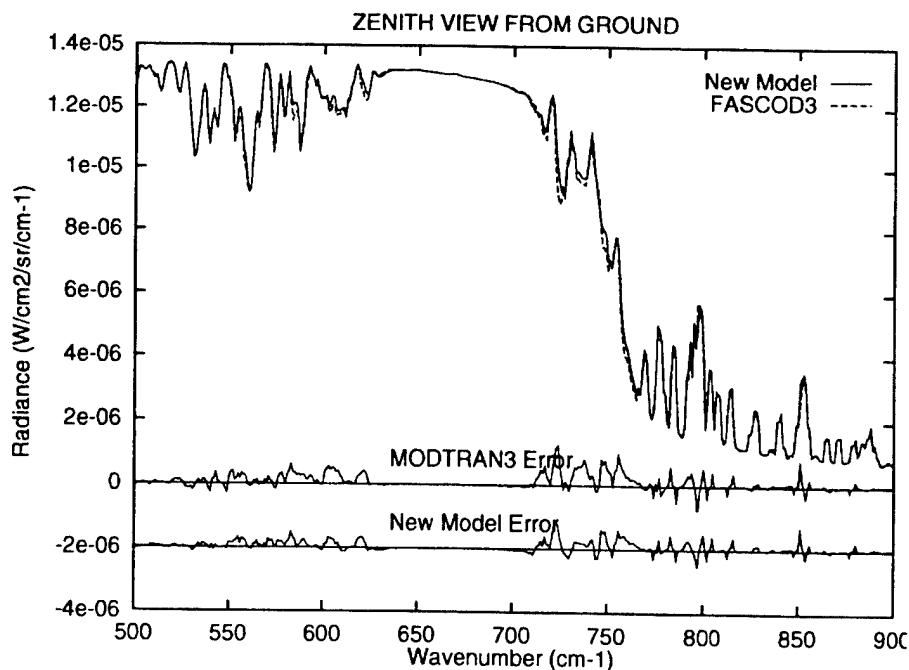
Figure 55. As in Figure 54, but for the 500 - 900 cm⁻¹ Region

6.6 Conclusions

The main conclusions of this investigation are:

(1) Improvements in the accuracy of MODTRAN3 have been achieved in a beta test version of the code, primarily by upgrading the line tail quasi-continuum and O_2 continuum models and replacing the standard band model with a more sophisticated two-line-group treatment . Over wide spectral ranges the RMS errors are reduced by up to 40% (not including the effect of the O_2 continuum modification), with larger improvements in accuracy for certain wavelengths and optical paths.

(2) Comparisons with FASCOD3 for typical remote sensing scenerios show that both the new code and MODTRAN3 have good overall accuracy. At 5 cm^{-1} resolution the average RMS transmittance errors are 2% or less, and average spectral radiance errors are in a similar proportion to radiances at nearby optically thick wavelengths. These results lend support to the use of MODTRAN for near-real-time remote measurement of atmospheric properties.

(3) An effective method has been developed and tested for correcting band model parameters for non-random (i.e., correlated) positions of the spectral lines. Errors due to line correlation are small at most wavelengths but were found to be large for NO_2.

(4) The MODTRAN upgrades developed during this investigation lead to a better match to exact spectral calculations in the 4 - 5 □m region, but their effect on water vapor determinations should be negligible since the errors are small to begin with and fairly random. There may be some improvement in temperature profiles determined from CO_2 radiation at long wavelengths, where the errors in the MODTRAN3 spectra are more systematic. This could have a small indirect effect on water vapor determinations and data-model comparisons since the relationship between absolute humidity (which is measured spectrally) and relative humidity (measured by most in-situ sensors) is temperature-sensitive.

Since the accuracy of an approximate model such as MODTRAN can depend strongly on the spectral region and the optical path, further comparisons with FASCODE should be performed for a wider variety of remote sensing test cases. For best accuracy, a correction for line position correlation should be implemented for NO_2 and perhaps other species. Finally, the increase in computation time due to the 2-line-group band model needs to be quantified.

83

7.0 NEW SOLAR IRRADIANCE DATA SETS IN MODTRAN

MODTRAN requires accurate values of solar irradiance at the top of the atmosphere for the computation of directly transmitted solar irradiance and the solar contribution to total path radiance. Currently, MODTRAN uses a table of solar irradiances computed by Kurucz, consisting of values from 51 to 50000 cm^{-1} at 1 cm^{-1} intervals. There is a continuing effort towards solar spectrum irradiance measurements. For example, recently Woods et al have examined the Upper Atmosphere Research Satellite (UARS) solar UV irradiances. MODTRAN has now been upgraded to include several solar irradiance data sets in addition to Kurucz's calculations. Additionally, the user now has the ability to use his/her own solar irradiance file. This feature will be useful as new calibrated upper atmosphere solar data become available.

The five files now available to MODTRAN have irradiance values from 51 to ~50000 cm^{-1} in step sizes of 1 cm^{-1}. These files are described very briefly below and in more detail in section 7.1.

- **newkur.dat**: This is the same as oldkur.dat (the original Kurucz data currently used in MODTRAN) but with a deficiency between 310-340 nm corrected

- **oldkur.dat**: This is the original Kurucz data currently used in MODTRAN.

- **chkur.dat**: This data (from 43478 to 125000 cm^{-1}), measured on Kitt Peak and elsewhere, is from *K. Chance* [private communication, 1997]; however, the data are replaced by the Kurucz data where O_2 lines occur and supplemented by the Kurucz data.

- **cebchkur.dat**: This is the ATLAS SSBUV data from 24603-49986 cm^{-1}, supplied by *R. Cebula* [private communication, 1997]. Below 24603 cm^{-1}, chkur.dat values are used.

- **thkur.dat**: This is the SOLSPEC data from *G. Thuillier* [private communication, 1997] and ranges from 11404-50221 cm^{-1}. Below 11404, values from newkur.dat are used.

For the above files, in the spectral region where data are available, values at consecutive integral wavenumbers are obtained either by interpolation or by integrating data within ±0.5 cm^{-1} of the wavenumber. In what follows, MODTRAN's solar data are discussed in some detail and compared against each other.

7.1 New Solar Irradiance Files

7.1.1 Kurucz Calculations

This is the original MODTRAN solar irradiance "data", but these are actually the result of extensive line-by-line calculations performed by Kurucz. (Gail, we should have a couple more sentences about Kurucz's method.) These values were recently corrected in the 310 to 340 nm region using measurements

carried out by an UARS instrument Solar Ultraviolet Spectral Irradiance Monitor (SUSIM). As the figures below will show, Kurucz's calculation generally holds up very well against measurements. Furthermore, it is the most comprehensive irradiance set available with irradiances at wavenumbers all the way down to 51 cm^{-1}. The tabulated irradiances have values from 51-50000 cm^{-1} (200 nm and greater) at 1 cm^{-1} intervals. The corrected Kurucz data is the default MODTRAN choice.

7.1.2 Corrected Chance Data - Kitt Peak Measurements

The data, between 800-230 nm (125000-43478 cm^{-1}), consist of two solar spectra which are joined together. For wavelengths greater than 305 nm the data is from the McMath Instrument (Kitt Peak) and was collected by Kurucz. The data has been mostly corrected for atmospheric absorption but some atmospheric effects still remained (see below). For wavelengths less than 300 nm the data is taken from Anderson and Hall. Between 300-305 nm (33333-32787 cm^{-1}), the spectrum is a combination of the two.

Chance recalibrated (in wavelength) the Anderson and Hall data using a set of solar reference lines. The Kurucz data was wavelength calibrated using a single O_2 line. Chance believes that the Kurucz calibration is only good to about 0.002 nm, and he plans to recalibrate for accuracy to better than 0.001 nm. A triangular scanning function with a FWHM of 0.01 nm was used to interpolate the spectrum to a fixed grid. Currently the spectrum goes from about 230-800 nm, but the data exists out to 1300 nm (but would require some calibration work to make available).

As the Chance data still were not corrected for O_2 absorption, the relevant O_2 lines were replaced with Kurucz values. This is an eminently reasonable compromise given the close general agreement of the Chance data with the Kurucz calculations.

7.1.3 Cebula Data - ATLAS SSBUV Measurements

This data, supplied by Richard Cebula of NASA, one of the coauthors of the paper by Woods et al, is the result Atmospheric Laboratory for Applications and Science (ATLAS) Shuttle Solar Backscatter UltraViolet (SSBUV) experiment. The SSBUV data covers 200.055-406.453 nm (49986-24603 cm^{-1}) with step size varying from 0.152 to 0.136 nm. The uncertainty in wavelength measurements is ±0.026 nm. The 2□ uncertainly in irradiance varies from 6% at 200 nm to 2.8% at 250 nm to 2.6% at 300-400 nm.

7.1.4 Thuillier Data - SOLSPEC Measurements

This data, obtained using the SOLSPEC instrument, is from 199.12-876.86 nm (50221.0-11404.3 cm^{-1}). It is comparable to the ATLAS SSBUV data but is taken at a much coarser step size; the step size is 0.36 nm at the lower wavelength end and changes to 0.9 nm at the higher wavelength end.

85

7.2 Bandpass Intercomparisons

The overlap of the wavelength regions for different data sets suggests five wavelength regions for intercomparison. Between 876.76-800.00 nm (interval 1) the Kurucz and SOLSPEC data; between 800.00-406.45 nm (interval 2) the Kurucz, Chance and SOLSPEC data; between 406.45-230.00 nm (interval 3) all data sets; between 230.00-200.06 nm (interval 4) the Kurucz, SOLSPEC and SSBUV data; and finally, between 800.00-230.00 nm the Kurucz, Chance and SOLSPEC sets can be compared.

Table 6 shows the bandpass integrals in these intervals. These values lead one to conclude that all four data sets are consistent with each other. However, a more rigorous comparison must be made by examining the spectral variations between the data sets.

Table 6. Wavelength Regions for Different Data Sets

877-800 nm Interval 1	800-406 nm Interval 2	406-230 nm Interval 3	230-200 nm Interval 4	800-230 nm Interval 55
KR 80	647	122	0.95	768
CH	645	118		764
CB		121	1.02	
TH 82	654	124	1.02	778

(KR = corrected Kurucz, CH = corrected Chance, CB = SSBUV, TH = SOLSPEC)

7.3 Spectral Comparisons

7.3.1 SSBUV and SOLSPEC Data Comparison Below 400 nm

The SSBUV and SOLSPEC measurements, both of which were carried out in the upper atmosphere, are compared against each other in the region where they overlap (200-407 nm) in Figure 56. The SSBUV data was degraded into 0.5 nm bins in the lower wavelength half of the region and into 0.75 nm bins in the upper half. The agreement between SSBUV and SOLSPEC is much better in the shorter wavelength region.

In the rest of the comparisons, we use the ATLAS SSBUV (from Cebula) data as benchmark measurements below 400 nm and the SOLSPEC data (from Thuillier) as benchmark measurements above 400 nm where the SSBUV data is not available. This is consistent with Cebula's claim that the accuracy of the SSBUV data is better at 400 nm than at shorter wavelengths and with the fact that the SSBUV and the SOLSPEC data agree reasonably well between 200-400 nm.
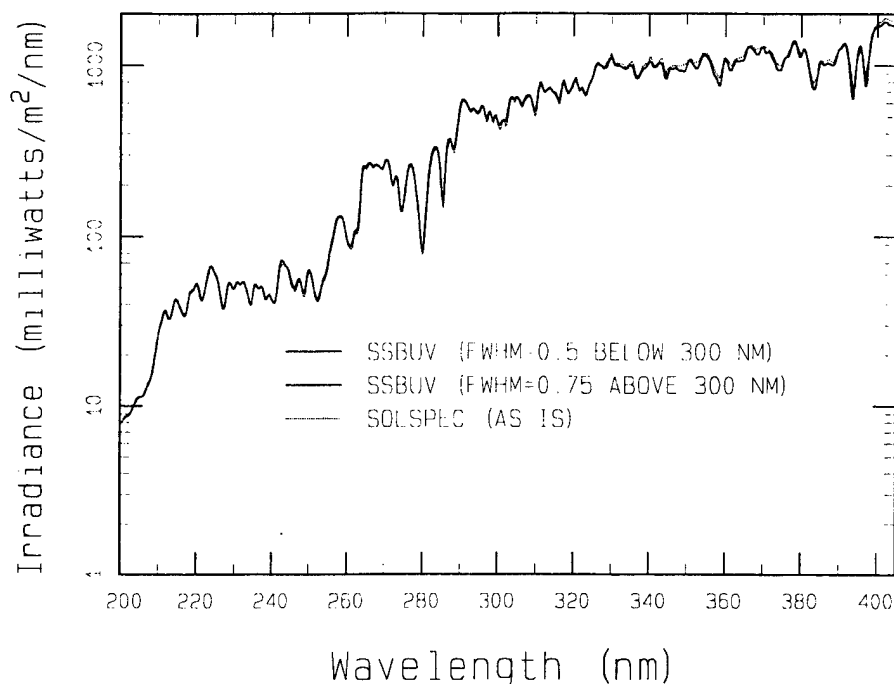
Figure 56. Comparison of the SSBUV and SOLSPEC Measurements in the 200-407 nm Spectral Region

7.3.2 Correction to Kurucz and Comparison to SSBUV Below 400 nm

As mentioned before the Kurucz data was deficient in the 310-340 nm region. This was corrected by using SUSIM data. Figure 57 shows the old and new Kurucz data plotted against the SSBUV benchmark data. Clearly, the newer Kurucz set is much closer to the SSBUV data. The same figure shows that in the 310-340 region, the new Kurucz set is also closer to the Chance measurements than the older Kurucz set. But when compared against the SSBUV data, the new Kurucz data reproduces the upper atmospheric SSBUV data better than the Chance set; the Chance data may still may contain some atmospheric effects.

The comparisons in Figure 57 establish the need to validate the correction to older Kurucz data set. They also show that in the wavelength region shown in Figure 57 the Kurucz calculation is more reliable than the Chance measurements. This is confirmed, as we shall see, for the entire wavelength region of MODTRAN. See Figure 58 for comparison in the 200-400 nm region; ratio plots, Figure 59, spanning this region nm also show that the corrected Kurucz data agree well with the SSBUV data whereas the Chance data are up to ± 20% off the measurements around 325 nm. (In all the radiance plots, data was degraded such that all the curves have similar undulations. This entailed degrading different set of data by triangular slits of differing halfwidth. The Chance and Kurucz numbers were degraded by 1.2 nm in Figure 56. The ratio plot of Figure 57 uses ratios evaluated at every 2 nm.)

87
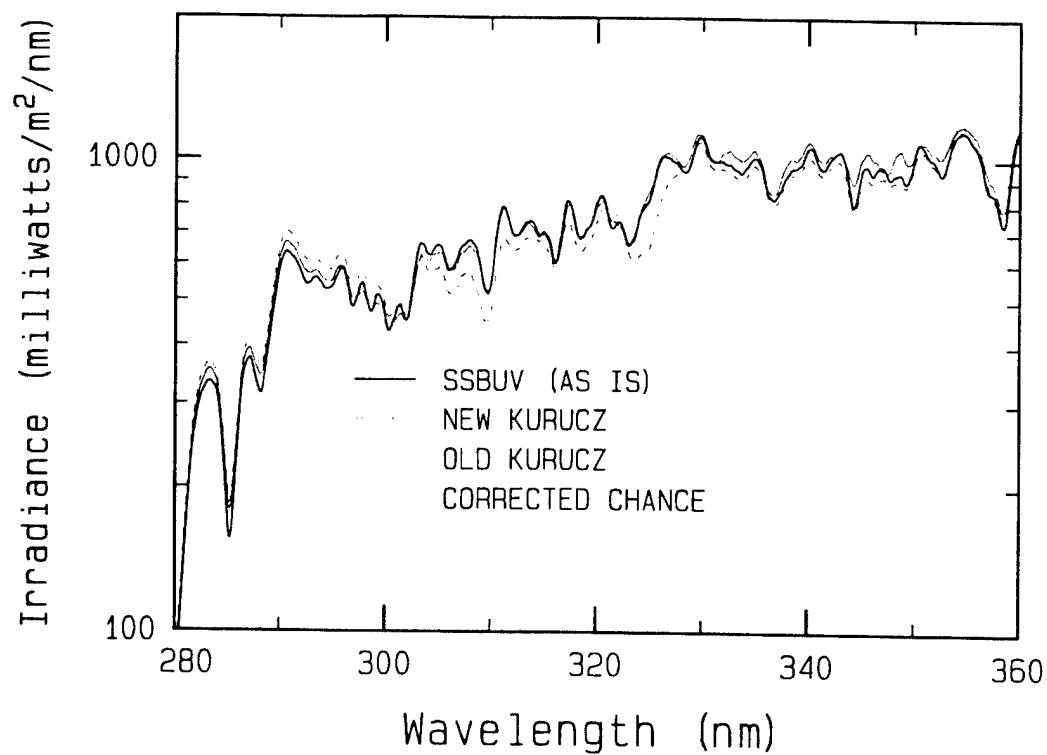
Figure 57. Comparison of the New and Old Kurucz Data with the SSBUV Measurements
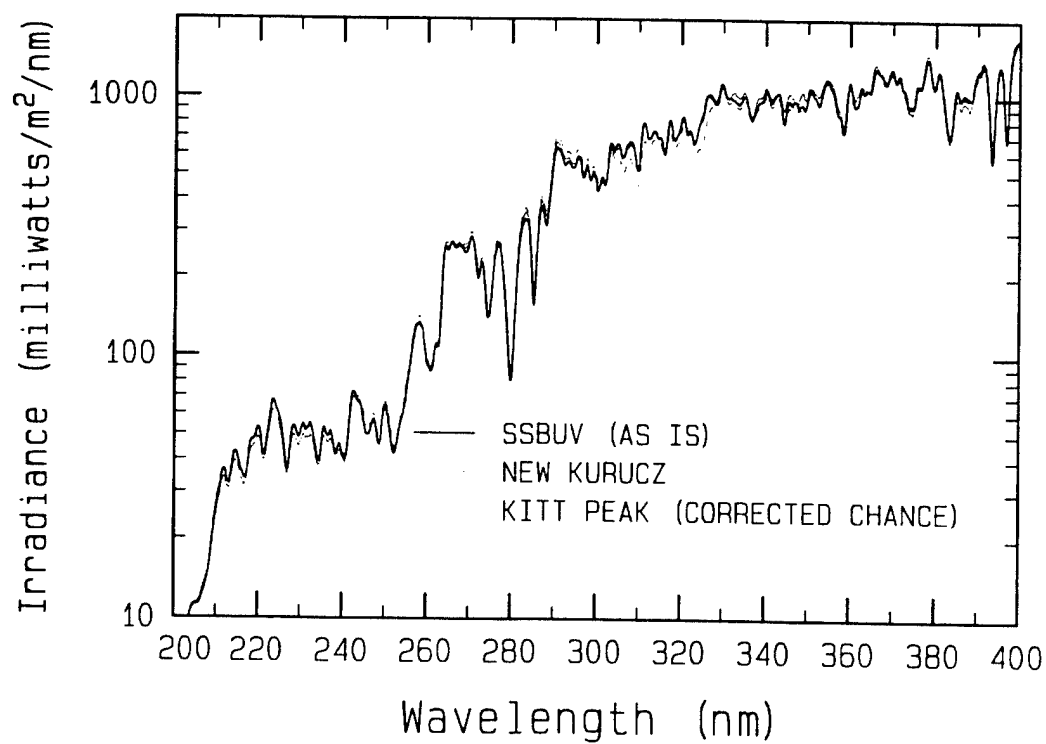
Figure 58. Comparison of the New Kurucz and Chance Data with the SSBUV Measurements

88
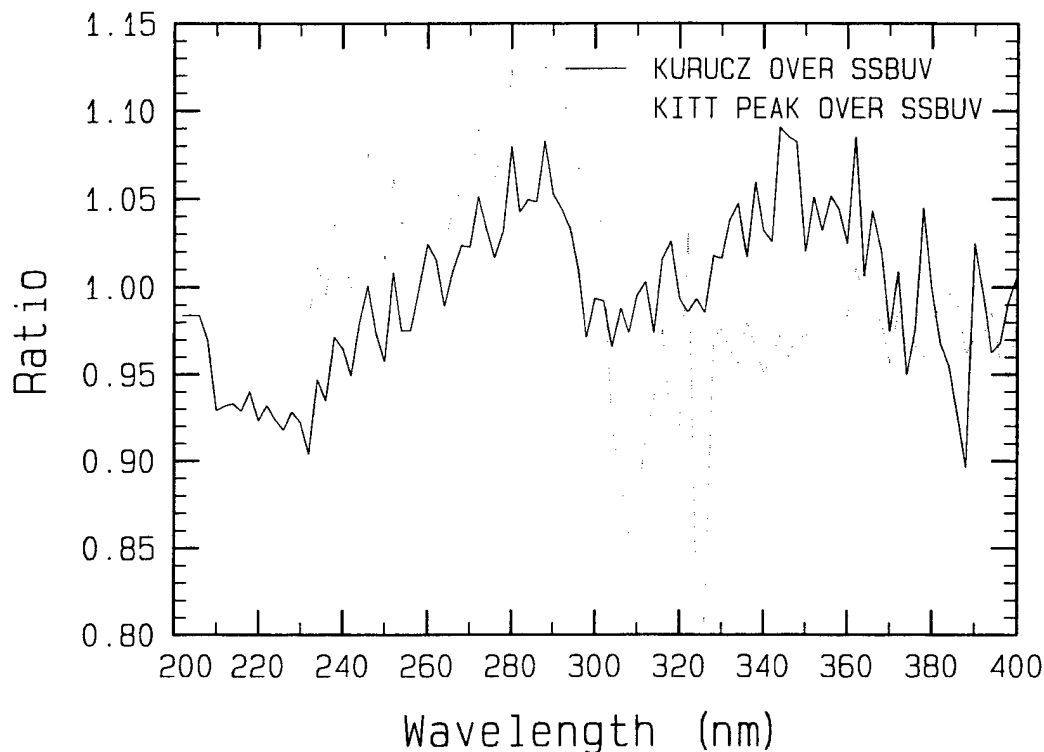
Figure 59. Comparison of the Ratio of the New Kurucz and Chance Data Sets to the SSBUV Measurements

7.3.3 Kurucz, Chance and SOLSPEC Data Above 400 nm

Figure 60 displays the Kurucz, Chance and the SOLSPEC data sets. Figure 61 shows the ratios of the data sets. With the exception of data around 720 nm, as shown in Figure 61, Kurucz and Chance agree well with the SOLSPEC data. Around this value the Chance data are off by about 15% from both Kurucz and the SOLSPEC data. This can be attributed to atmospheric effects due to H_2O.

7.4 Conclusions

The analysis and discussion in this section strongly support that the best available data below 400 nm in terms of resolution and accuracy the SSBUV data. The Kurucz calculations, after the 310-340 nm correction, agree well with this data set. Beyond, 400 nm, the only available data set is the SOLSPEC data. This data set is of low resolution, however. The Kurucz set also agrees with the SOLSPEC data remarkably well. The Kitt Peak measurements still have some unaccounted for atmospheric effects. Therefore, the corrected Kurucz data set is chosen as the MODTRAN default.

89
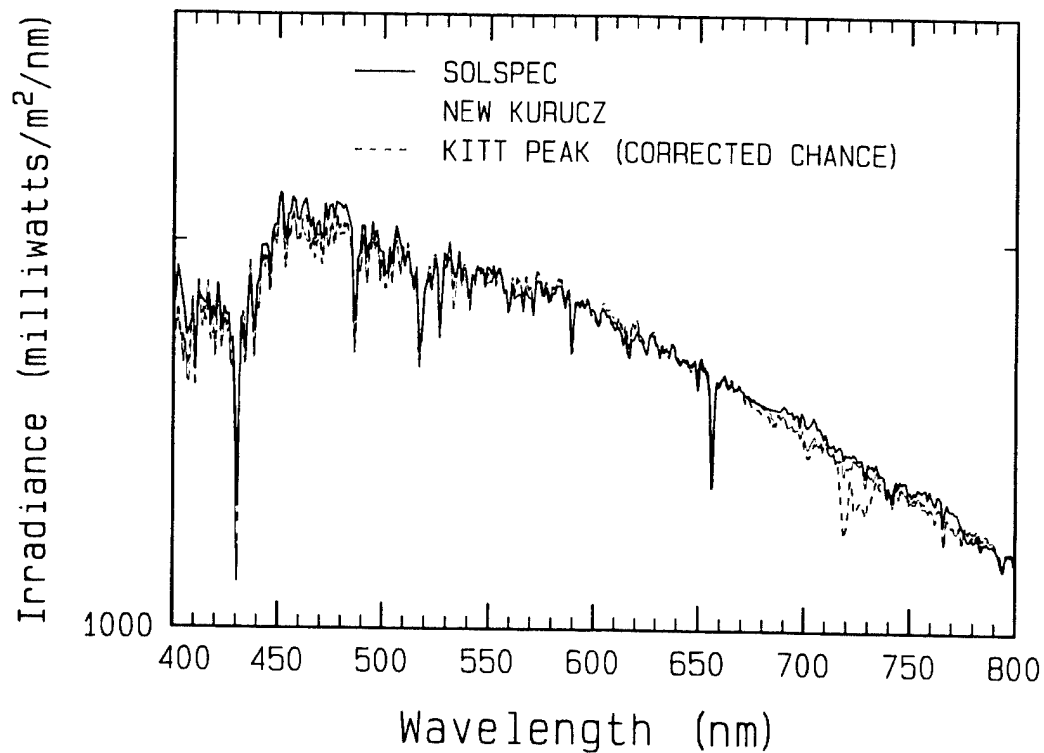
Figure 60. Comparison of the New Kurucz, Chance, and SOLSPEC Data Sets
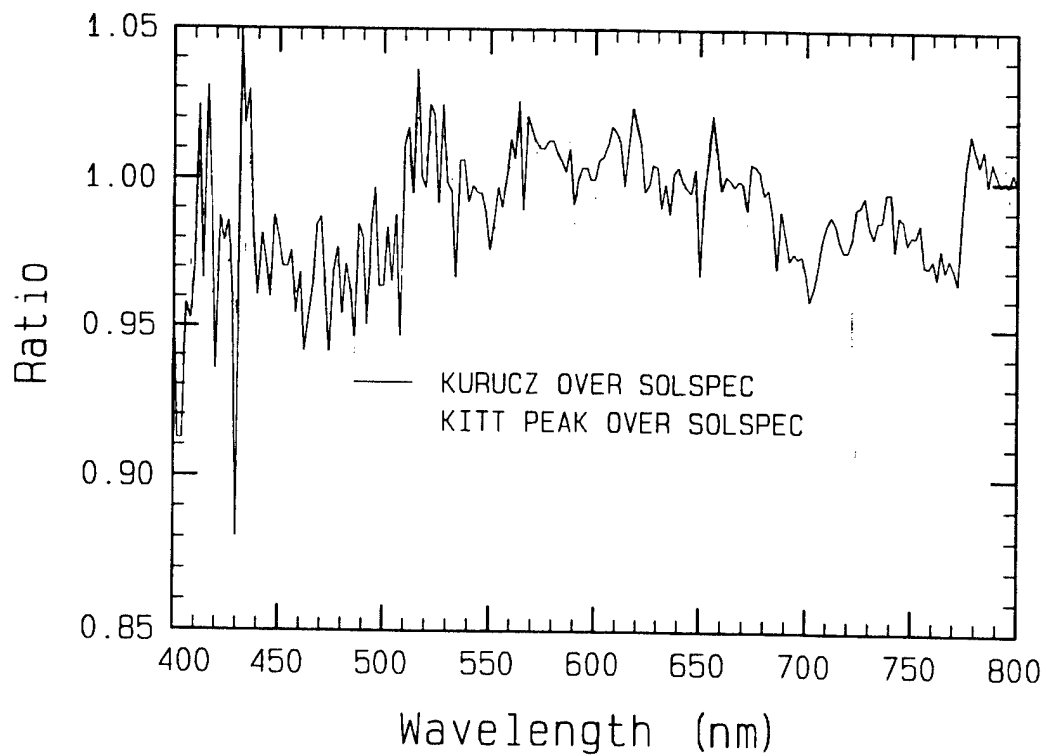
Figure 61. Comparison of the Ratio of the New Kurucz and Chance Data Sets to the SOLSPEC Measurements

8.0 INCORPORATION OF NOVAM INTO MODTRAN 3.7/4.0

The most recent compilation of the NOVAM (Navy Oceanic Vertical Aerosol Model) profiles offers a new set of aerosol descriptions, providing both optical and size distributions appropriate from the shipboard surface to 6 km, covering the spectral range from 0.2 micron to 40 microns at relatively sparse spectral resolution. Since the ozone retrievals currently implemented in the UV encompass an accounting of the aerosol background as stated above, the addition of NOVAM profiles to MODTRAN was deemed critically important.

8.1 NOVAM Code

SSI obtained the NOVAM code from NRaD through S. Gathman [Gathman and Davidson, 1993]. This code was released by R. A. Paulis under the authority of J. H. Richter, Oceanic and Atmospheric Sciences Division, Naval Command, Control and Ocean Surveillance Center, San Diego. The NOVAM code is an upgrade to NAM (Navy Aerosol Model) which is already in MODTRAN. NOVAM is based on extensive direct shipboard measurements carried out by several different agencies specializing in the marine environment. The inputs to the NOVAM code are radiosonde data consisting of altitude, temperature, pressure and relative humidity (RH), and other surface observation parameters such as optical visibility, wind speeds and surface IR extinction (1/km) at 10.6 microns; not all the inputs are required for implementation.

NOVAM recognizes three types of meteorological profiles characterized by existence or non-existence of temperature inversions. The cases are denoted numerically: 1. No inversion, 2. Two inversions, and 3. One inversion. The wavelength spectrum ranges from 0.2 to 40 microns; the actual spectral grid (in microns) is: 0.2, 0.3, 0.3371, 0.55, 0.6943, 1.06, 1.536, 2.0, 2.25, 2.5, 2.7, 3.0, 3.3923, 3.75, 4.5, 5.0, 5.5, 6.0, 6.2, 6.5, 7.2, 7.9, 8.2, 8.7, 9.0, 9.2, 10.0, 10.591, 11.0, 11.5, 12.5, 14.8, 15.0, 16.4, 17.2, 18.5, 21.3, 25.0, 30.0, 40.0. The model contains four classes of marine aerosols with three mode radii of 0.03, 0.24 and 2.0 microns, where the mode radius is the "size" of the most populous part (i.e., the peak) of the distribution at the RH of 80%. The 0.03 micron aerosol consists of two classes: soluble and insoluble. The other two sizes consist of soluble aerosols only.

The version of NOVAM from NRaD outputs surface layer altitudes, and the net extinction, absorption and asymmetry coefficients by <u>combining</u> the effect of all four aerosols. The output of NOVAM consists of aerosol size distribution parameters, and total extinction, absorption and

asymmetry values as a function of wavelength. In this study, NOVAM was modified to output this information as a function of wavelength for a series of altitude values beginning at the lowest "significant" radiosonde altitude (usually a few meters), extending into the lower troposphere. The NOVAM model is claimed to be valid up to 6 km. However, in consultation with Gathman [private communication, 1998], we have restricted the NOVAM aerosol profiles to reach no higher than 2km.

The set of NOVAM routines consists of about 6000 lines of FORTRAN code written in non-standard FORTRAN 77. NOVAM, however, needs only minimal modification so as to be acceptable to most FORTRAN compilers. Extensive modification of the code was ruled out in order to maintain an easily discernible correspondence between the modified and original versions.

The user should familiarize herself/himself with the NOVAM input files of which there are three: (i) the **Surface Observation Data File**, (ii) the **Radiosonde Profile File**, and (iii) a file called **novam.in**. For purposes of familiarizing with NOVAM, it is highly recommended that the user consult the above referenced NOVAM manual. In this report only a very brief description of the inputs and output are given. Questions regarding NOVAM's use in MODTRAN should be directed to the authors of this report.

Note that the NOVAM code supplied with this delivery has 13 inputs in the **Surface Observation File** as opposed to 9 as stated on page 9, Table 2, of the NOVAM manual. These inputs are the same as stated for positions 1 to 7. The revised Table 2 (Table 7) is described below. Values outside the stated range make the code use built-in default values. It is suggested that the user employ the default values when any of the specific data items are not available.

Table 7. Inputs for the NOVAM Surface Observation File

1. Sea Surface Temperature (°C)
2. Air Temperature (°C)
3. Relative Humidity (%)
4. Optical Visibility (km)
5. Current Real Wind Speed (m/s)
6. Averaged Wind Speed (24 hours, m/s)
7. Air Mass Parameter (1 to 30)
8. Cloud Cover Fraction (0 to 1)
9. Cloud Type (0 to 9)
10. Surface IR Extinction at 10.6 micron (1/km, 0.001 to 100.0)
11. Weather (0 to 11)
12. Height of Lowest Cloud (meters, negative value uses default)
13. Zonal/Seasonal Category (1 to 6)

The **Radiosonde Profile Data File** is in either of the formats described on page 15, Table 4 and Table 5, of the NOVAM manual. Table 4 contains data, each line of which consists of an altitude (m), potential temperature (°C)· and aerosol mixing ratio (g/kg). The relationship between the potential temperature (θ) and the usual air temperature (T) is given by the formula:

$$\theta = T \cdot (P_0/P)^{\kappa}, \quad \kappa = (C_p - C_v)/C_p \approx 0.288$$

where the C's are heat capacities at constant pressure and constant volume, $P_0 = 1013.25$ mb and both temperatures are in Kelvin. Potential temperature is the temperature attained by air at pressure P and temperature T where it is brought adiabatically (i.e., at constant entropy) to a standard pressure P_0 [Houghton, 1986]. Table 5 contains data, each line of which consists of a line number (an integer), log (base 10) of pressure in millibars multiplied by 10^4, the air temperature in °C, RH in percent and pressure in millibars multiplied by 10. As stated above, one needs the profile data either in the format of Table 4 and Table 5. Table 4 is said to be in 'n' format whereas Table 5 is said to be in 'r' format, presuming that 'n' denotes 'number' defined by mixing ratio, while 'r' denotes 'relative humidity.'

In addition to these files, NOVAM needs another file called **novam.in**. An example of **novam.in** is reproduced below:

1905sops

1905prof.txt

n

Here, **1905sops** is the **Surface Observation File** and **1905prof.txt** is the **Profile File** in the 'n' format as indicated by the last line. This file then specifies for the program where the necessary data files can be found.

The output of NOVAM, **novam.out**, now in a form suitable for MODTRAN, typically looks as follows. The *italicized* text will not appear in the output. The first number is 40 which is the number of wavelengths (in microns) which are then individually listed. The number 10 is the number of altitudes (in meters) which are then individually listed. Then the temperatures (in K) for each altitude are listed, followed by the pressures (in mb) and relative humidity (RH in %). Then for the

93

first wavelength (0.2 micron), the extinction coefficients (in 1/km) for each altitude is listed. The absorption coefficients (in 1/km) for each altitude is followed by the asymmetry parameters for each altitude. Then the same set of information of the second wavelength (.3 micron) are listed. This pattern continues.

40 *(number of wavelengths and wavelengths in microns)*

.2000	.3000	.3371	.5500	.6943	1.0600	1.5360	2.0000
2.2500	2.5000	2.7000	3.0000	3.3923	3.7500	4.5000	5.0000
5.5000	6.0000	6.2000	6.5000	7.2000	7.9000	8.2000	8.7000
9.0000	9.2000	10.0000	10.5910	11.0000	11.5000	12.5000	14.8000
15.0000	16.4000	17.2000	18.5000	21.3000	25.0000	30.0000	40.0000

10 *(number of altitudes and altitudes in m)*

20.9 123.6 226.3 329.1 393.8 458.6 523.4 572.0 620.7 669.3

(temperature in K)

287.65 286.49 285.57 284.85 285.37 285.95 285.65 287.65 288.91 288.45

(pressures in mb)

1010.70 999.40 988.10 976.80 969.66 962.55 955.50 949.60 943.73 937.90

(RH)

88.80 91.41 95.39 95.60 81.88 66.69 65.60 50.08 37.44 35.80

(spectral data for 0.2 microns)

```
.156E+00   .146E+00   .145E+00   .145E+00   .144E+00   .142E+00   .140E+00
.377E-01   .377E-01   .377E-01   (extinction)
.224E-03   .140E-03   .133E-03   .132E-03   .130E-03   .128E-03   .125E-03
.635E-06   .635E-06   .635E-06   (absorption)
.801E+00   .798E+00   .797E+00   .797E+00   .797E+00   .797E+00   .797E+00
.758E+00   .758E+00   .758E+00   (asymmetry)
```

(spectral data for 0.3 microns)

```
.150E+00   .140E+00   .139E+00   .139E+00   .137E+00   .135E+00   .133E+00
.283E-01   .283E-01   .283E-01
.377E-05   .255E-05   .245E-05   .243E-05   .240E-05   .236E-05   .233E-05
.488E-06   .488E-06   .488E-06
.804E+00   .800E+00   .799E+00   .799E+00   .799E+00   .799E+00   .799E+00
.777E+00   .777E+00   .777E+00
```

8.2 Incorporation Into MODTRAN

First all structure variables were eliminated and all non-standard system routines (such as **gettim**) were also eliminated from NOVAM. Several non-standard (i.e., non-FORTRAN 77) features were left intact. These include the DO ... ENDDO structure, longer than six character variable names and the use of the INCLUDE statement as these are acceptable by almost all modern compilers. The goal was to minimize changes to NOVAM and to use it almost "as is". The changes to the NOVAM code are briefly stated later.

Extensive changes to MODTRAN code had to be made to accommodate the way NOVAM treats its four aerosols. The reason changes were extensive is that, unlike MODTRAN's current requirement, NOVAM does not output an aerosol profile (varying with altitude) and spectral extinction and absorption coefficients (varying with wavelength but not with altitude). Instead NOVAM outputs both altitude and spectrally varying quantities which are products of profile and spectral parameters. Changes to NOVAM code itself, however, were kept to a minimum. This meant that in order to use NOVAM in MODTRAN the user must supply the required radiosonde input data to NOVAM, separate from the MODTRAN inputs. NOVAM is executed off-line and creates a file called **novam.out** (lower case in UNIX) which is used as input to MODTRAN (uppercase filename in UNIX). Note that NOVAM input files are currently separate and in addition to MODTRAN's usual input file (which is named **tape5**). If the altitudes in **tape5** overlap with those in the NOVAM output file, the meteorological parameters, such as humidity, pressure and temperature, used by MODTRAN will be those provided by NOVAM.

In a future upgrade, the requirement for NOVAM to have a separate input file can be eliminated; both MODTRAN and NOVAM will then use the information contained in the MODTRAN input file, **tape5**. This process will be facilitated by the prior development of a sonde compression scheme; SSI and PL/GPO have collaborated to write a program, called **SNDTP5**, which can compress radiosonde measurements, consisting of hundreds of altitude layers (such as those used by NOVAM), into a form more suitable for the finite layering appropriate (and generally just as accurate for transmittance and radiance calculations) for a MODTRAN **tape5**.

As mentioned NOVAM actually can model altitudes as high as 6000 meters. However, in consultation with E. Shettle [private communication, 1998] and S. Gathman [private communication,

95

1998], the maximum NOVAM altitude relevant for MODTRAN was determined to be 2 km. In reality, for most applications it will be less than 2 km. NOVAM distinguishes between three different temperature inversion cases. The code was modified to output these inversion layers explicitly which are then used in MODTRAN. This enables MODTRAN to use only a few layers and still accurately model the temperature effects. If the aerosol does not contain inversion layers, currently MODTRAN will introduce layers which are at most 100 m apart. Although adequate, this scheme may be improved so that layers are more closely spaced nearer to the surface (where the scale height is smaller/steeper) and are farther apart towards the top of the boundary layer (where the scale height is generally larger). This may allow using fewer layers without loss of accuracy.

In summary, NOVAM is simply used to generate a database of marine aerosol profiles and spectral information for MODTRAN. NOVAM does not at present generate angular phase functions. Instead, it has a database of asymmetry parameters from which Henyey-Greenstein phase functions can be computed. In principle, a Mie code can be used to generate the phase functions for NOVAM.

8.3 Some Results

Three typical (as provided in the NOVAM package) profiles of aerosol extinction and coincident temperature are shown if Figures 62a and 62b. Figure 63a, b, and c shows the simulated backscattered UV signatures associated with these profiles, as might be measured by a potential ozone monitor staring down from a space platform. These calculations use all three types of temperature inversions modeled in NOVAM. The calculation with no aerosol includes only the Rayleigh scattering component and is used as the measure of change imparted to the backscattered signature by low-lying aerosols. No attempt was made to smoothly incorporate these profiles into a total profile. Rather, the "default" US Standard temperature, pressure, and constituent (primarily ozone) profiles and background rural (23 km visibility) aerosols were employed above 0 - 2 km, the acceptable vertical range for the NOVAM input. The spectral range presented is only that reaching the surface and near-surface, as wavelengths shortward of 300 nm will be absorbed (in general) at higher altitudes. MODTRAN will accommodate simulations from 200 nm to the far-IR, including the aerosol impact, so the short spectral range depicted in these calculations is not a restriction.
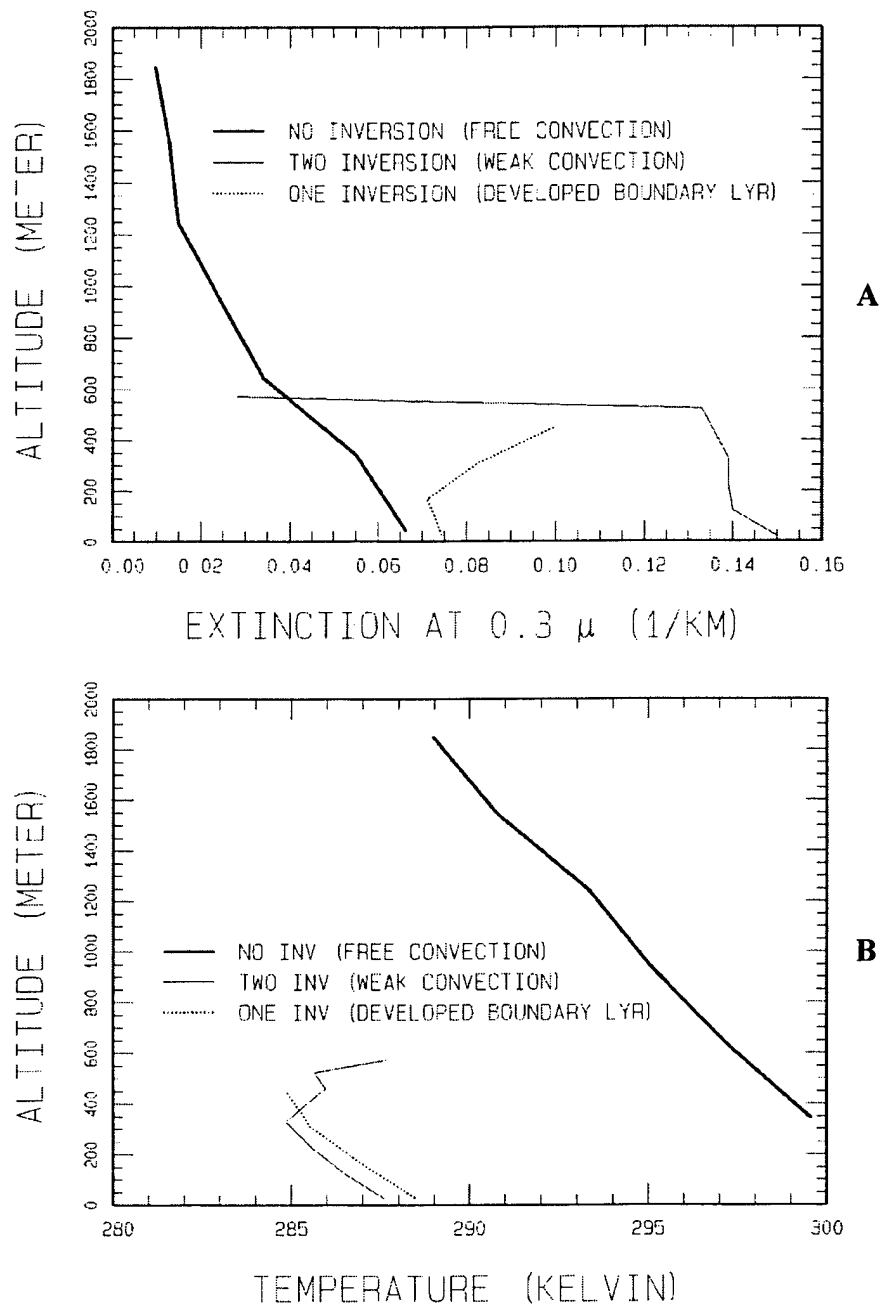
Figure 62a and 62b. The 3 aerosol and coincident temperature profiles (in extinction at 0.3 um and K, respectively) as a function of altitude. These profiles were chosen to capture the number of temperature inversions used as a parameter in NOVAM, 1 or no inversion, 2 or two inversions, and 3 for 1 inversion. There was no attempt to find the most perturbing case, so these can be considered typical. Note that MODTRAN merges these profiles into those describing the rest of the atmospheric profile from whatever source has been specified, 'default' or 'user-defined'. This can lead to very coarse discontinuities whose impact might need to be further explored.
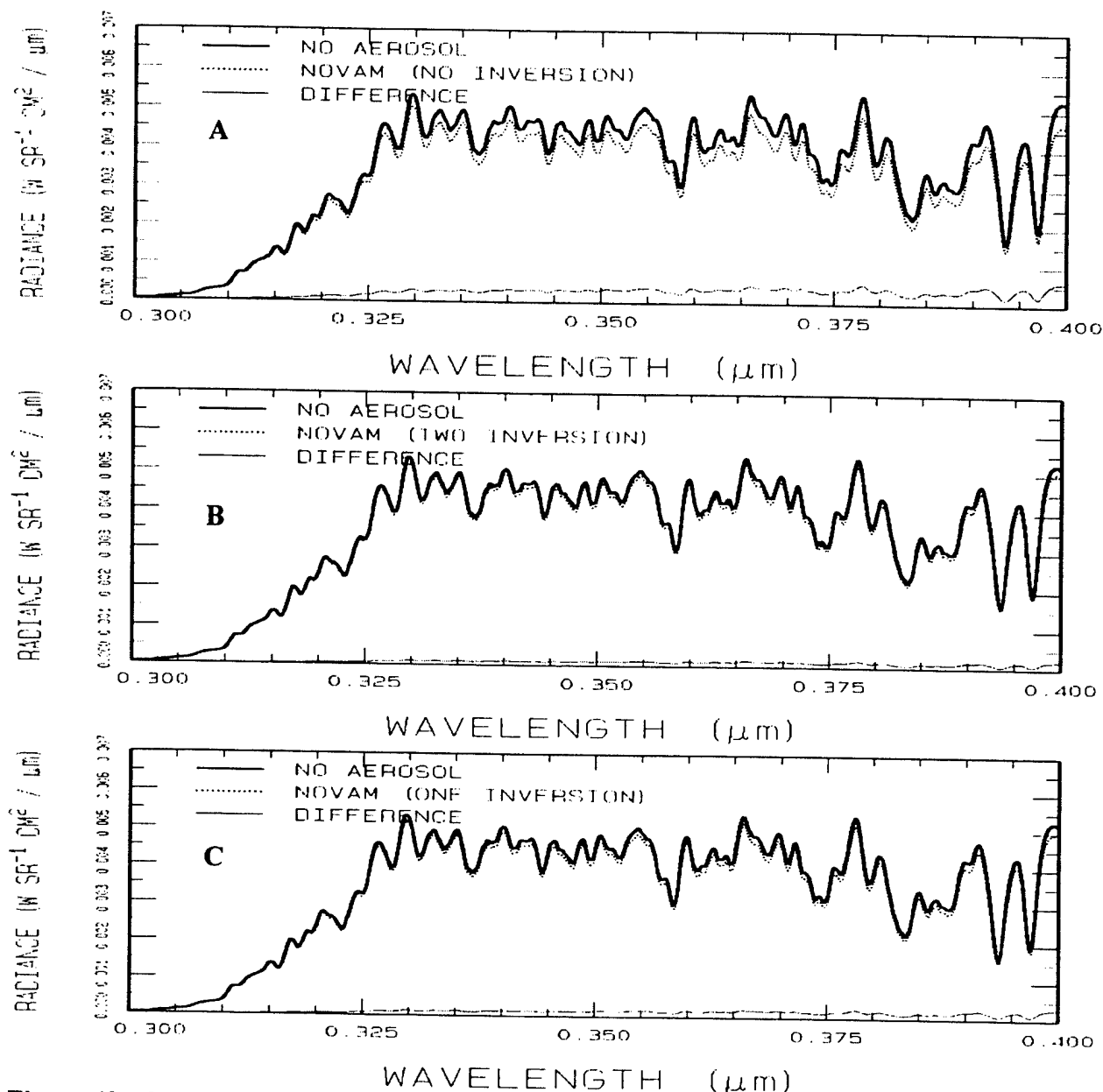
Figure 63a, b, c. As denoted, these represent typical sensitivity to the new NOVAM aerosol profiles shown in Figure 62. They plots are shown linearly to emphasize the impact at the longer wavelengths that 'see' to the surface, and, therefore, would be impacted by boundary-layer variability. At shorter wavelengths, <0.3 um), the stratospheric aerosol component might be important under extremes of volcanic loading. That sensitivity requires a logarithmic plot and has not been explored in this study.

8.4 Novam Input And Modtran Input Files

The NOVAM files were described earlier. So they are not reproduced here. In the delivered code, there are several **novam.in**, **Surface Observation** and **Radiosonde Profile** files.

98

The **tape5** used to run MODTRAN with NOVAM aerosols for the calculations in this report is shown below. The `N' in the third line invokes the NOVAM aerosol option in MODTRAN.

```
T   6    2    2    1    0    0    0    0    0    0    1    0    1       .0500
F   0F   0
    1N   0    0    0    0    0    0.000      .000      .000      .000
  0050.0000  .10     180.00000
      2    2    0    0
        45.  60.
          .3         .4      .0001      .0010 $      M1
      0
```

First NOVAM is executed to produce the **novam.out** file. This file then should be copied to the directory containing the MODTRAN executable as **NOVAM.OUT**; MODTRAN requires this file with the uppercase name.

8.5 Future Upgrades To Novam Implementation

There are at least six general areas in which the aerosol product in MODTRAN can be improved.

1. The first is to enable NOVAM to run from MODTRAN's input file, **tape5**. This task will enable MODTRAN to use radiosonde data consisting of several hundred altitude layers several of which can even be redundant. This will alleviate the need for NOVAM to have its own input file as is required in the current input scheme. Note that there still may be a need for the NOVAM input file, for example, to input surface observations.

2. MODTRAN does not now have phase functions for several aerosols (e.g., the desert aerosols) and for none of the cloud models. In the future this can be rectified by generation of the phase functions using the Mie code and incorporating them in MODTRAN.

3. The phase functions for NOVAM are also not available. In consultation with S. Gathman, they can be generated for the NOVAM aerosols and incorporated in MODTRAN.

4. The output of the Mie code can be put in a format so that user can include them in the MODTRAN input file without extensive editing.

5. Based on the El Chichon and Mt. Pinatubo erruptions, the content, size, type, and H_2SO_4 component of fresh and aging volcanic aerosols need to be altered from the default profiles now available within MODTRAN (Shettle, private communication).

6. MODTRAN currently merges NOVAM-generated profiles (e.g., xtinction and temperature) into those describing the rest of the atmospheric profile from whatever

99

source has been specified, 'default' or 'user-defined'. This could lead to very coarse discontinuities whose impact might need to be explored. General validation against real sonde data will provide additional confidence in the procedure.

8.6 Modifications To Novam To Code

As mentioned NOVAM modifications were kept to a bare minimum. Here is a list of types of coding changes to NOVAM.

1. All structure variables were replaced using this scheme:

    structure.member was replaced by **structure_member**

This of course meant that numerous corresponding changes to subroutine arguments had to be made.

2. The **driver3.f** routine was substantially changed to output the **novam.out** file described earlier.

3. The assym1 routine in the file **optics2.f** was substantially rewritten to fix an interpolation problem with the asymmetry parameters.

4. The calls to **gettim** were eliminated as it is not available on all machines.

5. **potential_temperature** was replaced by **potential_temp** as this variable and routine name is too long.

6. The file **drivesub2.f** was renamed **drivesb2.f** so that the new prefix has no more than eight characters which is the maximum for the PC environment.

7. As before the **sigfile** is created by calling it with **repeatflag** equal to .false.. In the same call, a new file called **invfile** is created with inversion and other extra layers to be used as MODTRAN layers. This file also contains pressure, air temperature (not potential temperature) and RH. It is created by modifying the routine **make_rdataary**. Later the driver (with **repeatflag**=.true.) reads the **invfile** and creates the **novam.out** file at these altitudes.

8. The driver checks to see that all altitudes in the invile which are greater than 2 km are discarded. Also discarded are the set of all top altitudes if the first altitude in the set has a relative humidity which is below 50%. That is because the NOVAM aerosols appear to be restricted to be in an environment of 50% humidity or higher.

9.0 MODTRAN 3.7/4.0 AEROSOL AND CLOUD UPGRADES

MODTRAN 3.7 and 4.0 contain several upgrades to the current aerosol and cloud models:

The four builtin aerosol models are no longer confined to fixed and essentially non-overlapping regions. Each can be independently moved to any region, and additionally, can be stretched, compressed and scaled. Because they can be moved independently, they can occupy overlapping regions.

The user-supplied spectral parameter input schemes for aerosols have been improved. Now the spectral grid can be arbitrary (i.e., not limited to the 47 fixed spectral points) and different for each aerosol. The scattering phase function can have wavelength dependence (not just angular dependence). Additionally, there can be now up to four (not just one) user-defined aerosol profiles. These upgrades, used in conjunction with the stand-alone Mie scattering code supplied with MODTRAN 3.7/4.0, allow the user to model the effects of aerosol more realistically than was previously possible.

A stand-alone Mie code was used to recompute the spectral parameters (extinction, absorption and the asymmetry parameters) of the builtin clouds on a spectral grid consisting of 788 points between 0.2 to 300 microns. This is a much needed improvement on the older grid of 47 points in the same spectral interval.

The upgrades were coded while still maintaining backward compatibility with earlier MODTRAN input files (tape5's). In the following each upgrade and ways to access it are described.

9.1 Moving, Stretching/Compressing & Scaling Builtin Aerosols

The user now has the ability to move MODTRAN's builtin aerosols from their original positions to arbitrary altitudes and also to compress and stretch them using two additional input lines. One important gain from this new scheme is the ability to move the tropopause to a more appropriate height rather than having it fixed at 10 km. (Note that this flexible aerosol scheme cannot be used in conjunction with NOVAM, the new Navy Oceanic Vertical Aerosol Model; however, NOVAM can be used with other upgrades. NOVAM refers to the Navy Oceanic Vertical Aerosol Model, which is part of the suite of aerosol models now in MODTRAN 3.7 and higher.)

The new flexibility is invoked by having the string ('A+') in CARD 2 in columns 1-2 as shown in the example below ('A+' stands for AEROSOL PLUS):

```
A+  1    0USS 0    0    0    0    0.000     .000     .000     .000  (CARD 2)
         .70      3.7      1.0           15.0                    1.0
       35.5      65.5      1.0           70.0           90.0  (CARD 2A+)
```

The string 'A+' triggers reading a new card, CARD 2A+, which actually consists of two lines of input and which are inserted immediately after the current CARD 2 and before CARD 2A (if clouds are being input). This new two-line card is necessary if and only if 'A+' is present.

CARD 2: APLUS, IHAZE, CNOVAM, ISEASN, ARUSS, IVULCN, ICSTL, ICLD, IVSA, VIS, WSS, WHH, RAINRT, GNDALT
FORMAT (A2, I3, A1, I4, A3, I2, 3(I5), 5F10.5)

CARD 2A+: ZAER11, ZAER12, SCALE1, ZAER21, ZAER22, SCALE2, ZAER31, ZAER32, SCALE3, ZAER41, ZAER42, SCALE4 (If APLUS='A+') FORMAT((3(1X, F9.0), 20X, 3(1X, F9.0)))

Only APLUS, CNOVAM and USS are new to CARD 2; all others have the same position and meaning as before. CMOVAM is a single character immediately after IHAZE and is set to 'N' for using NOVAM output by MODTRAN. Although CNOVAM and APLUS are both in CARD 2, NOVAM aerosols cannot be used in conjunction with APLUS aerosol enhancements.

USS, the other new variable in CARD 2, is a three-character string, for which the only menaingful value is 'USS' (for USER-SUPPLIED-SPECTRA). Previous to this upgrade, a user had to rely on builtin spectral databases for the builtin aerosols. The builtin spectra are provided on a very sparse spectral grid which is inadequate for many purposes. Now the user can supply a denser set of spectral data for the builtin aersols. The scheme for the spectral input is essentially the same as is currently done using CARD 2D2. This is expanded in more detail below.

There are 12 variables in the two lines of CARD 2A+ as enumerated above. The first set of three is for aerosol number 1; the second set of three, for aerosol 2; the third set, for aerosol 3 and the fourth set, for aerosol 4. The meanings of the numerical values for ZAERi1, ZAERi2 and SCALEi, i=1, 2, 3 and 4, are as follows:

ZAERi1   The base/bottom of aerosol I

ZAERi2 > ZAERi1   The top of aerosol I
       < ZAERi1   Translate original profile to new base, ZAERi1
       = ZAERi1   Set values to default, ignore SCALEi
                     (Also set to default when both ZAERi1 and ZAERi1 are blank)

SCALEi > 0.0   Multiply vertical profile by SCALEi
       = 0 or blank Multiply vertical profile by 1.0 (i.e., preserve column density)

The aerosols are linearly mapped into the new region and the column densities are preserved if SCALEi is unity. Note that since the cards are read using fixed formats, blanks are interpreted as zeros. By default, SCALEi is set to unity if blanks or 0.0 are input. Note that if the APLUS option is used, the two lines of CARD 2A+ must be present even if any of these lines are intended to consist of all blanks.

The oft-used current definition of an aerosol region leads to some inevitable confusion. The definition really should refer to the contiguous region where the aerosol concentration is non-negative and outside which it is zero. By this definition, the region of aerosol 1, for example, is from 0 to 3 km; the profile linearly decreases from a non-zero value at 2 km to zero at 3 km. Instead, in MODTRAN documentation this region is said to be from 0-2 km. In the MODTRAN 3.7 upgrade, the ZAERi1 and ZAERi2 values refer to the bounding altitudes which sandwich the entire region where the aerosol concentration is non-negative. Table 8 lists the default values of these bounding altitudes along with the commonly (but confusingly) referred-to region boundaries for each aerosol.

Table 8. Default Aerosol Region Boundaries.

Aerosol Region	Common Region Definition	Actual ZAERi1	Actual ZAERi2
1	0-2 km	0 km	3 km
2	2-10	2	11
3	10-30	10	35
4	30-100	30	100

9.2 User-Supplied Aerosol Parameter Upgrades

This section contains instructions for the MODTRAN 3.7/4.0 options that provide flexible wavelength-dependent specification of extinction, absorption, and asymmetry parameters and phase functions. These upgrades, used in conjunction with the stand-alone Mie code, allow aerosols to be modeled more realistically. The spectral grid can be arbitrary (i.e., not limited to the default 47 fixed spectral points of the previous MODTRAN) and different for each aerosol. The scattering phase function can have wavelength dependence in addition to angular dependence. There can be up to four user-defined aerosol profiles. In addition, utility programs are provided which allow MODTRAN to be run with the Navy Oceanic Vertical Aerosol Model (NOVAM).

9.2.1. User-Supplied Aerosol Spectral Parameters (ARUSS Option)

Previous to this upgrade, the user could provide extinction, absorption and asymmetry parameters only for user-supplied aerosol profiles (IHAZE=7 or ICLD=11) which are in fact the extinction values at 0.55 μm. Furthermore, the spectral parameters were limited to the 47 wavelengths. This was done using CARDs 2D, 2D1 and 2D2 with IHAZE=7 or ICLD=11.

There have been two generalizations to user-supplied aerosol spectral data:

- Now the user can supply spectral data on an arbitrary grid for IHAZE=7 or ICLD=11. For this ARUSS (in CARD 2) needs to be set to the three-character string 'USS'. Additionally, the meaning of the IREG(N), N=1, 2, 3 and 4, variables in CARD 2D has been generalized; when > 1, they now specify the number of wavelengths at which data is supplied.

- The user can also supply spectral data for the default aerosol profiles, as selected by IHAZE, ISEASN and IVULCN (IHAZE≠7 and ICLD ≠11), instead of relying on the sparse built-in databases of MODTRAN. This is also done by setting ARUSS to the character string 'USS'. The USS option can also be used in conjunction with the APLUS option.

The relevant cards for these upgrades are CARD 2D, 2D1 and 2D2 as described below.

Note the units of extinction and absorption parameters in MODTRAN. THE EXTINCTION AND ABSORPTION COEFFICIENTS ARE ACTUALLY UNITLESS, BECAUSE THEY ARE OBTAINED BY DIVIDING THE ACTUAL VALUES BY EXTINCTION AT 0.55 μm:

$$K_{EXT}(\lambda) = EXT(\lambda)/EXT(0.55~\mu m);~~K_{ABS}(\lambda) = ABS(\lambda)/EXT(0.55~\mu m).$$

CARD 2D: IREG(1), IREG(2), IREG(3), IREG(4)   (if IHAZE=7 or ICLD=11 or ARUSS='USS')
FORMAT(4I5)

> **CARD 2D1:**   AWCCON, TITLE (CARDs 2D1 and 2D2 needed if IREG(1) > 0)
> FORMAT(E10.3, 18A4)

> **CARD 2D2:**   (VX(1, I), EXTC(1, I), ABSC(1, I), ASYM(1, I), I=1, IREG(1) or 47)
> (if ARUSS is not set)
> FORMAT(3(F6.2, 2F7.5, F6.4))

> **CARD 2D1:**   AWCCON, TITLE (if IREG(2) > 0)
> FORMAT(E10.3, 18A4)

> **CARD 2D2:**   (VX(2, I), EXTC(2, I), ABSC(2, I), ASYM(2, I), I=1, IREG(2) or 47) (if ARUSS is not set)
> FORMAT(3(F6.2, 2F7.5, F6.4))

> **CARD 2D1:**   AWCCON, TITLE (if IREG(3) > 0)
> FORMAT(E10.3, 18A4)

> **CARD 2D2:**   (VX(3, I), EXTC(3, I), ABSC(3, I), ASYM(3, I), I=1, IREG(3) or 47) (if ARUSS is not set)
> FORMAT(3(F6.2, 2F7.5, F6.4))

> **CARD 2D1:**   AWCCON, TITLE (if IREG(4) > 0)
> FORMAT(E10.3, 18A4)

> **CARD 2D2:**   (VX(4, I), EXTC(4, I), ABSC(4, I), ASYM(4, I), I=1, IREG(4) or 47) (if ARUSS is not set)
> FORMAT(3(F6.2, 2F7.5, F6.4))

CARDs 2D1 and 2D2 are repeated up to four times, one pair for each aerosol. However, the two cards for aerosol i are needed if and only if IREG(N) > 0. The only differences between the present and prior forms are in CARD 2D and CARD 2D2. Now CARD 2D has four integer values denoting the number of spectral grid points for each of the four aerosols; IREG(N) = number of spectral grid points for aerosol N. CARD 2D2 is the list of the spectral parameters: VX is the wavelength in microns, EXTC is the extinction coefficient, ABSC is the absorption coefficient and ASYM is the

asymmetry parameter. Previously IREGs were all set to 1 or 0. A value of 1 meant that spectral parameters had to be read using CARD 2D2 and the number of spectral points were fixed at 47. (Actually the VX array was not used at all because the 47 wavelengths were already fixed in the code at an earlier point.) Now, VX is a 2D-array; the first dimension identifies the aerosol and the second is the wavelength index. The user must input VX values in microns and in increasing order; that is, the first VX must be the lowest wavelength. The VX array may differ for each aerosol.

The meaning of IREG is summarized and further clarified below:

VALUE OF ARUSS	VALUE AND MEANING OF IREG(i)
ARUSS=' '	IREG(N) = 0 No user-supplied spectral data
	IREG(N) = 1 User-supplied data for the earlier set of 47 fixed grid points. Although VX array is read, they are not used; instead the 47 wavelengths are used.
ARUSS='USS'	IREG(N) = 0 No user-supplied data
	IREG(N) = M User-supplied data for M arbitrary wavelengths

9.2.2. User-Supplied Aerosol Phase Functions (CARDS 3b1, 3b2, 3c1-3c6)

The user-supplied phase function input scheme has also been upgraded. As before, the user-supplied phase functions are read in if IPH (CARD 3A2) is set to 1. Now, the user-supplied phase functions can vary with wavelength in addition to angle. This upgrade is actually independent of the A+ and USS upgrades, and it necessitates a "generalized" form of CARD 3B1:

CARD 3B1: **NANGLS, NWLF** (if IPH=1)
FORMAT(2(I5))

NWLF is the new variable which can be either 0 or a positive integer; 0 means that the phase function has no wavelength dependence whereas a positive integer means that the phase function will be specified on a wavelength grid with that many points. The phase function array, F, now has three indices: aerosol index, angle index and the wavelength index.

If NWLF = 0 or blank, CARD 3B2 is used as before:

CARD 3B2: **(ANGF(I), F(1, I, 1), F(2, I, 1), F(3, I, 1), F(4, I, 1), I=1, NANGLS)**
FORMAT(5E10.3) (if IPH=1, NWLF=0)

If NWLF > 0, CARD 3B2 is replaced by CARDs 3C1-3C6:

106

CARD 3C1: (ANGF(I), I=1, NANGLS)   (read angles if IPH=1, NWLF > 0),
FORMAT(8(1X, F9.0))

CARD 3C2: (WLF(J), J=1, NWLF)   (read wavelengths, in microns,
FORMAT(8(1X, F9.0))   if IPH=1, NWLF > 0)

CARD 3C3: (F(1, I, J), J=1, NWLF)   (read phase function for aerosol 1
FORMAT(8(1X, E9.3))   if IPH=1, NWLF > 0; repeat NANGLS times)

CARD 3C4: (F(2, I, J), J=1, NWLF)   (read for aerosol 2,
FORMAT(8(1X, E9.3))   repeat NANGLS times)

CARD 3C5: (F(3, I, J), J=1, NWLF)   (read for aerosol 3,
FORMAT(8(1X, E9.3))   repeat NANGLS times)

CARD 3C6: (F(4, I, J), J=1, NWLF)   (read for aerosol 4,
FORMAT(8(1X, E9.3))   repeat NANGLS times)

In this upgrade, the wavelength grid and the angle grid is the same for each of the four aerosols. Furthermore, the phase function must be supplied either for all aerosols or no aerosol. For each, all CARDs 3C3 are supplied first, then all CARDs 3C4, all 3C5, and finally all 3C6; the CARDs for the subsequent aerosol then follow.

9.2.3. User-Supplied Aerosol Profiles (CARD 2C3)

Prior to these upgrades, the user could only input one aerosol profile by using the user-selected profile option, MODEL=7, IRD2=1. Now the user can have up to four user-defined aerosol profiles with MODEL=7, IRD2=2. (MODEL=0 is not allowed.)

This upgrade cannot be used with the A+ upgrade option; the APLUS option is ignored if MODEL=7 and IRD2=2 or 1. The A+ option allows the built-in aerosols to be shifted around, whereas this upgrade allows the user to input aerosol profiles (up to all four) with greater control. The four profiles can only be input as altitude-dependent aerosol extinction coefficients at 0.55 μm. Previously the single user-defined aerosol profile could be either the altitude-dependent extinction coefficient or the altitude-dependent liquid water content (in gm/m³). For backward compatibility the previous option for the single aerosol profile is maintained.

107

This upgrade is achieved by a generalization of CARD 2C3. For this purpose AHAZE was changed from a scalar variable to an array, AHAZE(4). The two versions of CARD 2C3 are shown below:

CARD 2C3: AHAZE(1), EQLWCZ, RRATZ, IHA1, ICLD1, IVUL1, ISEA1, ICHR1
(if IRD2=1)
FORMAT(10X, 3F10.0, 5I5)

CARD 2C3: AHAZE(1), RRATZ, AHAZE(2), AHAZE(3), AHAZE(4) (if IRD2=2)
FORMAT(10X, F10.0, 10X, 4F10.0)

The variables missing in the newer version of CARD 2C3 (IRD2=2) are not needed for specifying aerosols. However, ICLD1 (IRD2=1) allows the user to specify cloud profiles in addition to aerosol profiles with the restriction that a cloud extinction and an aerosol extinction cannot be specified at the same altitude using CARD 2C3. The price of the current upgrade is the elimination of the cloud extinction at an altitude for having the luxury of inputing up to four aerosol extinctions. However, user-specified cloud profiles may be entered using CARD 2E1.

As mentioned, in lieu of extinction an aerosol profile could also be given as liquid water content in gm/m^3. The conversion factor for converting liquid water content (gm/m^3) to extinction coefficient is given by AWCCON. AWCCON can also be user-specified by using CARD 2D (IHAZE=7 or ICLD=11). However, since in the present upgrade, the aerosol profiles cannot be stated in terms of liquid water content, AWCCON values in CARD 2D1 are not used.

9.3 Example tape5 File

Here is an example of a tape5 which has both the A+ and ARUSS aerosol options. Notice the CARD 2A+ following CARD 2 (which contains 'A+' as its first two characters). Also note that user-supplied spectral data are used for a built-in aerosol profile.

```
M    4    3    0    1    0    0    0    0    0    0    1    0   -1          .0500
F    OF   0
A+   1    1USS 0    0    0    0    0.000     0.000     0.000     0.000
          .5                  1.0   (CARD 2A+)
(This blank line must be here or this line should have zeros)   (CARD 2A+)
     40    0    0    0   (CARD 2D)
  0.000e+00region #1 desert summer aerosol
    0.201.016680.434950.8797     0.301.016680.434950.8797     0.341.019360.447350.8857
    0.551.000000.219350.7980     0.691.037040.167430.7666     1.061.114910.037210.7143
```

108

```
 1.541.208350.043480.7689     2.001.047120.042120.8557     2.250.905020.035770.8936
 2.500.770220.050250.9116     2.700.667040.086210.9281     3.000.628860.114680.9247
 3.390.812440.122180.8623     3.750.788880.100130.8493     4.500.677650.104040.8524
 5.000.608420.104880.8551     5.500.511680.115510.8706     6.000.362390.150330.9038
 6.200.337160.150810.9065     6.500.311720.152880.9079     7.200.670350.206630.7748
 7.900.285240.129920.8881     8.200.301080.188320.8855     8.700.600290.258340.7717
 9.000.829650.339030.6736     9.200.831530.346750.6684    10.000.808380.344870.6558
10.590.692100.275960.6814    11.000.669310.250000.6748    11.500.625310.232900.6805
12.500.526480.201000.7023    14.800.493950.190370.6708    15.000.487910.188070.6700
16.400.466220.177020.6539    17.200.461220.172020.6408    18.500.442030.181610.6366
21.300.485200.268970.5959    25.000.457050.223520.5460    30.000.401790.258470.5494
40.000.368010.239470.4688
004.90000              180.00000
     2500       02600          25          5
       0
```

9.4 Cloud Spectral Upgrades

A Mie code was used to recompute the sepectral parameters of the five builtin clouds, cumulus, altostratus, stratus, stratus/strato-cumulus and nimbostratus, on a dense grid of 788 spectral points between 0.2 and 300 microns, with the density of the spectral points heavily weighted towards the shorter wavelengths. This new grid is a much needed improvement on the older grid of 47 points in the same wavelength region. The aerosol optical properties were also retabulated at the 788 grid points, but the data is simply an interpolation of the lower resolution data; in other words, no new Mie calculation was performed for the aerosols.

10. ACKNOWLEDGEMENTS

110

11. REFERENCES

Adler-Golden, S. M. and M. W. Matthew, "SHARC-3 Calculations of Atmospheric Radiance in the Solar Terminator Region," SSI-TR-229, Spectral Sciences Inc., Burlington, MA (1993).

Adler-Golden, S. M., "Description of the SHARC Atmospheric Generator," SSI-TR-232, Spectral Sciences Inc., Burlington, MA (1993).

Adler-Golden, S. M.A. Berk, J. Vail, F. von Esse, D. Smith, L. Jeong, and R. Sharma, "Spectral and Radiometric Comparisons of CIRRIS-1A Data and SAMM Code Calculations," SSI-TR-241, Spectral Sciences Inc., Burlington, MA (1994).

Ahmadjian, M. A., R. M. Nadile, J. O. Wise, and B. Bartschi, "CIRRIS-1A Space Shuttle Experiment." *J. Spacecr. Rockets*, **27**, 669, 1990.

Anderson, G. P., J. H. Chetwynd, S. A. Clough, E. P. Shettle, and F. X. Kneizys, "AFGL Atmospheric Constituent Profiles (0-120 km)," AFGL-TR-86-0110 (1986). ADA175173

Anderson, G. P. and L. A. Hall, "Solar Irradiance between 2000-3100 Angstroms with Spectral Band Pass of 1 Angstroms," *J. Geophys. Res.*, **94**, 6435-6441, 1989.

Anderson, G. P., J. H. Chetwynd, J.-M. Theriault, P. K. Acharya, A. Berk, D. C. Robertson, F. X. Kneizys, M. L. Hoke, L. W. Abreu, and E. P. Shettle, "MODTRAN2: Suitability for Remote Sensing," Proceedings of the Workshop on Atmospheric Correction of LANDSAT Imagery, Torrance, CA (1993).

Armstrong, P. S., S. J. Lipson, J. R. Lowell, W. A. M. Blumberg, D. R. Smith, R. M. Nadile, and J. A. Dodd, "Analysis of Comprehensive CIRRIS-1A Observations of Nitric Oxide in the Thermosphere," *EOS Trans. AGU*, **74**, F225, 1993.

Berk, A. L. S. Bernstein, G. P. Anderson, P. K. Acharay, D. C. Robertson, J. H. Chetwynd, and S. M. Adler-Golden, "MODTRAN Cloud and Multiple Scattering Upgrades with Application to AVIRIS," *Remote Sens. Environ.*, **65**, 367, 1998.

Bernstein, L. S., A. Berk, P. K. Acharya, D. C. Robertson, G. P. Anderson, J. H. Chetwynd, and L. M. Kimball, "Very Narrow Band Model Calculations of Atmospheric Fluxes and Cooling Rates," *J. Atmos. Sci.*, **53**, 2887, 1996.

Bingham, G., "Calibration/Data Reduction," presented at the *CIRRIS-1A Data and Lessons Learned Review*, Air Force Research Laboratory, Hanscom AFB, MA (October 1991).

Clough, S. A., F. X. Kneizys, G. P. Anderson, E. P. Shettle, J. H. Chetwynd, L. W. Abreu, and L. A. Hall, "FASCOD3: Spectral Simulation," Proceedings of the International Radiation Symposium, Eds. Lenoble and Geleyn, Deepak Publishing, 1988.

Bingham, G. E., D. K. Zhou, Y. Yang, A. Steed, G. P. Anderson, and R. M. Nadile, "Greenhouse Gas Concentration Profiles Retrieved from CIRRIS-1A Measurements in the 7-13 μm Window During STS-39," *Eos Trans. AGU*, **74**, F173, 1993.

Chanin, M. L., "Advances in Mesospheric Studies by Rayleigh Lidar Techniques," presented at the *AGU Chapman Conference on the Upper Mesosphere and Lower Thermosphere*, Asilomar, CA (November 1992).

Dodd, J. A., S. J. Lipson, J. R. Lowell, P. S. Armstrong, W. A. M. Blumberg, R. M. Nadile, S. M. Adler-Golden, W. J. Marinelli, K. W. Holtzclaw, and B. D. Green, "Analysis of Hydroxyl Earthlimb Emissions. Kinetic Model for State-to-State Dynamics of OH(v,N)," *J. Geophys. Res.*, **99**, 3559, 1994.

Duff, J. W., F. Bien, and D. E. Paulsen, "Classical Dynamics of the $N(^4S) + O_2(X^3\Sigma g) \rightarrow NO(X^2\Pi) + O(^3P)$ Reaction," *Geophys. Res. Lett.*, **21**, 2043 (1994).

Gathman, S.G. and K. L. Davidson, "The Navy Oceanic Vertical Aerosol Model," TR 1634, Naval Command Control and Ocean Surveillance Center, San Diego, CA (1993).

Goody, R. M. and Y. L. Yung, "Atmospheric Radiation: Theoretical Basis," Oxford University Press, NY, 1989.

Hedin, A. E., "Extension of the MSIS Thermospheric Model into the Middle and Lower Atmosphere," *J. Geophys. Res.*, **96**, 1159, 1991.

Hegblom, E. R., "Interactive Data Processing System," presented at the *CIRRIS-1A Data and Lessons Learned Review*, Air Force Research Laboratory, Hanscom AFB, MA (October 1991).

Houghton, J.T., The Physics of Atmospheres, Cambridge University Press,1986.

Kurucz, R.L., "The Solar Irradiance by Computation," PL-TR-95-2060, Air Force Geophysics Laboratory, Hanscom Air Force Base, MA, May 1995.

Kurucz, R.L., "Atomic and Molecular Data for Opacity Calculations," Revista Mexican de Astonomia y Astrofisica, 23, 1992; "Finding the Missing Solar Ultraviolet Opacity," ibid, 1992; "Remaining Line Opacity Problems for the Solar Spectrum," ibid, 1992.

Lacis, A. A., and V. Oinas, "A Description of the Correlated k Distribution Method for Modeling Nongray Gaseous Absorption, Thermal Emission, and Multiple Scattering in Vertically Inhomogeneous Atmospheres," *J. Geophys. Res.*, **96**, 9027, 1991.

Ludwig, C. B., W. Malkmus, J. E. Reardon, and J. A. L. Thomson, "Handbook of Infrared Radiation for Combustion Gases," NASA Report SP-3000 (1973).

Makhlouf, U., R. H. Picard, and J. R. Winick, "Photochemical Dynamical Modeling of the Measured Response of Airglow to Gravity Waves: 1. Basic Model for OH Airglow," *J. Geophys. Res.*, **100**, 11289, 1994.

Rinsland, C. P., R. Zander, J. S. Namkung, C. B. Farmer, and R. H. Norton, "Stratospheric Infrared Continuum Absorptions Observed by the ATMOS Instrument," *J. Geophys. Res.*, **94**, 16303, 1989.

Rothman, L. S., C. P. Rinsland, A. Goldman, S. T. Massie, D. P. Edwards, J.-M. Flaud, A. Perrin, V. Dana, J.-Y. Madin, J. Schroeder, A. McCann, R. R. Gamache, R. B. Wattson, K. Yoshino, K. Chance, K. W. Jucks, L. R. Brown, V. Nemtchinov, and P. Varanasi, "The HITRAN Molecular Database and HAWKS (HITRAN Atmospheric Workstation): 1996 Edition," *J. Quant. Spectrosc. Radiat. Transfer,* **60**, 665, 1998.

Sharma, R. D., H. Dothe, and J. W. Duff, "Model of the 5.3 μm Radiance During the Sunlit Terrestrial Thermosphere," *J. Geophys. Res.*, **103**, 14753, 1998.

Sharma, R. D., J. H. Brown, A. Berk, P. K. Acharya, J. Gruninger, J. W. Duff, and R. L. Sundberg, "User's Manual for SAMM, SHARC and MODTRAN Merged," PL-TR-96-2090, Air Force Research Laboratory, Hanscom AFB, MA (1996). ADA310349

Smith, D. R., R. M. Nadile, E. Richards, R. Hegblom, and R. Gibson, "Diurnal Variability of IR Emission Profiles Near the Terminator as Observed by the CIRRIS 1A Experiment From the Space Shuttle,: *EOS Trans. AGU*, **73**, S111, 1992.

Smith, D. R., W. A. M. Blumberg, R. M. Nadile, S. J. Lipson, E. R. Huppi, N. Wheeler, and J. A. Dodd, "Observation of High-N Hydroxyl Pure Rotation Lines in Atmospheric Emission Spectra by the CIRRIS-1A Space Shuttle Experiment," *Geophys. Res. Lett.*, **19**, 593, 1992.

Smith, D. R., P. De, S. Adler-Golden, and C. Roth, "Empirical Correlations in Thermospheric NO Density Measured from Rockets and Satellites," *J. Geophys. Res.*, **98**, 9453, 1993.

Smith, D. R. and M. Ahmadjian, "Observation of Nitric Oxide Rovibrational Band Head Emissions in the Quiescent Airglow During the CIRRIS-1A Space Shuttle Experiment," *Geophys. Res. Lett.*, **20**, 2679, 1993.

Summers, M. E., "Zonally Averaged Trace Constituent Climatology," NRL-MR-7641-93-7416, Naval Research Laboratory, Washington, DC (1993).

Sundberg, R. L. J. W. Duff, J. H. Gruninger, L. S. Bernstein, R. D. Sharma, M. W. Matthew, S. M. Adler-Golden, R. J. Healey, J. H. Brown, and D. C. Robertson, "SHARC, a Model for Calculating Atmospheric Infrared Radiation Under Non-Equilibrium Conditions," in *The Upper Mesosphere and the Lower Thermosphere: A Review of Experiment and Theory, Geophysical Monograph Series*, **87**, 287, 1995.

Winick, J. R., R. H. Picard, U. Makhlouf, E. T. P. Lee, W. A. M. Blumberg, D. R. Smith, R. M. Nadile, A. Paboojian, P. P. Wintersteiner, and R. A. Joseph, "Analysis of the 4.3 μm Limb Emission Observed From STS-39," *EOS Trans. AGU*, **73**, F418, 1992.

Wise, J. O., R. L. Carovillano, H. C. Carlson, R. G. Roble, S. Adler-Golden, R. M. Nadile, and, M. Ahmadjian, "CIRRIS 1A Global Observations of 15 μm-CO_2 and 5.3-μm NO Limb Radiance in the Lower Thermosphere during Moderate to Active Geomagnetic Activity," *J. Geophys. Res.*, **100**, 21357, 1995.

Woods, T.N., D.K. Prinz, G.J. Rottman, J. London, P.C. Crane, R.P. Cebula, E. Hilsenrath, G.E. Brueckner, M.D. Andrews, O.R. White, M.E. VanHoosier, L.E. Floyd, L.C. Herring, B.G. Knapp, C.K. Pankratz and P.A. Reiser, "Validation of the UARS Solar Ultraviolet Irradiances: Comparison with the ATLAS 1 and 2 Measurements," *J. Geophys. Res.*, **101**, 9841-9569, 1996.

Zhou, D. K., W. R. Pendleton Jr., G. E. Bingham, A. J. Steed, and R. M. Nadile, "Shuttle-Induced Optical Contamination Observed from STS-39 by CIRRIS-1A," *Eos Trans. AGU*, **74**, F467, 1993.